DEFINING A REGULATORY ROLE FOR THE HSV GLYCOPROTEIN B MEMBRANE PROXIMAL REGION IN MEMBRANE ASSOCIATION

Spencer S. Shelly

A DISSERTATION

in

Cell and Molecular Biology

Presented to the Faculties of the University of Pennsylvania

in

Partial Fulfillment of the Requirements for the

Degree of Doctor of Philosophy

2013

Supervisor of Dissertation

_____

Roselyn J. Eisenberg
Professor of Microbiology

Co-Supervisor of Dissertation

_____

Gary H. Cohen
Professor of Microbiology

Graduate Group Chairperson

_____

Daniel S. Kessler, Associate Professor of Cell and Developmental Biology

Dissertation Committee
Paul F. Bates, Professor of Microbiology
Jeffrey M. Bergelson, Professor of Pediatrics
Harvey M. Friedman, Professor of Medicine
Yan Yuan, Professor of Microbiology

DEDICATION

For my wife and daughter

ACKNOWLEDGMENTS

The work presented in this thesis could not have been completed without the tremendous support provided by many individuals.

I would like to express my gratitude to my advisors, Gary Cohen and Roselyn Eisenberg, for allowing me to join the laboratory and for the tremendous support and guidance they provided in all aspects of this work. Their continuous enthusiasm and dedication is inspiring. Also, I need to thank Michael Atchison for his personal support and his commitment to the VMD/PhD program. I must also thank the members of my thesis committee Paul Bates, Jeff Bergelson, Harvey Freidman, and Yan Yuan for helping me throughout this process. My thanks to Sara Cherry and the members of the Cherry laboratory where I learned a great deal.

I also thank the fantastic group of people that makes up the Cohen/Eisenberg laboratory. A big thanks to the entire lab past and present, including Doina Atanasiu, Chwan Hong Foo, John Gallagher, Huan Lou, Manuel Ponce-de-Leon, Wan Ting Saw, Katie Stiles, and Chuck Whitbeck. I'd especially like to thank Tina Cairns who helped with many aspects of this project, and made completion of this work possible.

I'm incredibly grateful for my wonderful wife and daughter, and their constant support and encouragement. Lastly, I would like to thank my parents for their unconditional support.

ABSTRACT

DEFINING A REGULATORY ROLE FOR THE HSV GLYCOPROTEIN B MEMBRANE PROXIMAL REGION IN MEMBRANE ASSOCIATION

Spencer S. Shelly

Roselyn J. Eisenberg

Gary H. Cohen

Herpes simplex virus (HSV) entry requires four essential glycoproteins (gD, gH/gL, and gB) to enable fusion between the virion envelope and the cellular membrane. The fusion cascade is activated by gD binding to one of its receptors, nectin-1 or HVEM. Glycoprotein B (gB), a class III viral fusion protein, mediates the fusion reaction, while data indicates that gH/gL acts as a regulator of gB. gB is trimeric and has a 773 amino acid ectodomain with a highly hydrophobic membrane proximal region (MPR) (residues 731-773) and two fusion loops (FL) per protomer. The post-fusion structure of gB was solved from the gB(730t) construct, which is truncated to remove the hydrophobic MPR residues. In this dissertation I investigated the MPRs influence on gBs ability to interact with membranes. I hypothesize that the MPR regulates fusion loop exposure by interacting with the fusion loops and masks them until fusion begins. To investigate this process I constructed a series of MPR deletion, truncation, and point mutations using

both full-length mammalian expression vectors and purified baculovirus expressed protein. I found that deletions in the MPR from full-length gB resulted in a disruption in cell surface expression in transfected cells. This suggests the MPR is necessary for proper folding or transport of gB. Soluble gB MPR truncations [gB(759t), gB(749t), gB(739t)] were expressed and purified using the baculovirus expression system, and compared to MPR-less gB(730t) and full MPR containing gB(773t). I found that gB containing an MPR segment were all compromised in their ability to bind liposomes in comparison to gB(730t), which lacks any MPR residues. Supporting our hypothesis we found that residues 731 to 739 were sufficient prevent liposome association and mutation of two aromatic residues, F732 and F739, to alanine in gB(739t) restored gBs ability to bind liposomes. Together, my data suggests the MPR does indeed regulate gBs ability to associate with liposomes, and that aromatic residues in the MPR are important for this function. This supports our model that the MPR masks the gB FLs to prevent premature membrane association and adds another layer of regulation to the HSV entry cascade.

TABLE OF CONTENTS

Page

LIST OF TABLES

CHAPTER 1

LIST OF ILLUSTRATIONS

CHAPTER 1

CHAPTER 2

CHAPTER 3

APPENDIX

CHAPTER 1

GENERAL INTRODUCTION

Herpesvirus overview

The viral family Herpesviridae consists of over 200 members infecting nearly every species of animal (39). Herpesviridae family members are traditionally classified on the basis of virion architecture. They contain an electron-opaque core of double-stranded DNA surrounded by an icosadeltahedral capsid. The capsid is surrounded by a proteinaceous tegument and is surrounded by an envelope spiked with glycoproteins (Figure I-1) (39, 143). There are eight known human herpesviruses (Table I-1), which along with all herpesviruses are further divided into three subfamilies, alphaherpesvirus, betaherpesvirus, and gammaherpesvirus. These subdivisions are based on genome organization, biological properties, and cellular tropism. Alpha-herpesviruses have a broad host range, wide cellular tropism, a short replication cycle, destroy infected cells, and infect sensory ganglia where latency is often established. The human alphaherpesviruses include varicella zoster virus (VZV) and Herpes simplex virus type 1 and type 2 (HSV-1 and HSV-2) (39). The betaherpesviruses have long replication cycles and infect secretory glands and lymphoreticular cells. Betaherpesvirus infected cells become enlarged and are known as cytomegalia, and the human viruses include human cytomegalovirus (HCMV), human herpes virus-6 (HHV-6), and human herpes virus-7 (HHV-7) (39). T-lymphocytes or B-lymphocytes are the usual target cells of the gammaherpesviruses, which have the most restricted host range of the three herpesvirus subfamilies. The gammaherpesviruses infecting humans include Epstein Barr virus (EBV) and Kaposi's sarcoma associated herpesvirus (KSHV) (39).

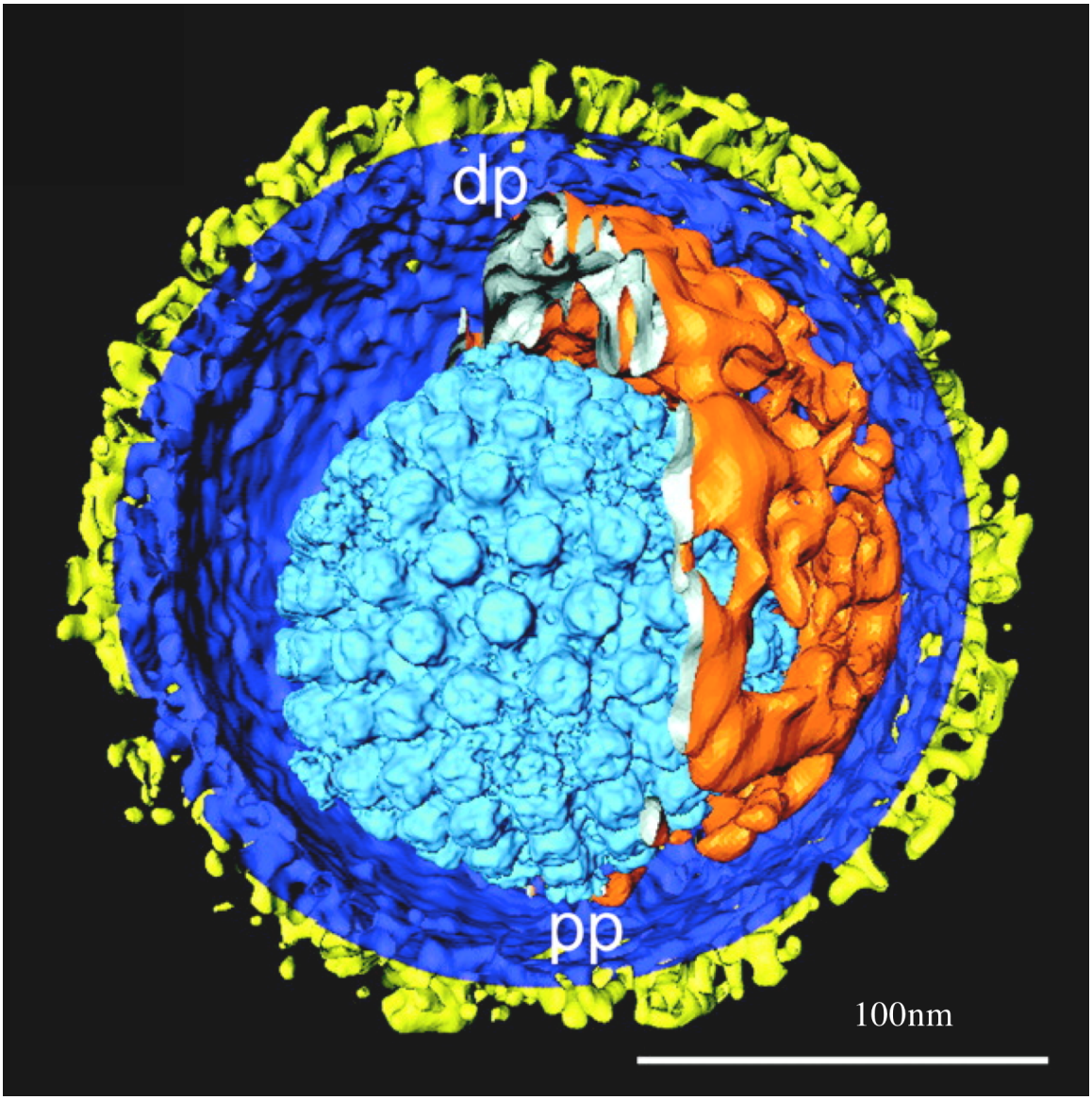

Figure I-1. Structure of HSV-1 virion. The icosahedral capsid (cyan) contains the dsDNA genome, and is surrounded by the tegument layer (orange, portions removed). The tegument is surrounded by the host-derived lipid bilayer (blue), which is studded with the viral glycoproteins (yellow). Adapted from Grunewald *et al* (48).

Abbrev.	Vernacular name	Designation	Subfamily
HSV-1	Herpes simplex virus 1	HHV-1	α
HSV-2	Herpes simplex virus 1	HHV-2	α
VZV	Varicella-zoster virus	HHV-3	α
EBV	Epstein-Barr virus	HHV-4	γ
CMV	Cytomegalovirus	HHV-5	β
HHV-6	Human herpesvirus 6	HHV-6	β
HHV-7	Human herpesvirus 7	HHV-7	β
KSV	Kaposi's sarcoma-associated herpesvirus	HHV-8	γ

Table I-1. Human herpesvirus classification. The eight human herpesvirus are listed above with their vernacular name, official designation, and herpesvirus subfamily classification. Adapted from Fields Virology (39).

HSV-1 and HSV-2 are prevalent in the United States with seroprevalence of 58% and 17% of the adult population respectively (148). HSV-1 is the oral form of the virus and typically causes lesions of the oral mucosa. The genital form, HSV-2, causes lesions of the genital tissues. Closer analysis of HSV-2 seroprevalence in the U.S. reveals women are infected at twice the rate of men, 23.1% versus 10.9% (148). In those infected HSV establishes a latent infection in sensory ganglia that persists for the lifetime of the host (39). HSV symptoms are rarely life threatening but cause varying degrees of morbidity. Active HSV infection in immunocompetent adults can range from being asymptomatic to the formation of oral or genital mucosal lesions (131). HSV can cause corneal infections resulting in keratitis and rarely blindness or fatal encephalitis in healthy individuals. Infection of neonates and the immunocompromised can result in disseminated HSV that is life threatening (131). Approximately 1500 cases of neonatal disseminated HSV are diagnosed each year in the United States (28) with a mortality rate of 47% (144).

Virion structure

Four compartments make up the HSV virion, which are the genome, capsid, tegument, and envelope with glycoproteins (Figure I-1) (48, 140). HSV is a large, enveloped virus with a diameter of 125-200 nm and contains an approximately 150 kilobase pair linear double-stranded DNA with a G + C content of nearly 68% (39). The genome contains two covalently linked segments, called the long (L) and short (S) unique segments, which are linked by inverted repeats. The repeats allow rearrangement of the

unique sequences yielding four possible genome arrangements (53). The HSV genome encodes at least 70 polypeptides (39).

The HSV genome is enclosed by an icosahedral capsid made from four major components (VP5, VP19C, VP23, VP26) and has been resolved by electron microscopy in detail (152). VP5 is the major capsid protein, which oligomerizes to form ring-shaped capsomers, while one VP19C and two VP23 molecules form timers. VP26 is located at tips of the capsomers (39).

The capsid is surrounded by the closely associated tegument layer, which is made of at least 22 proteins (140). Tegument proteins have multiple roles immediately upon virus entry. These functions include virion host shut-off (vhs) by UL41 to halt host protein synthesis (85). VP16 is an essential viral transcription factor and US11 prevents the shutdown of protein synthesis by protein kinase R (PKR) (2, 106).

A lipid bilayer surrounds the genome, capsid, and tegument known as the viral envelope. The envelope is derived from host lipid membrane and contains eleven glycoproteins (gB, gC, gD, gE, gG, gH, gI, gJ, gL, gM, gN) and at least three non-glycosylated proteins (39). While five of these glycoproteins (gD, gB, gH, gL, gC) are involved in entry four (gD, gB, gH, gL) are necessary and sufficient for the fusion with susceptible cell membranes (55, 105). Glycoprotein C has dual functions including a dispensable role in viral attachment and in immune evasion blocking the complement pathway (57, 59, 83).

HSV replication cycle

HSV transmission occurs through epithelial mucosa of the human host, usually by direct contact between infected and uninfected tissues. The steps of infection include viral attachment to the cell surface followed by fusion of the viral and cellular membranes allowing viral entry (122). Viral replication occurs at the site of entry leading to cell death and viral spread to innervating axons of the peripheral nervous system. Retrograde transport along microtubules carriers the viral capsid with tegument proteins to the neurons cell body and nucleus (32). Several tegument proteins, VP16 and US11, are important to shutdown host synthesis and viral protein production as discussed above.

Lytic infection of sensory neurons leads to destruction of the neuron, but often a latent infection is established where the virus persists without neuronal destruction. In the sensory neurons life-long latent infection is established in the trigeminal or superior cervical ganglion for HSV-1 and the sacral ganglia for HSV-2 (93). During latent infection the virus is protected from the host immune response in the immune privileged neuronal site and the low level of HSV transcription. The latent HSV genome exists as a circularized extrachromosomal episome in the neuronal nucleus, and only one viral transcript called the latency associated transcript (LAT) is detectable in the cell (15). In an incompetently understood process the latent virus can response to stimuli like stress or UV light and reactivate to produce infectious particles. Reactivation leads to viral capsid formation and anterograde transport down the axon to the axonal termini where virions are assembled (93, 135). Ultimately a secondary lytic infection of the epithelial mucosa occurs near the area of the previous primary infection with lesion formation or

asymptomatic viral shedding (91, 93). To complete this complex replication cycle HSV infects multiple cell types, and this correlates with the wide cellular tropism exhibited by the virus in tissue culture.

HSV has the ability to infect epithelial, endothelial, fibroblasts, and neurons in its human host (39). HSV also non-productively infects monocytes and T cells (107). In vitro HSV infects most cell types tested, which is likely due to its ability to use multiple cellular receptors.

As described above, attachment is mediated by envelope glycoproteins, and four glycoproteins (gD, gB, gH, gL) are necessary and sufficient for attachment and fusion with susceptible cell membranes (55, 105). The details of viral entry and membrane fusion process will be discussed below. HSV fuses either at the cell membrane or undergoes endocytosis and fuses with an endocytic vesicle releasing the viral capsid into the cytoplasm. The capsid binds to the retrograde molecular motor dynein and is transported along microtubules to the nuclear pore (32, 33, 35). Viral DNA is then released into the nucleus were it circularizes forming an extra-chromosomal episome.

Expression of HSV genes products is highly regulated cascade using the cellular RNA polymerase II (109). Three groups of genes have been defined based on the timing of there expression: immediate-early (IE), early (E), and late (L) (39). Generally, the immediate-early genes serve regulatory functions, the early genes participate in translation and DNA replication, and late genes are structural proteins. Activation of IE gene transcription requires the presence of tegument proteins (VP16) and cellular factors (Oct1) prior to viral protein synthesis (126). Six IE proteins (ICP0, ICP4, ICP22, ICP27,

ICP47, US1.5) are transcribed and translated two to four hours post infection (hpi) and several are involved in the induction of E gene expression (39). Early gene transcription reaches its peak 4-8 hpi, and several E proteins replicate cellular function such as thymidine kinase (ICP36) and ribonucleotide reductase (ICP6). DNA polymerase (UL30), DNA binding proteins (UL42, UL29), ORI binding protein (UL9), and helicase/primase complex (UL5, UL8, UL52 are the seven E proteins necessary and sufficient to carry out viral DNA replication (16). The onset DNA replication leads to a reduction in E expression and the increase in expression of L genes encoding structural elements of the virion including glycoproteins.

HSV DNA replication initiates after the linear viral genome is delivered to the nucleus and circularized. DNA replication is thought to originate by a bidirectional theta mechanism, which is followed by rolling-circle replication resulting in head-to-tail concatemers of HSV genomes (16). DNA concatemers are cleaved into individual genome segments during packaging into the preformed viral capsids. The resulting nucleocapsid are enveloped by bud through the inner nuclear membrane (141), but competing theories for the HSV egress route have been presented.

Historically, the double envelopment model has been the most widely accepted model. In this model capsid particle are enveloped by the inner nuclear membrane envelope, fuse with the outer nuclear membrane, and are released to the cytoplasm. The capsids then association with tegument proteins and are re-enveloped by a cytoplasmic organelle, likely budding into the Trans Golgi Network for maturation and transported through the vesicular secretory pathway (23, 90). A second model provides two

pathways for egress. First, a minority of capsids are enveloped by the inner nuclear membrane and travel intraluminally through the Rough ER (RER) to Golgi cisternae and package in to transport vesicles. A second, primary route allows capsids direct passage from the nucleus to the cytoplasm through enlarged nuclear pores. In the cytoplasm they can bud into cytoplasmic membranes (23, 78). Whatever the mode of envelopment the end result is infectious HSV particles surrounded in a glycoprotein studded envelope.

Viral entry strategies

Viral entry pathways are determined by interactions at the cell surface, and these critical interactions regulate the process viral genetic material uses to cross the cellular lipid bilayer. Both non-enveloped and enveloped viruses must accomplish this task. The non-enveloped viruses, lacking a lipid bilayer of their own, must transfer their genome across the cellular bilayer. Enveloped viral genomes must transit both the viral and cellular bilayers (51). The strategy used by each virus is dictated by the particular cellular conditions encountered at the site of penetration (137)

Non-enveloped viruses, lacking a lipid bilayer, use three main strategies to get their genetic material across the cellular membrane. These strategies include transient lipid rearrangement, pore formation, and gross membrane disruption (98). Non-enveloped viral particles often require additional maturation steps, such as proteolysis and conformational alteration to be primed for cellular invasion. At the target cell each virus type is primed by a specific set of signals including receptor binding, low pH, protease cleavage, chaperone-assisted morphological changes, or divalent cation

chelation. These triggers regulate capsid rearrangements known broadly as uncoating and help ensure the virus is in the proper state and location when activated for entry. Poliovirus, a member of the family Picornaviridae binds its cellular receptor CD155 and undergoes a conformational change exposing an amphipathic α-helix in the capsid protein (54, 89). The α-helix is important for membrane penetration, pore formation, and ultimately genome release into the cytoplasm (98, 139). Membrane pore formation, as described above for Picornaviridae, is also employed by the Parvoviridae and Reoviridae families, to facilitate genome release into the cytoplasm (1, 38, 62, 139). Other non-enveloped viruses such as adenovirus cause gross membrane disruption by lytic factor release facilitating genome entry into the cell (84).

Enveloped viruses depend on a mechanism capable of facilitating fusion between the viral and cellular membranes for their genetic material to gain entry. Fusion between two bilayer membranes is a thermodynamically favorable process with a high kinetic barrier of 40-50 kcal/mol (71). In enveloped viruses fusion proteins provide this mechanism and catalyze membrane fusion by overcoming the kinetic barrier using the free energy of conformational change. The described viral fusion proteins contain several common characteristics. They are type I membrane proteins with a large ectodomain and two membrane-interacting regions, the C-terminal transmembrane anchor and a hydrophobic patch or fusion peptide. Also, they have a cytoplasmic tail and are trimeric in their post-fusion state (51, 145). Viral fusion proteins are membrane bound with large ectodomains folded into a metastable pre-fusion state (51). To

overcome the high energy barrier of membrane fusion a fusion protein undergoes conformational change and uses the energy released to drive fusion.

Viral Fusion Proteins

Three classes of viral fusion proteins, class I, class II and class III, are recognized based on their structure and mechanism of fusion, and are exemplified by influenza hemagglutinin (HA), tick-borne encephalitis virus (TBEV) E protein, and vesicular stomatitis virus (VSV) glycoprotein G respectively (Figure I-2) (95, 96, 111, 113, 120). Across these three classes of viral fusion proteins the route for catalyzing viral-cell fusion is believed to follow a similar process using the free energy liberated by conformational change to bring the viral and cellular membranes together (Figure I-3) (51). Fusion proteins while diverse in sequence and structure all catalyze fusion using the same general process resulting a trimeric active state and post fusion structure. Unique regulatory steps are present in each class, and even for each particular virus, providing control mechanisms for the fusion process (145).

The surfaces of mature enveloped viral particles are covered in fusion proteins in a metastable fusion-competent state (Figure I-3A). A triggering event, specific to each fusion protein, leads to conversion into to a prehairpin intermediate homotrimer. The prehairpin intermediate (Figure I-3B) forms a bridge between the viral membrane and target membranes connected though the C-terminal transmembrane anchor and the hydrophobic fusion peptide, respectively. Next a series of conformational changes, or fold-back steps occur bring the two membrane inserted elements, the fusion peptide and

transmembrane anchor, together to create a trimer-of-hairpins (Figure I-3C-D) (25, 88). Through the fold-back process the membrane becomes distorted, progressing through hemifusion, small fusion pore formation, and finally the establishment of a stable large fusion pore (Figure I-3D) (51, 145). Ultimately, formation of a stable six-helix bundle results in the fusion of the viral and cellular membranes and allows the transfer of the viral nucleocapsid into the cytoplasm to initiate replication (Figure I-3E).

Class I Fusion Proteins

Class I fusion proteins are trimeric pre-fusion and post-fusion with a characteristic long central α-helical coiled-coil, two heptad repeat regions, and N-terminal fusion peptide, which is initially concealed at the primer interface (51, 145). Typically, the class I fusion protein is translated as a single polypeptide and cleaved into 2 proteins during post-translational processing or upon exposure to low pH in the endosome. The fusion active portion contains the membrane anchor and remains attached to the viral membrane, while the second portion contains the receptor binding motif (145).

Fusion between the viral and cellular membranes occurs generally as outlined above. Briefly, the fusion protein is attached to the viral membrane by the transmembrane domain and to the cellular membrane by insertion of the fusion peptide. Conformational changes, initiated by a trigger (receptor binding or low pH), drive the fusion protein into a hairpin intermediate-state. Then self-association of the heptad repeat regions support the formation of a stable six-helix bundle (6HB) in the

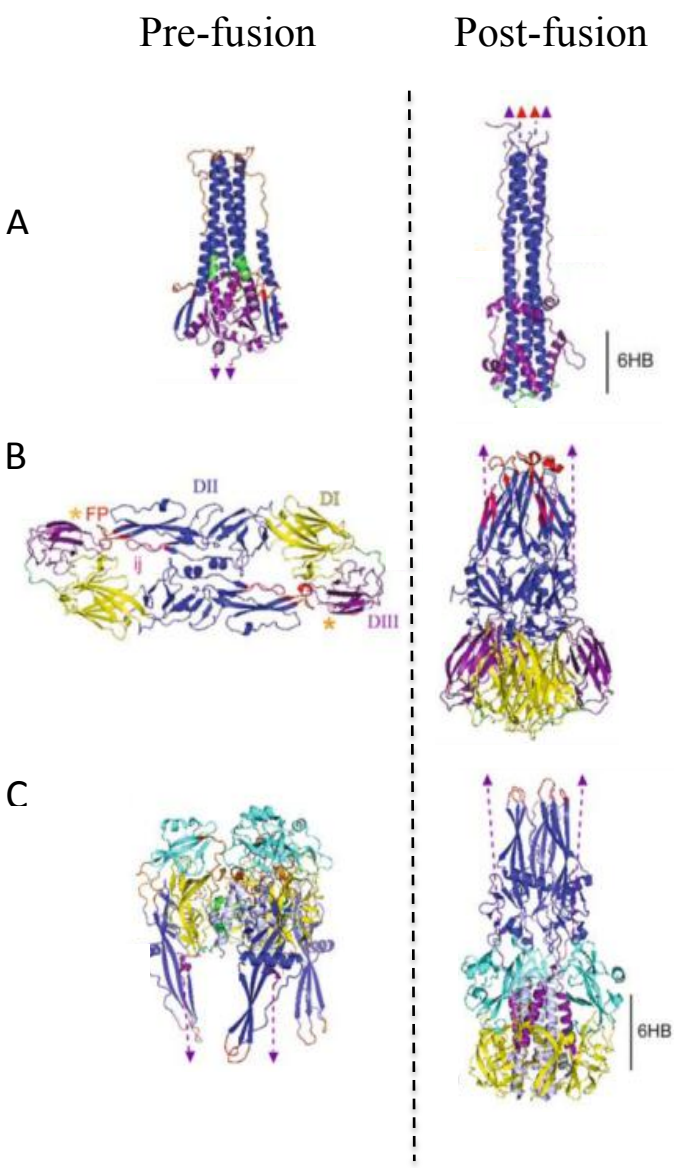

Figure I-2. Class I, II, III fusion proteins; pre-fusion and post-fusion structures. (A) Class I fusion protein Influenza virus HA2 crystal structures is shown. (B) Class II fusion protein TBEV E protein crystal structures. (C) Class III fusion protein VSV G protein crystal structures. (A-C) The pre-fusion states are on the left and post-fusion states on the right. Functional domains are identified by color. Adapted from White *et al* (145).

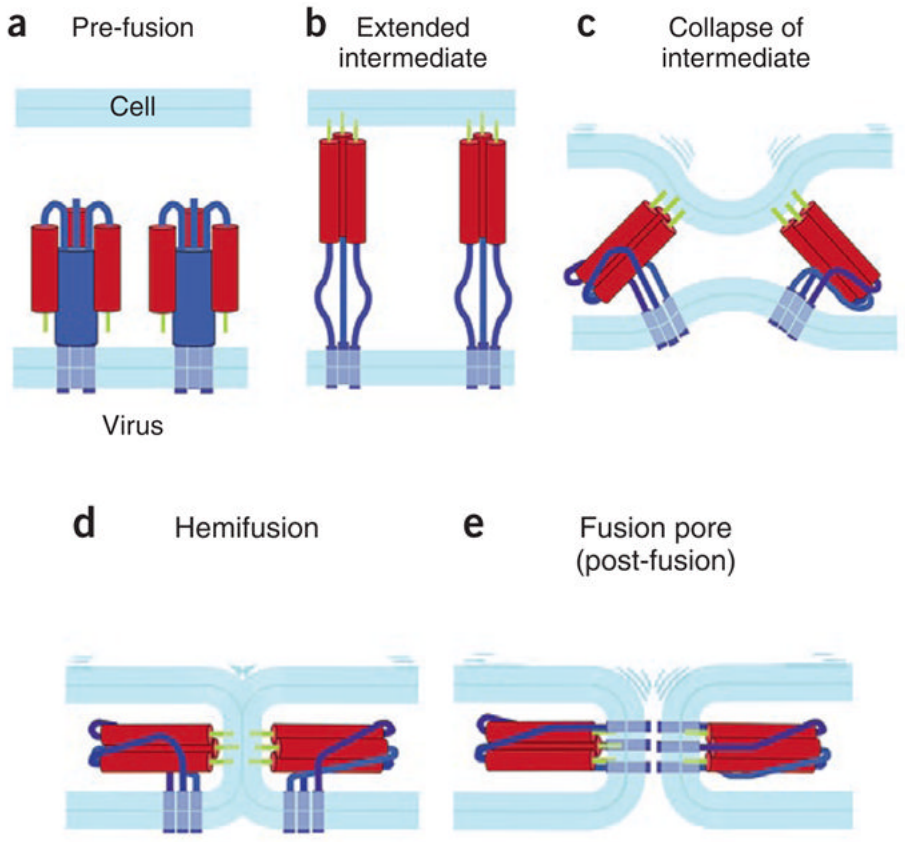

Figure I-3. Model of membrane fusion. (A-E) The proposed sequence of events of membrane fusion mediated by viral fusion proteins. Class I, II, III fusion proteins are thought to all follow this similar general series of steps to promote membrane fusion. Adapted from Harrison *et al* (51).

trimeric post-fusion form resulting in membrane fusion (145).

Viruses containing class I fusion proteins include paramyxoviruses, retrovirues, filovirues, coronaviruses, and orthomyxoviruses (17, 42, 75, 100). Influenza, a member of the Orthomyxoviridae family, contains the prototypical class I fusion protein, HA, which serves a model for the class. A 220 kDa homotrimer with both receptor binding and fusion activity, HA's pre-fusion form was the first crystallized fusion protein, and HA remains one of the best studied viral fusion proteins (Figure I-2A) (145, 146). HA consists of two disulfide-linked subunits, HA_1 and HA_2, derived by proteolytic cleavage of the HA_0 precursor. Cleavage of HA_0 occurs in the trans-golgi network (TGN) and HA_1 contains the receptor binding domain, while HA_2 forms the central α-helical coiled-coil region and contains the fusion active region with the heptad regions (HR1 and HR2) and the fusion peptide (51, 120). The placement of the receptor binding domain and the fusion functional domain on separate proteins is typical of class I fusion proteins.

Binding to the host ligand, sialic acid, through the HA_1 subunit leads to endocytosis of the influenza virion (120). Exposure to low pH following endocytosis induces irreversible conformational change in HA and release of the fusion peptide from its protected position allowing insertion into the target membrane. The pre-hairpin intermediate form the fusion peptide is inserted into the target membrane and the transmembrane domain anchors HA to the viral envelope. Now fusion protein spans the distance between the viral and target membranes (18, 145). Next, HA_2 folds back as the HR regions come together drawing the transmembrane domain and fusion peptide together with their associated viral and cellular membranes, respectively. In the final

post-fusion form HA has folded back on itself to form a trimer of hairpins with a long central trimeric alpha-helical core packed at the C-terminal region by three shorter helices, also referred to as the 6 helix bundle (6HB) (Figure I-2A) (27). Through conformation change this class I fusion protein has moved from a high energy metastable prefusion state to a more stable lower energy postfusion state and used the energy released to drive membrane fusion (51, 145).

Class II Fusion Proteins

The viral glycoproteins E1 of Semliki forest virus (SFV) and E protein of Tick-borne encephalitis virus (TBEV) are class II fusion proteins from Alphavirus and Flavivirus genera, respectively (Figure I-2B). These are small, enveloped, positive-sense RNAviruses with a nucleocapsid and a lipid bilayer containing the viral transmembrane (TM) proteins. SFV E1 and TBEV E protein class II glycoproteins have distinct primary sequences with little homology, but they have significant secondary and tertiary structural homology (67). Class II fusion proteins are thought to use a by a similar fold-back process as class I fusion proteins to bring the membranes together and facilitate fusion (145).

Several key factors distinguish SFV E1 protein and TBEV E protein from class II fusion proteins from class I fusion proteins informing the class separation (77). Class II fusion proteins are primarily composed of β-sheets with little α-helical content, have internal fusion loops at the tip of β-strands, are anti-parallel dimers lying flat on the virion surface in their pre-fusion form, and require a regulatory protein for proper folding

(67, 145). Class II proteins associate with a regulatory protein during post-translational processing. The regulatory protein may function to maintain the protein in its native metastable (67). Cotranslation with a regulatory protein in class II fusion proteins differentiates them from class I fusion proteins that do not associate with a regulatory protein in this way.

SFV fusion protein E1 is cotranslationally expressed with regulatory protein p62. After insertion into the endoplasmic reticulum the p62-E1 complex folds and continues transport along the secretory pathway toward the plasma membrane (67). Late in the secretory pathway the p62 is cleaved by the cellular protease furin. Furin cleavage of p62 is a critical regulator step and produces an E2 transmembrane protein that remains stably associated with the p62/E1 dimer (68). E2 contains the receptor binding domain and shields the internal fusion loops on E1 from premature exposure. Each SFV virion buds from the plasma membrane covered with 80 trimers of E2/E1 heterodimers laying flat on the surface with T=4 icosahedral symmetry (46, 68, 114, 145).

SFV and TBEV both undergo receptor-mediated endocytosis and require a low pH to trigger fusion. As the pH decreases SFV E2/E1 dimer undergoes a conformational change allowing exposure of the E1fusion loop and its insert into the target membrane(67). This conformational change also results reorganization of E1 into trimmers, which are necessary for hairpin formation and fold-back leading to membrane fusion and a trimeric post-fusion structure.

Class III Fusion Proteins

Class III fusion proteins were initially characterized through the surprising structural homology between vesicular stomatitis virus (VSV) glycoprotein G and HSV-1 glycoprotein B, which contain no sequence homology and are a negative-stranded RNA virus and a DNA virus, respectively (56, 111). VSV is a member of the Rhabdoviridae family, while HSV represents the large Herpesviridae family (39). The VSV G structure has been resolved at neutral and low pH providing a picture of the pre-fusion and post-fusion structures (Figure I-2C) (111, 113). Analysis of these structures revealed characteristics found in both class I and class II fusion proteins, but an overall structural organization that was different than any previously described fusion protein (110). The resolved structures showed that VSV G fusion proteins are trimeric pre-fusion and post-fusion like a class I fusion protein and contain central α-helical structural elements. Class III fusion proteins also contain β-sheets and have internal fusion loops, both important secondary structural motifs of class II fusion proteins (111). Importantly, class III fusion proteins appear to use conformational changes to power the formation of a hairpin structure that pull the viral and target membranes together in a similar manner as both class I and II fusion proteins indicating a common overall framework for achieving membrane fusion.

Comparison of HSV-1 gB structure and VSV G post-fusion structure reveals similar folds and, likely, a common evolutionary origin not evident in primary sequence comparison (56, 111, 127). Other class III fusion proteins identified based on structural homology to VSV G include Epstein-Barr virus (EBV) gB and baculovirus gp64 (9, 66). In comparison to VSV G where both pre-fusion and post-fusion structures have been

resolved, the gBs and gp64 are presumed to be post-fusion conformations. They are homotrimeric with a long central coiled-coil like class I, and internal bipartite fusion loops similar to the single fusion loop in a class II fusion protein (117).

VSV is a small, negative sense, enveloped RNA virus with a bullet shaped morphology resembling other Rhabdoviruses, such as rabies virus (39). VSV has been widely used as a model system due to its broad cell tropism, one of the broadest of any enveloped virus, and the ability to grow large quantities of virus at high titers (39, 74). Many aspects of this bullet shaped rhabdovirus, from entry and fusion to replication and assembly, are well characterized (39). VSV is a virus of economic concern for the livestock industry causing significant morbidity, but its extensive study is largely due to its tractability in experimental systems.

The VSV receptor remains unidentified, but may aspects of its entry have been well-characterized biochemically and through structural analysis. The VSV envelope is covered with a single protein, the 495 amino acid, type I transmembrane protein spikes know as glycoprotein (G), which functions in both attachment and entry (30). Following receptor binding VSV is taken into endocytic pathway of target cells by clathrin-mediated endocytosis (65). Exposure to acidic pH of the endsome induces significant conformational changes in VSV G resulting in fusion and ultimately nucleocapsid release (111, 113).

Earlier biochemical analysis identified three conformational states in G; prefusion, activated hydrophobic, and post-fusion (44, 110). The post-fusion state was recognized as antigenically distinct from the first two, and a shift toward the post-fusion

state observed upon exposure to low pH. Interestingly, these antigenic changes observed in G at low pH were reversible upon return to neutral pH, a property not observed in class I and class II fusion proteins (43, 112).

As described above, the pre-fusion and post-fusion VSV G ectodomain structures have been resolved (Figure I-2C), and were identified along with HSV-1 gB to represent a new class of fusion proteins, class III (56, 111, 113). To mediate viral entry into cells VSV G and baculovirus gp64 are sufficient, and serve the attachment, receptor binding, and fusion functions without the need for other viral proteins (14, 110, 150). HSV gB is not sufficient to mediate fusion on its own even through its structure resembles post-fusion VSV G. HSV requires three other proteins, gD and gH/gL heterodimer, along with gB for successful entry and fusion. (105).

Herpesvirus entry

Herpesviruses encompass a large family of enveloped viruses with a conserved fusion mechanism. Nine human herpesviruses have been characterized, and in excess of 130 herpesviruses have been identified in all species (39). They are dispersed across the three subfamilies; alpha-, beta-, and gammaherpesviruses. The alphaviruses are HSV types 1 and type 2 (HSV-1 and HSV-2) and varicella-zoster virus (VZV). The betaherpesviruses include cytomegalovirus (CMV) and human herpesviruses 6A, 6B, and 7 (HHV-6A, HHV-6B and HHV-7). The two gammaherpesviruses are Epstein-Barr virus (EBV) and Kaposi' sarcoma herpesvirus (KSHV) also known as human herpesvirus 8 (HHV-8) (55). Across all herpesvirses entry and fusion is mediated by homologs of

three highly conserved proteins, gB and gH/gL (Figure I-4). In addition to these conserved entry proteins a receptor binding protein is necessary, and a wide variety are used throughout the Herpesviridae (Figure I-4). HSV and its entry requirements are further evaluated below.

HSV entry has historically been reported to occur at the plasma membrane by direct fusion as seen in Vero cells (Figure I-5A) (147). Entry through the endosomal pathway has also been reported, under both neutral and acidic conditions (99). Interestingly, the mode of entry varies by cell type, but in all cases gD and the core fusion machinery gH/L and gB are necessary. Entry through the endocytic pathway seems to predominate in HeLa, CHO-K1 expressing gD-receptor nectin-1, and primary human keratinocytes, and requires acidification for successful fusion (Figure I-5B) (99). B78H1 mouse melanoma cells expressing gD receptor nectin-1 are reported to use the endocytic pathway for entry but without a requirement for low pH as seen in the cell types above (Figure I-5C) (92). HSV's ability to infect a wide variety of cell types may be a function of the multiple receptors it can bind to initiate successful entry, and this variety may contribute to the varied entry pathways.

HSV employs four glycoproteins proteins in a complex entry mechanism, and each is required for successful entry. These four proteins are gD, gH, gL, and gB (Figure I-6). Glycoprotein D (gD) is the receptor binding protein for HSV and has three known cellular receptors, which are herpes virus entry mediator (HVEM), nectin-1, and 3-OS-modified heparan sulfate moieties (121). The core herpes fusion machinery includes gH/gL heterodimer and gB, which are highly conserved throughout all herpesviruses.

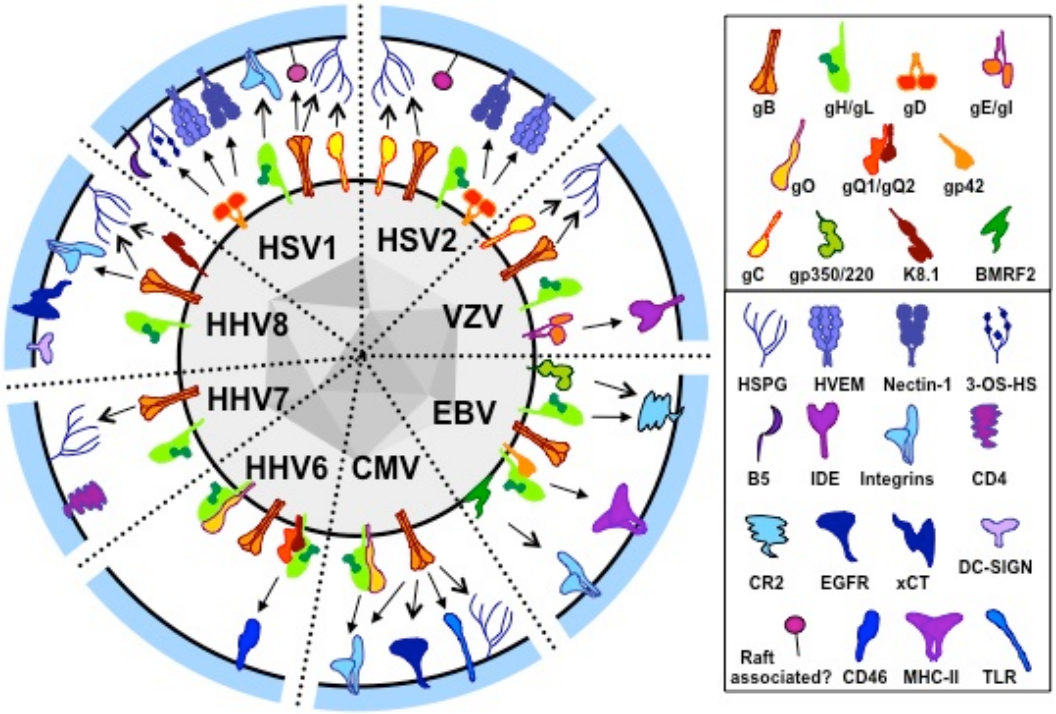

Figure I-4. Entry proteins of human herpesviruses. All eight human herpesviruses require gB and gH/L for entry. Recepter binding is performed by gD in the alphaherpesviruses except for VZV, which uses gE. Betaherpeseviruses and gammaherpesvirues bind receptor(s) using gB, gH/gL, or an accessory protein. Adapted from Heldwein and Krummenacher (55).

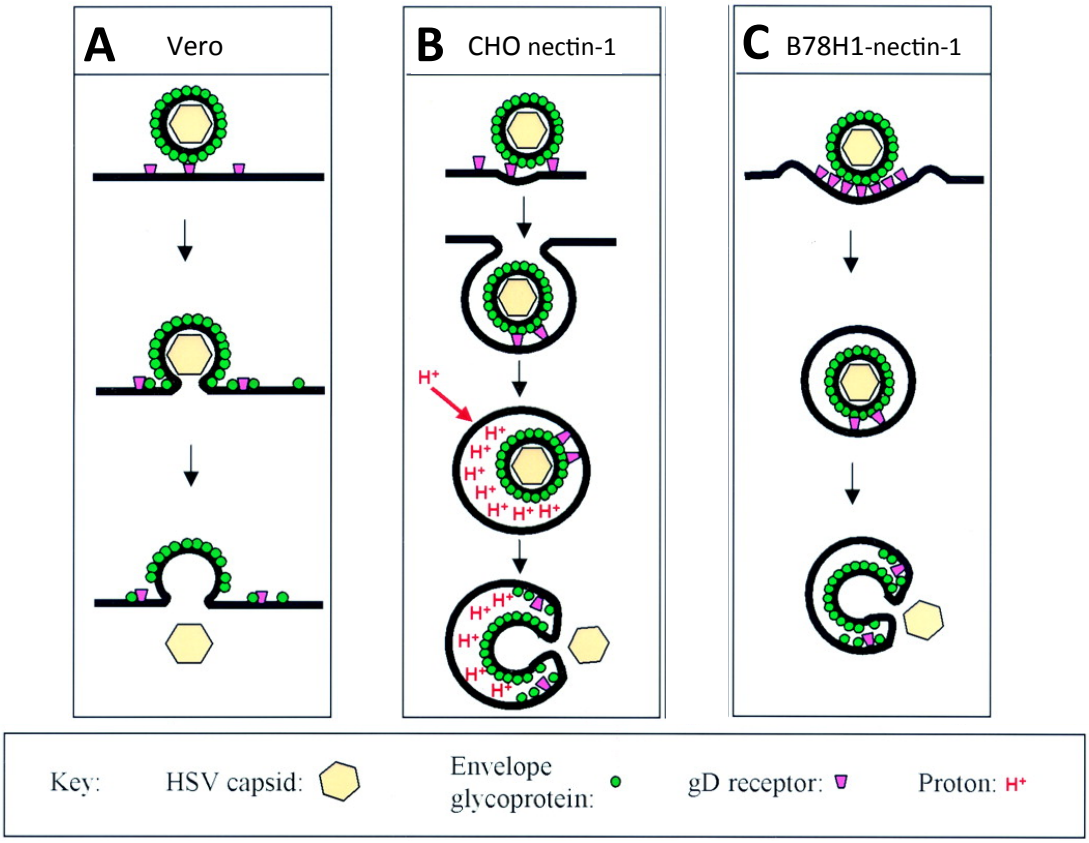

Figure I-5. Routes of HSV entry. (A) Entry into Vero cells occurs at the plasma membrane and is pH-independent. (B) HSV enters CHO-nectin-1 expressing cells by pH-dependent endocytosis, but cannot enter CHO cells without nectin-1. (C) Like CHO cells, B78 cells require a transformation with a gD receptor. Here B78 cells are transfected with nectin-1. Entry into these cells is by pH-independent endocytosis. Adapted from Milne *et al* (92).

Importantly, the four glycoproteins (gD, gH/gL, gB) and a receptor (HVEM or nectin-1) are necessary and sufficient to complete cell fusion (4, 138).

gC

Glycoprotein C (gC) is a nonessential glycoprotein that plays a role to aid entry by binding heparin sulfate proteoglycans (HSPG) fostering virus-cell attachment (55). Initial viral attachment occurs through the non-essential glycoprotein gC and independently through gB by binding heparan sulfate proteoglycans (HSPG) (12, 123). Cells deficient in proteoglycan synthesis have a significant reduction in viral infection, but remain permissive to HSV indicating HSPG is not essential for infection (10). Additionally, gC mutant HSV virions remain infectious, albeit at a lower level, while gB null virions are non-infectious (21, 57). These data support that gC and HSPG binding are nonessential for HSV entry, while gB is essential. gB, the focus of this thesis, will be discussed further in later sections.

gD

HSV-1 gD, the receptor binding protein, binds one of three cellular ligands, and plays an important role in virus tropism. gD is a 369 amino acid type 1 membrane protein with a immunoglobulin V-like fold at its core as seen by its crystal structure. N- and C- terminal extension wrap around the core, and gD is thought to form a homodimer on the virion surface (Figure I-6). Understanding of gD binding to its main cellular ligands, HVEM or nectin-1, has been significantly advanced by successful crystallization

of gD in complex with each ligand (24, 31). Glycoprotein D binding with its receptors is essential for viral entry, and data supports that this binding transmits a single downstream that allows gH/gL and gB to complete fusion with the cell membrane. *In vivo* both gD receptors, HVEM and nectin-1, seem to be relevant for continued infection. Patient isolated virus samples retain the ability to use either receptor no matter the location of the lesion from which virus was collected (70).

HVEM is a tumor necrosis factor-like receptor found in the greatest abundance on T cells (Figure I-6). HVEM is widely expressed, but is found at high levels in the spleen, thymus, lungs, B cells, monocytes, and T cells (72). For HSV entry HVEM is a functional receptor in in activated T cells, oral epithelial cells, and corneal fibroblasts (61, 97, 134). HVEM has several natural ligands providing stimulatory signals (LIGHT, lymphotoxin alpha) and inhibitory signals (BTLA and CD160) that together modulate the immune response (47, 52, 87, 116). Interestingly, HSV does not replicate successfully in T cells (128). This provides the intriguing possibility that gD-HVEM interactions may modulate the host immune response, possibly aiding virus replication and latency.

Nectin-1, a cell adhesion molecule located at adhesion junctions, is found at sites distinct from HVEM, and is abundant on epithelial cells, fibroblasts, and on neurons (94, 97, 130). Nectin-1 and its family members (nectin-2, -3, -4) contain three Ig-like domains, a transmembrane domain, and cytoplasmic tail (Figure I-6). Nectin-1 acts as a receptor for HSV-1 and HSV-2, and is the primary receptor on epithelial cells and neurons (61, 119). Nectin-1 is also a receptor for pseudorabies virus (PRV) and bovine herpesvirus type-1 (BHV-1), both alphaviruses like HSV (45).

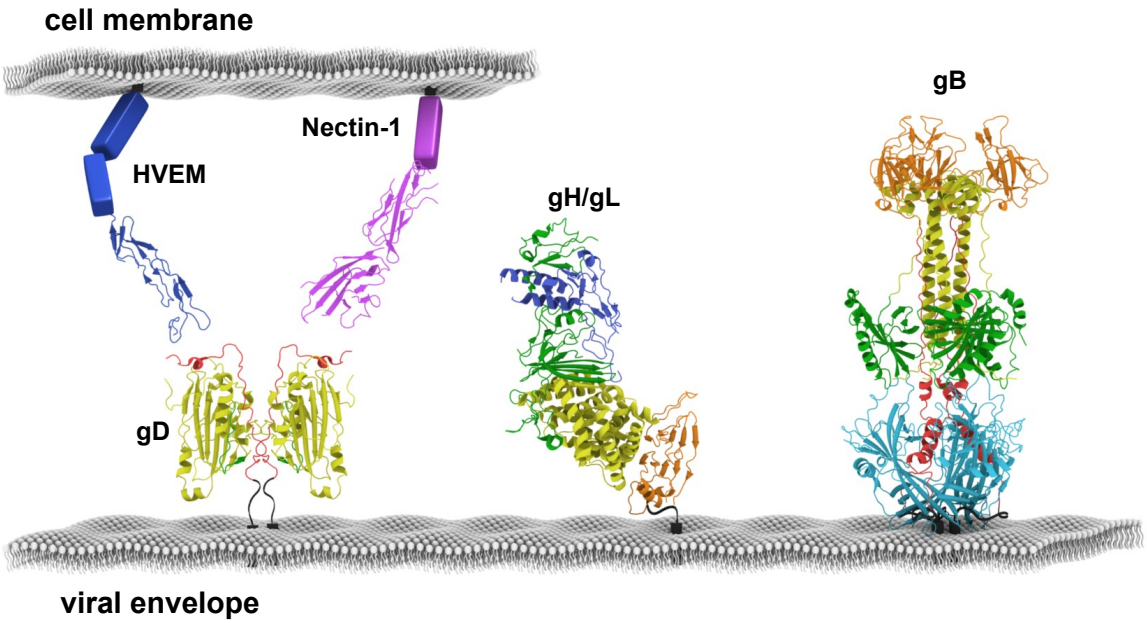

Figure I-6. Proteins required for HSV entry. Four essential glycoproteins (gB, gD, and gH/gL) are required for HSV entry. gD interacts with one of the key cellular receptors, HVEM or nectin-1. The crystal structures of each glycoprotein and receptor are depicted. Adapted from Eisenberg *et al* (36).

The third gD receptor, heparan sulfate proteoglycans (HSPG) are carbohydrate chains covalently linked to proteins. HSPGs are secreted into the extracellular matrix or are cell associate. They are expressed ubiquitously on mammalian cells and interact with growth factors, cytokines, chemokine, and morphogens. HSPGs have a wide variety of important functions in development, morphogenesis, cell adhesion, and hemostasis (37). HSPGs are made of a core protein and one or more linear polysaccharide, or glycosaminoglycan (GAG), chain covalently attached in the ER. The HS undergo a series of processing reactions in the Golgi to deacetylate, sulphonate, and otherwise modify the chains for its specific role and location (13).

3-O-sulfated heparan sulfate (3-OS-HS) only functions as a receptor for HSV-1. 3-OS-HS binds gD in several cell lines (HeLa, Vero), and is an important receptor for primary corneal fibroblast infection (118) (101, 133).

gH/gL

The gH/gL heterodimer is a part of the core herpesvirus fusion machinery and is highly conserved. HSV-1 gH is a 838 amino acid with a large ectodomain and membrane anchor, while gL is 224 amino acids protein without a transmembrane segment (26). The heterodimer requires formation of the 1:1 gH/gL complex where gL functions as a chaperone essential for proper processing and trafficking of gH (103). gH/gL is a major target for HSV neutralizing antibodies supporting its importance in the entry process (103). Several studies have suggested gH/gL may have fusogenic properties due to identification of fusion activity of gH derived synthetic peptides and the predicted

presence of heptad repeat regions in gH (40, 41). Recently, the gH/gL crystal structure was solved for HSV-2 as well as EBV and a fragment of PRV gH, and had no structural homology to a known fusion protein. Additionally, the predicted heptad repeat region formed helices excluding a role in fusion (Chowndary 2010)(6, 86). An interaction necessary for cell-cell fusion was identified between gH/gL and gB using bimolecular complementation (4, 5). Additionally, gH/gL and gB cofloatation with liposomes was observed at low pH (22). These data support the idea that interaction between gH/gL is necessary for fusion.

HSV glycoprotein B

Glycoprotein B is the most highly conserved herpesvirus entry proteins protein. gB is 904 amino acid protein produced from a 934 amino acid polypeptide with the 30 amino acid signal sequence cleaved during the maturation process (Figure I-7). gB contains a 697 amino acid ectodomain, a 68 amino acid membrane proximal and transmembrane domain, and a 109 amino acid cytoplasmic domain. The membrane proximal and transmembrane region spans amino acids 731-794, and contains three hydrophobic domains. Residues 731-773 contain the two hydrophobic domains and are named the membrane proximal region (MPR). The third hydrophobic region represents the transmembrane domain anchoring gB to the viral membrane (108).

gB is structurally homologous to VSV G and baculovirus gp64, but does not share sequence homology with these fusion proteins (56, 66, 111). This structural homology identified gB as a class III fusion protein. gB is trimeric with two fusion loops per

protomer, β-sheets, PH domain, and a long central α-helices (56). gB was suspected to have fusion activity before the structure was resolved due several pieces of data. In the early studies of HSV a syncytial phenotype was observed, and the genotype was localized to point and truncation mutants in gB (20, 132). Mutational analysis of the putative fusion loop region through point mutants and linker insertions identified mutations that altered gB's ability to mediate cell-cell fusion (49, 50, 82). Point mutations in the putative gB fusion loops (W174, Y179, H263, R264) decreased or completely abrogated the ability of soluble gB (730t) to associate with liposomes (49). These data further support a role for gB in fusion and entry.

Detailed analysis of the gB crystal structure identified five distinct structural domains in the 85Åx80Åx160Å elongated trimer, which resembles the size and shape of spikes observed on HSV-1 virions by electron microcopy (56, 125). The crystallized construct contained HSV-1 residues 133 to 730, and was produced in a baculovirus expression system as a soluble protein (Figure I-7). The soluble protein was then purified by immunoaffinity chromatography and named gB730t. The resulting trimeric structure contains three protomers, each with five domains. Domain I (residue 153 to 363) forms the base and contains a PH-like domain and a β-sandwich made of 2 β-sheets. PH domains facilitate phosphoinositol binding and protein-protein interactions, which may be important for gB function (76). Importantly, the two proposed fusion loops occupy the folds in two adjacent β-strands of each protomer and project toward the membrane (56). The specific properties of gB fusion loops will be discussed in a later section.

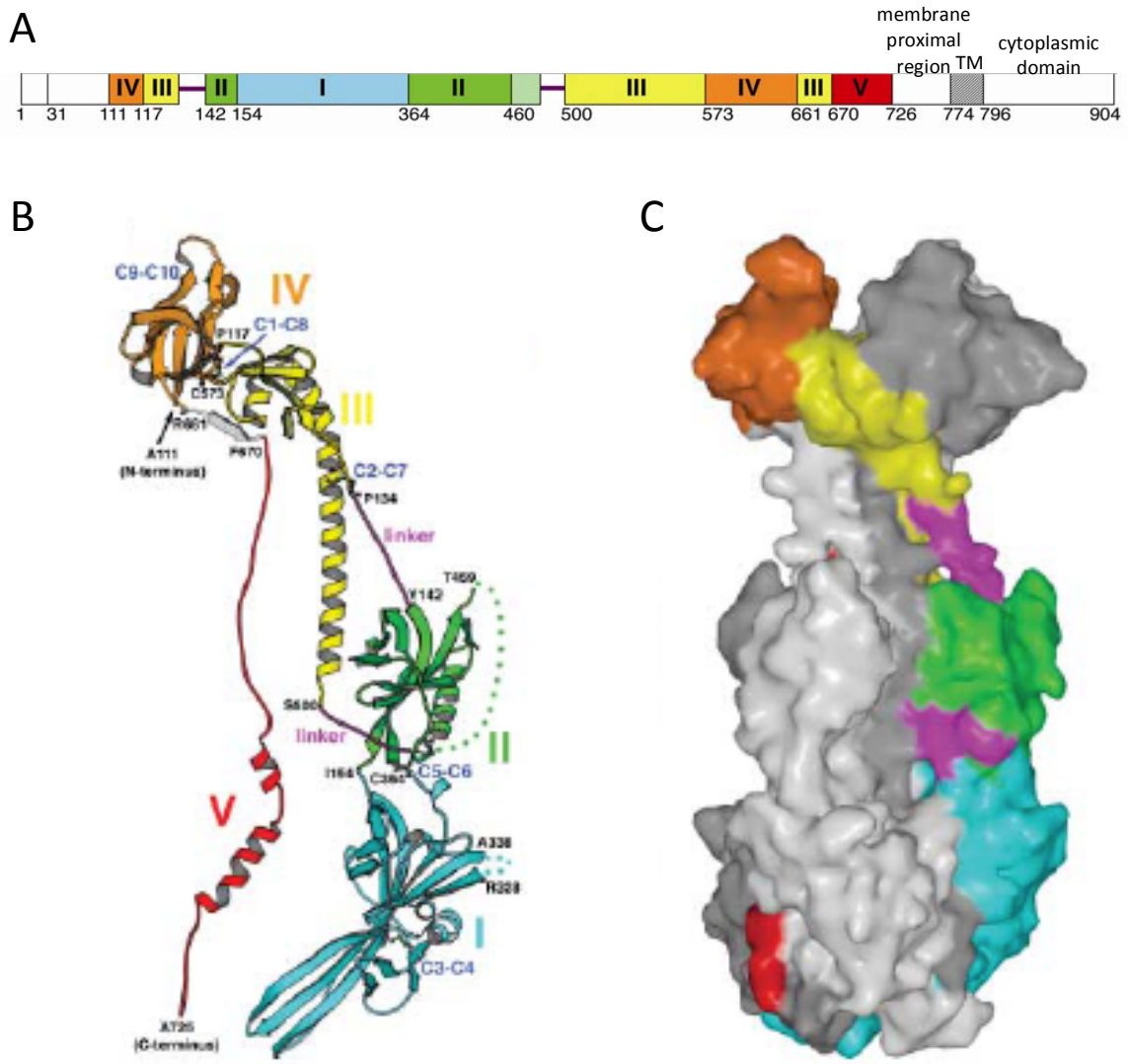

Figure I-7. Structure of HSV gB. (A) domain architecture of gB. Domains are highlighted in different colors with their first residue position shown. (B) Ribbon diagram of a single gB protomer with domains labeled and colored identically to (A). (C) Surface representation of gB trimer with domains of one protomer colored according to (A). Adapted from Heldwein *et al* (56).

Domain II is formed by two discontinuous segments and forms another PH-like domain. Domain III is made of 3 discontinuous segments and contains a long α-helix that with the adjacent protomers forms the central coiled-coil of gB with many essential trimer contacts (56). Domain III bears a strong similarity to the central coil-coiled in class I fusion proteins.

Domain IV, the crown, is also formed by two discontinuous segments that are linked by a disulfide bond forming a globular structure at the top of the structure (56). No structural relatives have been described for this region. Notably, several neutralizing monoclonal antibodies have been mapped to similar surface epitopes suggesting domain IV is exposed on the virion surface (56, 58).

Domain V is a long extension (residues 670 to 725) stretching from the top to the bottom of gB. This long extension fits in the groove between the other two protomers, but has no contact with any other portion of its own protomer. These interactions may help stabilize the trimer. The crystallized structure ends at amino acid 725, leaving the remaining C-terminal portion of the ectodomain, the transmembrane domain, and the cytoplasmic domain unresolved. The missing ectodomain contains the hydrophobic MPR (residues 731-773) that was removed from the soluble gB construct used for crystallization due to its hydrophobic character (56). Chapter II will focus on investigating what role the MPR plays in gB fusion.

The available evidence suggests that the HSV gB structure is the post-fusion form due to similarities with the extended post-fusion VSV G. In the future examination of a second, presumably pre-fusion gB structure would provide evidence that the current

structure is the post-fusion form (111). Several studies report conformational changes in gB when exposed to low pH (22, 34). Analysis of a low pH structure of gB detected a major shift in the position of fusion loop 2, but no global pH-dependent changes in the fusion protein were noted. This fusion loop 2 shift is hypothesized to be important for endocytic entry of HSV, but the observed changes are not the global rearrangements one would anticipate for the pre-fusion form (124). Antigenic changes detected in soluble gB at low pH caused a change in the oligomeric structure toward the monomeric state. Upon return to a neutral pH these changes were reversible (34). Reversibility from pre-fusion to post-fusion is a key characteristic of VSV G and class III fusion proteins, and it appears gB has a reversible component to its conformational changes due to pH. Significantly, the conformational changes detected in gB antigenically and by crystal structure do not appear as profound as those observed for VSV G (110, 111). Using structural data to develop a model of the gB pre-fusion structure and its transition to post-fusion provides detailed analysis of fusion protein. Until a pre-fusion structure is solved a variety of techniques including targeted mutations, antigenic analysis, and lipid binding assays are used to continue to dissect gB's role in HSV entry and fusion.

Using the presumed post-fusion structure of gB, and the homologous VSV G structural data, targeted mutagenesis was used to evaluate the proposed HSV fusion loops. The two HSV gB fusion loops (FL), aa 173 to 179 and 258 to 265, in domain I were mutated at structurally significant residues. Mutation of gB FL residues W174, Y179, and A261 resulted in loss cell-cell of fusion, and mutations at W174, Y179, H263, R264 led to impairment or loss of liposome association (49, 50). The availability of the

crystal structure allowed characterization of regions important for viral fusion and infection led to a functional map of the gB structure as described below.

gB Functional Regions

Mapping functional regions (FRs) using neutralizing antibodies is a common way to identify important regions. Numerous studies have used monoclonal antibodies to identify FRs of gB (3, 49, 50, 82, 104). Careful characterization of a 67 monoclonal antibody panel to HSV gB identified eleven neutralizing antibodies and facilitated the identification of functional regions. An overlapping peptide panel was used to identify epitopes and then the epitopes were mapped onto the HSV-1 gB ectodomain structure identifying four FRs (11). The four FRs are spread over the entire ectodomain with some spanning multiple structural domains (Figure I-8).

FR1 includes the domains I and V, contains the putative fusion loops, and is recognized by several neutralizing monoclonal antibodies. Monoclonal antibody SS55 was mapped to domain I, and is a potent neutralizer. Another FR1 virus neutralizing antibody, SS144, mapped to the long α-helix of domain V near the carboxy-terminus of the gB crystal structure (11). Interestingly, both SS55 and SS144 block soluble gB(730t) from associating with liposomes in a coflotation assay (49). The presence of the putative fusion loops, multiple neutralizing antibodies, and the disruption of liposome association strongly suggests FR1 is important for virus entry and fusion.

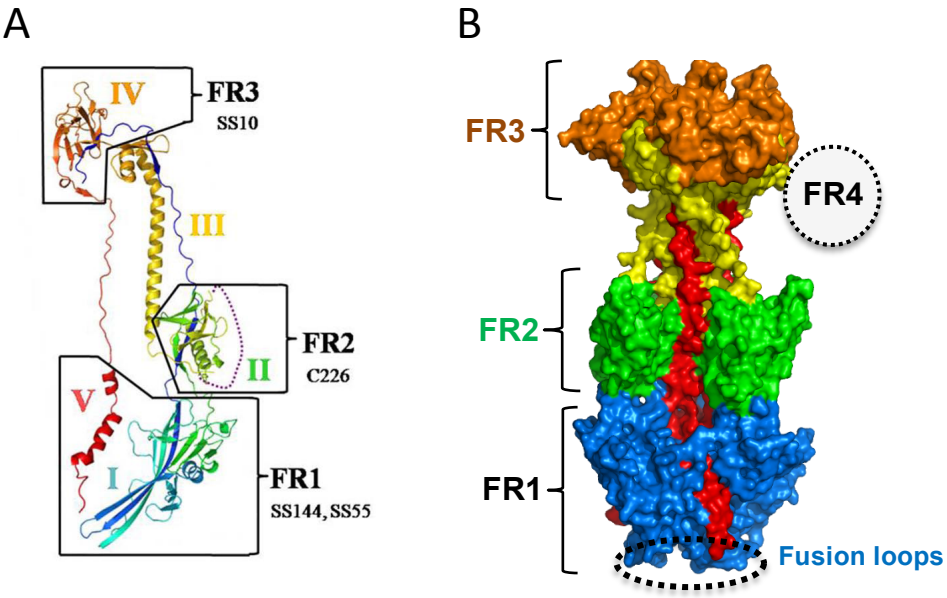

Figure I-8. gB functional regions. HSV gB FRs are defined by the epitopes of neutralizing MAbs: SS55/SS106/SS144 (FR1, blue and red, fusion domain), C226/H1838/H1781 (FR2, green, gH/gL interaction domain), SS10/SS67-69 (FR3, orange, receptor-binding domain). The epitope of MAb H1817 (FR4, dotted circle) maps to the unresolved N-terminus. (A) Ribbon diagram of gB protomer with functional regions outlined in black. Representative monoclonal antibodies used to define these regions are listed. (B) Space filling model of gB trimer with functional regions labeled. The fusion loops are indicated at the bottom of the structure. Adapted from Hannah et al and Eisenberg et al (36, 49).

FR2 is on the outer surface of domain II, and represented by C226 neutralizing antibody. C226 type-common recognizing both gB1 and gB2, and identifies domain II as critical to HSV entry. FR3 encompasses residues located in domain III and domain IV includes the epitope of neutralizing antibody SS10. The SS10 epitope includes residues 640-670, which are highly conserved among herpesviruses (56). This epitope is in domain IV at the top or crown of the structure opposite the viral membrane in the presumed post-fusion structure. Interestingly, SS10 blocks soluble gB's ability to bind to cells, but does not interfere with gB liposome association (11, 49). FR4 is formed by a region of the gB N-terminus that was not solved in the crystal structure, and contains the gB heparin sulfate binding region (11, 12).

Membrane Proximal Region

The membrane proximal region (MPR) is a portion of the ectodomain adjacent to the transmembrane domain of viral fusion proteins. The MPRs of viral fusion proteins all show an abundance of hydrophobic and aromatic residues (W, Y, F), and thus have high hydrophobic character. In contrast, the number and spacing of these aromatic residues vary with each fusion protein (7) (29). Mutations in the MPR of multiple fusion proteins including HIV1 gp41 (115), HPIV 2 F protein (136), SV5 F protein (151), VSV glycoprotein G (63, 64), baculovirus gp64 (79), and HSV gB (82) indicate they play important roles in the regulation of membrane fusion. It is thought that the aromatic and hydrophobic properties of MPRs indicate a function in bridging the gap at the lipid interface between aqueous and hydrophobic environments (7, 69).

The seventeen residue membrane proximal region of HIV-1 gp41 is known as the membrane proximal external region (MPER), and is involved in virion assembly and infection (115). The structure of this tryptophan rich region of gp41 was recently solved. The MPER crystal structure places three aromatic side chains per monomer facing towards the membrane on a non-classical coiled-coil structure (19). These aromatic residues are positioned for membrane insertion and data supports the notion that gp41 MPER structural motif aids the generation of viral membrane curvature and ultimately fusion (19). The deletion of seventeen residues of the MPER or mutation of five conserved tryptophan residues to alanine abolished cell-cell fusion. Single tryptophan mutations resulted in decreased infectivity (115). Interestingly, the epitope for a broadly neutralizing antibody, 2F5, is located in the MPER highlighting the importance of this structure in infection (60).

The twelve residue membrane-proximal region of the human parainfluenza virus type 2 (HPIV2) F protein, is necessary for fusion activity but not surface expression (136). Importantly, three residues (N475, F476, and F477) were identified to be critical for cell fusion activity, and when singly mutated to alanine F protein was unable to mediate hemifusion. The inability of the F protein MPR mutants to initiate hemifusion indicates the MPR is involved in lipid mixing (136).

The SFV class II fusion protein E1 has a MPR that is thought to play a role in the conformational change during fusion. Although structural data is unavailable, site-directed antigenic analysis revealed that at neutral pH epitopes on the MPR are unavailable. Upon low pH triggering and E2/E1 heterodimer dissociation the MPR

became accessible to antibodies (81). In the post-fusion conformation the MPR again became inaccessible and appears to pack on the trimer core aiding hairpin formation. After further conformational change during hairpin formation the MPR epitopes again became inaccessible (80, 81). Interestingly, neither E1 protein MPRs conserved length nor any specific residue was required for membrane fusion, but large insertions or deletions do decrease fusion (80).

The 42 amino acid VSV glycoprotein G MPR is absent from the solved crystal structures of VSV G, but significant mutational analysis has been performed on the region to inform its function (7). A significant degree of sequence homology exists between the C-terminal regions of the vesciculoviruses suggesting a functional role for this region. The MPR is hypothesized to stretch from the crown to the TMD in the VSV G post-fusion structure (111). One hypothesized role for the MPR is as a flexible tether to position VSV G properly between the viral and cellular membrane (110). Additionally, there are mutation of conserved aromatic residues (W and F) singly or together had little effect on cell-cell fusion. This is in contrast to tryptophan residues that have been shown to be important in HIV-1 gp41 MPR fusion activity (63, 115). Further mutational analysis identified significant reduction in cell-cell fusion and infectivity when 13 residues (N449 to W461) of the MPR were deleted. Insertions also decreased fusion activity and infectivity (63). These studies strongly support a role for the VSV G in membrane fusion, but its specific function remains elusive.

Although the transmembrane domain and MPR are not included in the resolved structures of pre- and post-fusion VSV glycoprotein G the fusion loops are mapped and

the structure suggests they are in close proximity to the transmembrane region (111, 113). One interpretation of these observations is that the MPRs simply functions as a flexible tether from the transmembrane domain and allows the proper alignment of the fusion protein with the membrane required for fusion to proceed (110). Alternatively, as suggested above the MPR may play a role at the lipid interface to assist destabilizing of membranes and promote lipid mixing (64, 129). Others have hypothesized a role for the MPR to regulate fusion more directly, for example in HSV-1 gB the fusion loops may be masked by the hydrophobic MPR preventing premature exposure to membrane (50).

As outlined above the MPRs of both class I and class II fusion proteins play a role in cell-cell fusion. The lack of structural data for most MPRs limits our understanding of the specific role the MPR plays in fusion. The MPR of class III VSV G is also important for successful viral membrane fusion, but specific residues, such as tryptophan like gp41 have not been identified as critical to function. Analysis of HSV gB MPR, also excluded from the crystal structure, may provide insight into gB specifically and class III fusion proteins generally.

Structural data is not available for HSV gB MPR since the crystallized construct was truncated just prior to the MPR at residue 730 (56). Exclusion of the MPR (731-773) was due to the negative effect a highly hydrophobic region like the MPR can have on the ability to crystal the protein (Figure I-9). Although there is no available structure of a class III fusion protein MPR several studies have assessed its functional importance in herpesvirus gB. While mutations in the HIV1 gp41 and VSV G MPRs do not disrupt their expression and folding, the herpesvirus gB MPR appears sensitive to mutation

resulting in defective protein folding and decreased cell surface expression (63, 82, 108, 115, 142, 149). Misfolding and low surface expression of mutants made it difficult to assess the gB MPRs functional role. However, the few HSV gB MPR mutants that are expressed on the cell surface are impaired in cell-cell fusion or virus entry (82, 142). Generally, it is thought that in the pre-fusion form a fusion protein must mask its fusion loops to prevent premature virus activation or interactions that would result in decreased virus infectivity. In the post-fusion structure of HSV gB the fusion loops are not masked by another portion of the solved structure, which does not include the MPR (56). In contrast the fusion peptides of class I are protected within the trimer interface and fusion loops of class II proteins are masked at the dimer interface (96, 145). Hannah et al. (50) proposed that due to its hydrophobic nature the HSV1 gB MPR could mask the hydrophobic fusion loops in the pre-fusion state. Interestingly, purified EBV gB truncated to remove the C-terminus including the MPR self-associated forming rosettes visible on electron microscopy (8). This association, presumably through the hydrophobic fusion loops, supports the speculation that masking of these hydrophobic fusion loops may prevent self-association or premature inactivation of fusion proteins.

Aims of present work

Each protomer of the gB trimer includes two fusion loops (a.a. 173-179 and 258-265) and a MPR (a.a. 731-773) (20, 49, 50, 56, 102, 108). The goal of my dissertation has been to further define the role the gB fusion loops and MPR play in HSV membrane fusion and its regulation. The construct used for gB crystallization lacked

A

730-AMFAGLGAFFEGMGDLGRAVGKVVMGIVGGVVSAVSGVSSFMSN-773

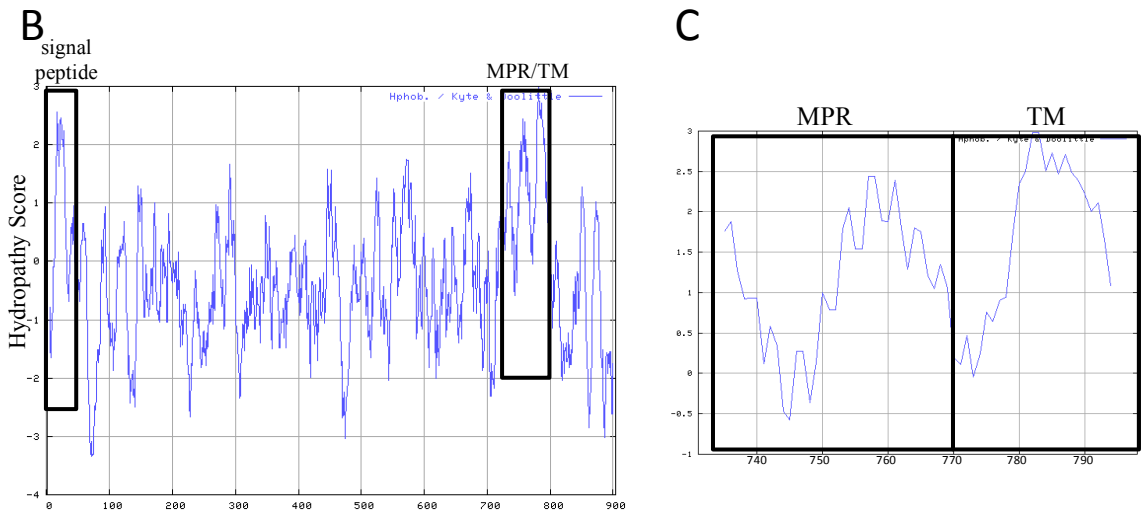

Figure I-9. gB membrane proximal region. (A) The amino acid sequence of the HSV gB membrane proximal region (MPR). (B) Kyte-Doolittle hydropathy plot of gB sequence. The signal sequence in demarcated by a box at the amino terminus of gB. The putative MPR and TM domains are marked by black box. A positive peak greater then 1.6 indicates a high hydrophobicity score. (C) An expanded view of MPR/TM boxed region in (B) showing a high hydrophobicity score. Web based Kyte-Doolittle calculator web.expasy.org/protscale/ and Kyte and Doolittle (73).

the MPR and the putative fusion loops were exposed with no mechanism to prevent premature membrane interactions (56).

The forty-three amino acid MPR has a highly hydrophobic character and this region was excluded from the crystalized gB construct due to its potential to decrease the probability of successful crystal formation. In the second chapter of this dissertation various gB MPR deletion and truncation mutants were constructed. The deletion mutants, expressed in mammalian cells in a full-length gB background, were not efficiently expressed on the cell surface. Next recombinant baculovirus expressed C-terminal gB MPR truncations were assayed for their membrane binding ability. I found that despite the presence of fusion loops, purified soluble gB containing as few as the first nine MPR residues (gB739t) was deficient in the ability to bind liposomes. In comparison, gB(730t) lacking the entire MPR has been shown to bind liposomes (49). Remarkably, mutation of two aromatic residues to alanine in the short nine amino acid MPR was sufficient to restore the liposome binding ability of the soluble gB protein (117). Together, these data suggest an important interaction within FR1 involving the MPR that regulates liposome binding.

REFERENCES

1. **Agosto, M. A., T. Ivanovic, and M. L. Nibert.** 2006. Mammalian reovirus, a nonfusogenic nonenveloped virus, forms size-selective pores in a model membrane. Proc Natl Acad Sci U S A **103:**16496-16501.
2. **Arnosti, D. N., C. M. Preston, M. Hagmann, W. Schaffner, R. G. Hope, G. Laughlan, and B. F. Luisi.** 1993. Specific transcriptional activation in vitro by the herpes simplex virus protein VP16. Nucleic Acids Res **21:**5570-5576.
3. **Atanasiu, D., W. T. Saw, G. H. Cohen, and R. J. Eisenberg.** 2010. Cascade of events governing cell-cell fusion induced by herpes simplex virus glycoproteins gD, gH/gL, and gB. J Virol **84:**12292-12299.
4. **Atanasiu, D., J. C. Whitbeck, T. M. Cairns, B. Reilly, G. H. Cohen, and R. J. Eisenberg.** 2007. Bimolecular complementation reveals that glycoproteins gB and gH/gL of herpes simplex virus interact with each other during cell fusion. Proc Natl Acad Sci U S A **104:**18718-18723.
5. **Atanasiu, D., J. C. Whitbeck, M. P. de Leon, H. Lou, B. P. Hannah, G. H. Cohen, and R. J. Eisenberg.** 2010. Bimolecular complementation defines functional regions of herpes simplex virus gB that are involved with gH/gL as a necessary step leading to cell fusion. J Virol **84:**3825-3834.
6. **Backovic, M., R. M. DuBois, J. J. Cockburn, A. J. Sharff, M. C. Vaney, H. Granzow, B. G. Klupp, G. Bricogne, T. C. Mettenleiter, and F. A. Rey.** 2010. Structure of a core fragment of glycoprotein H from pseudorabies virus in complex with antibody. Proc Natl Acad Sci U S A **107:**22635-22640.

7. **Backovic, M., and T. S. Jardetzky.** 2009. Class III viral membrane fusion proteins. Curr Opin Struct Biol **19:**189-196.

8. **Backovic, M., G. P. Leser, R. A. Lamb, R. Longnecker, and T. S. Jardetzky.** 2007. Characterization of EBV gB indicates properties of both class I and class II viral fusion proteins. Virology **368:**102-113.

9. **Backovic, M., R. Longnecker, and T. S. Jardetzky.** 2009. Structure of a trimeric variant of the Epstein-Barr virus glycoprotein B. Proc Natl Acad Sci U S A **106:**2880-2885.

10. **Banfield, B. W., Y. Leduc, L. Esford, K. Schubert, and F. Tufaro.** 1995. Sequential isolation of proteoglycan synthesis mutants by using herpes simplex virus as a selective agent: evidence for a proteoglycan-independent virus entry pathway. J Virol **69:**3290-3298.

11. **Bender, F. C., M. Samanta, E. E. Heldwein, M. P. de Leon, E. Bilman, H. Lou, J. C. Whitbeck, R. J. Eisenberg, and G. H. Cohen.** 2007. Antigenic and mutational analyses of herpes simplex virus glycoprotein B reveal four functional regions. J Virol **81:**3827-3841.

12. **Bender, F. C., J. C. Whitbeck, H. Lou, G. H. Cohen, and R. J. Eisenberg.** 2005. Herpes simplex virus glycoprotein B binds to cell surfaces independently of heparan sulfate and blocks virus entry. Journal of virology **79:**11588-11597.

13. **Bishop, J. R., M. Schuksz, and J. D. Esko.** 2007. Heparan sulphate proteoglycans fine-tune mammalian physiology. Nature **446:**1030-1037.

14. **Blissard, G. W., and J. R. Wenz.** 1992. Baculovirus gp64 envelope glycoprotein is sufficient to mediate pH-dependent membrane fusion. Journal of virology **66:**6829-6835.

15. **Bloom, D. C.** 2004. HSV LAT and neuronal survival. Int Rev Immunol **23:**187-198.

16. **Boehmer, P. E., and I. R. Lehman.** 1997. Herpes simplex virus DNA replication. Annu Rev Biochem **66:**347-384.

17. **Bosch, B. J., R. van der Zee, C. A. de Haan, and P. J. Rottier.** 2003. The coronavirus spike protein is a class I virus fusion protein: structural and functional characterization of the fusion core complex. Journal of virology **77:**8801-8811.

18. **Bullough, P. A., F. M. Hughson, J. J. Skehel, and D. C. Wiley.** 1994. Structure of influenza haemagglutinin at the pH of membrane fusion. Nature **371:**37-43.

19. **Buzon, V., G. Natrajan, D. Schibli, F. Campelo, M. M. Kozlov, and W. Weissenhorn.** 2010. Crystal structure of HIV-1 gp41 including both fusion peptide and membrane proximal external regions. PLoS Pathog **6:**e1000880.

20. **Bzik, D. J., B. A. Fox, N. A. DeLuca, and S. Person.** 1984. Nucleotide sequence specifying the glycoprotein gene, gB, of herpes simplex virus type 1. Virology **133:**301-314.

21. **Cai, W. Z., S. Person, C. DebRoy, and B. H. Gu.** 1988. Functional regions and structural features of the gB glycoprotein of herpes simplex virus type 1. An analysis of linker insertion mutants. J Mol Biol **201:**575-588.

22. **Cairns, T. M., J. C. Whitbeck, H. Lou, E. E. Heldwein, T. K. Chowdary, R. J. Eisenberg, and G. H. Cohen.** 2011. Capturing the herpes simplex virus core fusion complex (gB-gH/gL) in an acidic environment. J Virol.

23. **Campadelli-Fiume, G., and B. Roizman.** 2006. The egress of herpesviruses from cells: the unanswered questions. Journal of virology **80:**6716-6717; author replies 6717-6719.

24. **Carfi, A., S. H. Willis, J. C. Whitbeck, C. Krummenacher, G. H. Cohen, R. J. Eisenberg, and D. C. Wiley.** 2001. Herpes simplex virus glycoprotein D bound to the human receptor HveA. Mol Cell **8:**169-179.

25. **Chernomordik, L. V., and M. M. Kozlov.** 2008. Mechanics of membrane fusion. Nature structural & molecular biology **15:**675-683.

26. **Chowdary, T. K., T. M. Cairns, D. Atanasiu, G. H. Cohen, R. J. Eisenberg, and E. E. Heldwein.** 2010. Crystal structure of the conserved herpesvirus fusion regulator complex gH-gL. Nature structural & molecular biology **17:**882-888.

27. **Colman, P. M., and M. C. Lawrence.** 2003. The structural biology of type I viral membrane fusion. Nat Rev Mol Cell Biol **4:**309-319.

28. **Corey, L., and A. Wald.** 2009. Maternal and neonatal herpes simplex virus infections. N Engl J Med **361:**1376-1385.

29. **Cosset, F. L., and D. Lavillette.** 2011. Cell entry of enveloped viruses. Adv Genet **73:**121-183.

30. **Da Poian, A. T., F. A. Carneiro, and F. Stauffer.** 2005. Viral membrane fusion: is glycoprotein G of rhabdoviruses a representative of a new class of viral fusion proteins? Braz J Med Biol Res **38:**813-823.

31. **Di Giovine, P., E. C. Settembre, A. K. Bhargava, M. A. Luftig, H. Lou, G. H. Cohen, R. J. Eisenberg, C. Krummenacher, and A. Carfi.** 2011. Structure of herpes simplex virus glycoprotein D bound to the human receptor nectin-1. PLoS Pathog **7:**e1002277.

32. **Diefenbach, R. J., M. Miranda-Saksena, M. W. Douglas, and A. L. Cunningham.** 2008. Transport and egress of herpes simplex virus in neurons. Rev Med Virol **18:**35-51.

33. **Dohner, K., A. Wolfstein, U. Prank, C. Echeverri, D. Dujardin, R. Vallee, and B. Sodeik.** 2002. Function of dynein and dynactin in herpes simplex virus capsid transport. Mol Biol Cell **13:**2795-2809.

34. **Dollery, S. J., C. C. Wright, D. C. Johnson, and A. V. Nicola.** 2011. Low-pH-dependent changes in the conformation and oligomeric state of the prefusion form of herpes simplex virus glycoprotein B are separable from fusion activity. Journal of virology **85:**9964-9973.

35. **Douglas, M. W., R. J. Diefenbach, F. L. Homa, M. Miranda-Saksena, F. J. Rixon, V. Vittone, K. Byth, and A. L. Cunningham.** 2004. Herpes simplex virus type 1 capsid protein VP26 interacts with dynein light chains RP3 and Tctex1 and plays a role in retrograde cellular transport. The Journal of biological chemistry **279:**28522-28530.

36. **Eisenberg, R. J., D. Atanasiu, T. M. Cairns, J. R. Gallagher, C. Krummenacher, and G. H. Cohen.** 2012. Herpes virus fusion and entry: a story with many characters. Viruses **4:**800-832.

37. **Esko, J. D., and S. B. Selleck.** 2002. Order out of chaos: assembly of ligand binding sites in heparan sulfate. Annu Rev Biochem **71:**435-471.

38. **Farr, G. A., L. G. Zhang, and P. Tattersall.** 2005. Parvoviral virions deploy a capsid-tethered lipolytic enzyme to breach the endosomal membrane during cell entry. Proc Natl Acad Sci U S A **102:**17148-17153.

39. **Fields, B. N., D. M. Knipe, and P. M. Howley.** 2007. Fields' virology, 5th ed. Wolters Kluwer Health/Lippincott Williams & Wilkins, Philadelphia.

40. **Galdiero, S., A. Falanga, M. Vitiello, M. D'Isanto, C. Collins, V. Orrei, H. Browne, C. Pedone, and M. Galdiero.** 2007. Evidence for a role of the membrane-proximal region of herpes simplex virus Type 1 glycoprotein H in membrane fusion and virus inhibition. Chembiochem **8:**885-895.

41. **Galdiero, S., M. Vitiello, M. D'Isanto, A. Falanga, C. Collins, K. Raieta, C. Pedone, H. Browne, and M. Galdiero.** 2006. Analysis of synthetic peptides from heptad-repeat domains of herpes simplex virus type 1 glycoproteins H and B. J Gen Virol **87:**1085-1097.

42. **Gallaher, W. R., C. DiSimone, and M. J. Buchmeier.** 2001. The viral transmembrane superfamily: possible divergence of Arenavirus and Filovirus glycoproteins from a common RNA virus ancestor. BMC Microbiol **1:**1.

43. **Gaudin, Y.** 2000. Reversibility in fusion protein conformational changes. The intriguing case of rhabdovirus-induced membrane fusion. Subcell Biochem **34:**379-408.

44. **Gaudin, Y., R. W. Ruigrok, M. Knossow, and A. Flamand.** 1993. Low-pH conformational changes of rabies virus glycoprotein and their role in membrane fusion. Journal of virology **67:**1365-1372.

45. **Geraghty, R. J., C. Krummenacher, G. H. Cohen, R. J. Eisenberg, and P. G. Spear.** 1998. Entry of alphaherpesviruses mediated by poliovirus receptor-related protein 1 and poliovirus receptor. Science **280:**1618-1620.

46. **Gibbons, D. L., M. C. Vaney, A. Roussel, A. Vigouroux, B. Reilly, J. Lepault, M. Kielian, and F. A. Rey.** 2004. Conformational change and protein-protein interactions of the fusion protein of Semliki Forest virus. Nature **427:**320-325.

47. **Gonzalez, L. C., K. M. Loyet, J. Calemine-Fenaux, V. Chauhan, B. Wranik, W. Ouyang, and D. L. Eaton.** 2005. A coreceptor interaction between the CD28 and TNF receptor family members B and T lymphocyte attenuator and herpesvirus entry mediator. Proc Natl Acad Sci U S A **102:**1116-1121.

48. **Grunewald, K., P. Desai, D. C. Winkler, J. B. Heymann, D. M. Belnap, W. Baumeister, and A. C. Steven.** 2003. Three-dimensional structure of herpes simplex virus from cryo-electron tomography. Science **302:**1396-1398.

49. **Hannah, B. P., T. M. Cairns, F. C. Bender, J. C. Whitbeck, H. Lou, R. J. Eisenberg, and G. H. Cohen.** 2009. Herpes simplex virus glycoprotein B associates with target membranes via its fusion loops. J Virol **83:**6825-6836.

50. **Hannah, B. P., E. E. Heldwein, F. C. Bender, G. H. Cohen, and R. J. Eisenberg.** 2007. Mutational evidence of internal fusion loops in herpes simplex virus glycoprotein B. J Virol **81:**4858-4865.

51. **Harrison, S. C.** 2008. Viral membrane fusion. Nature structural & molecular biology **15:**690-698.

52. **Harrop, J. A., P. C. McDonnell, M. Brigham-Burke, S. D. Lyn, J. Minton, K. B. Tan, K. Dede, J. Spampanato, C. Silverman, P. Hensley, R. DiPrinzio, J. G. Emery, K. Deen, C. Eichman, M. Chabot-Fletcher, A. Truneh, and P. R. Young.** 1998. Herpesvirus entry mediator ligand (HVEM-L), a novel ligand for HVEM/TR2, stimulates proliferation of T cells and inhibits HT29 cell growth. The Journal of biological chemistry **273:**27548-27556.

53. **Hayward, G. S., R. J. Jacob, S. C. Wadsworth, and B. Roizman.** 1975. Anatomy of herpes simplex virus DNA: evidence for four populations of molecules that differ in the relative orientations of their long and short components. Proc Natl Acad Sci U S A **72:**4243-4247.

54. **He, Y., S. Mueller, P. R. Chipman, C. M. Bator, X. Peng, V. D. Bowman, S. Mukhopadhyay, E. Wimmer, R. J. Kuhn, and M. G. Rossmann.** 2003. Complexes of poliovirus serotypes with their common cellular receptor, CD155. Journal of virology **77:**4827-4835.

55. **Heldwein, E. E., and C. Krummenacher.** 2008. Entry of herpesviruses into mammalian cells. Cell Mol Life Sci **65:**1653-1668.

56. **Heldwein, E. E., H. Lou, F. C. Bender, G. H. Cohen, R. J. Eisenberg, and S. C. Harrison.** 2006. Crystal structure of glycoprotein B from herpes simplex virus 1. Science **313:**217-220.

57. **Herold, B. C., D. WuDunn, N. Soltys, and P. G. Spear.** 1991. Glycoprotein C of herpes simplex virus type 1 plays a principal role in the adsorption of virus to cells and in infectivity. Journal of virology **65:**1090-1098.

58. **Highlander, S. L., D. J. Dorney, P. J. Gage, T. C. Holland, W. Cai, S. Person, M. Levine, and J. C. Glorioso.** 1989. Identification of mar mutations in herpes simplex virus type 1 glycoprotein B which alter antigenic structure and function in virus penetration. Journal of virology **63:**730-738.

59. **Hook, L. M., J. M. Lubinski, M. Jiang, M. K. Pangburn, and H. M. Friedman.** 2006. Herpes simplex virus type 1 and 2 glycoprotein C prevents complement-mediated neutralization induced by natural immunoglobulin M antibody. Journal of virology **80:**4038-4046.

60. **Huarte, N., A. Araujo, R. Arranz, M. Lorizate, H. Quendler, R. Kunert, J. M. Valpuesta, and J. L. Nieva.** 2012. Recognition of Membrane-Bound Fusion-Peptide/MPER Complexes by the HIV-1 Neutralizing 2F5 Antibody: Implications for Anti-2F5 Immunogenicity. PLoS One **7:**e52740.

61. **Hung, S. L., Y. Y. Cheng, Y. H. Wang, K. W. Chang, and Y. T. Chen.** 2002. Expression and roles of herpesvirus entry mediators A and C in cells of oral origin. Oral Microbiol Immunol **17:**215-223.

62. **Ivanovic, T., M. A. Agosto, L. Zhang, K. Chandran, S. C. Harrison, and M. L. Nibert.** 2008. Peptides released from reovirus outer capsid form membrane pores that recruit virus particles. Embo J **27:**1289-1298.

63. **Jeetendra, E., K. Ghosh, D. Odell, J. Li, H. P. Ghosh, and M. A. Whitt.** 2003. The membrane-proximal region of vesicular stomatitis virus glycoprotein G ectodomain is critical for fusion and virus infectivity. Journal of virology **77:**12807-12818.

64. **Jeetendra, E., C. S. Robison, L. M. Albritton, and M. A. Whitt.** 2002. The membrane-proximal domain of vesicular stomatitis virus G protein functions as a membrane fusion potentiator and can induce hemifusion. J Virol **76:**12300-12311.

65. **Johannsdottir, H. K., R. Mancini, J. Kartenbeck, L. Amato, and A. Helenius.** 2009. Host cell factors and functions involved in vesicular stomatitis virus entry. Journal of virology **83:**440-453.

66. **Kadlec, J., S. Loureiro, N. G. Abrescia, D. I. Stuart, and I. M. Jones.** 2008. The postfusion structure of baculovirus gp64 supports a unified view of viral fusion machines. Nat Struct Mol Biol **15:**1024-1030.

67. **Kielian, M.** 2006. Class II virus membrane fusion proteins. Virology **344:**38-47.

68. **Kielian, M., and F. A. Rey.** 2006. Virus membrane-fusion proteins: more than one way to make a hairpin. Nat Rev Microbiol **4:**67-76.

69. **Killian, J. A., and G. von Heijne.** 2000. How proteins adapt to a membrane-water interface. Trends Biochem Sci **25:**429-434.

70. **Krummenacher, C., F. Baribaud, M. Ponce de Leon, I. Baribaud, J. C. Whitbeck, R. Xu, G. H. Cohen, and R. J. Eisenberg.** 2004. Comparative usage of herpesvirus entry mediator A and nectin-1 by laboratory strains and clinical isolates of herpes simplex virus. Virology **322:**286-299.

71. **Kuzmin, P. I., J. Zimmerberg, Y. A. Chizmadzhev, and F. S. Cohen.** 2001. A quantitative model for membrane fusion based on low-energy intermediates. Proc Natl Acad Sci U S A **98:**7235-7240.

72. **Kwon, B. S., K. B. Tan, J. Ni, K. O. Oh, Z. H. Lee, K. K. Kim, Y. J. Kim, S. Wang, R. Gentz, G. L. Yu, J. Harrop, S. D. Lyn, C. Silverman, T. G. Porter, A. Truneh, and P. R. Young.** 1997. A newly identified member of the tumor necrosis factor receptor superfamily with a wide tissue distribution and involvement in lymphocyte activation. The Journal of biological chemistry **272:**14272-14276.

73. **Kyte, J., and R. F. Doolittle.** 1982. A simple method for displaying the hydropathic character of a protein. J Mol Biol **157:**105-132.

74. **Lawson, N. D., E. A. Stillman, M. A. Whitt, and J. K. Rose.** 1995. Recombinant vesicular stomatitis viruses from DNA. Proc Natl Acad Sci U S A **92:**4477-4481.

75. **Lee, J. E., M. L. Fusco, A. J. Hessell, W. B. Oswald, D. R. Burton, and E. O. Saphire.** 2008. Structure of the Ebola virus glycoprotein bound to an antibody from a human survivor. Nature **454:**177-182.

76. **Lemmon, M. A.** 2007. Pleckstrin homology (PH) domains and phosphoinositides. Biochem Soc Symp**:**81-93.

77. **Lescar, J., A. Roussel, M. W. Wien, J. Navaza, S. D. Fuller, G. Wengler, and F. A. Rey.** 2001. The Fusion glycoprotein shell of Semliki Forest virus: an icosahedral assembly primed for fusogenic activation at endosomal pH. Cell **105:**137-148.

78. **Leuzinger, H., U. Ziegler, E. M. Schraner, C. Fraefel, D. L. Glauser, I. Heid, M. Ackermann, M. Mueller, and P. Wild.** 2005. Herpes simplex virus 1 envelopment follows two diverse pathways. Journal of virology **79:**13047-13059.

79. **Li, Z., and G. W. Blissard.** 2009. The pre-transmembrane domain of the Autographa californica multicapsid nucleopolyhedrovirus GP64 protein is critical for membrane fusion and virus infectivity. Journal of virology **83:**10993-11004.

80. **Liao, M., and M. Kielian.** 2006. Functions of the stem region of the Semliki Forest virus fusion protein during virus fusion and assembly. Journal of virology **80:**11362-11369.

81. **Liao, M., and M. Kielian.** 2006. Site-directed antibodies against the stem region reveal low pH-induced conformational changes of the Semliki Forest virus fusion protein. Journal of virology **80:**9599-9607.

82. **Lin, E., and P. G. Spear.** 2007. Random linker-insertion mutagenesis to identify functional domains of herpes simplex virus type 1 glycoprotein B. Proc Natl Acad Sci U S A **104:**13140-13145.

83. **Lubinski, J. M., L. Wang, A. M. Soulika, R. Burger, R. A. Wetsel, H. Colten, G. H. Cohen, R. J. Eisenberg, J. D. Lambris, and H. M. Friedman.** 1998. Herpes simplex virus type 1 glycoprotein gC mediates immune evasion in vivo. Journal of virology **72:**8257-8263.

84. **Maier, O., D. L. Galan, H. Wodrich, and C. M. Wiethoff.** 2010. An N-terminal domain of adenovirus protein VI fragments membranes by inducing positive membrane curvature. Virology **402:**11-19.

85. **Matis, J., and M. Kudelova.** 2001. Early shutoff of host protein synthesis in cells infected with herpes simplex viruses. Acta Virol **45:**269-277.

86. **Matsuura, H., A. N. Kirschner, R. Longnecker, and T. S. Jardetzky.** 2010. Crystal structure of the Epstein-Barr virus (EBV) glycoprotein H/glycoprotein L (gH/gL) complex. Proc Natl Acad Sci U S A **107:**22641-22646.

87. **Mauri, D. N., R. Ebner, R. I. Montgomery, K. D. Kochel, T. C. Cheung, G. L. Yu, S. Ruben, M. Murphy, R. J. Eisenberg, G. H. Cohen, P. G. Spear, and C. F. Ware.** 1998. LIGHT, a new member of the TNF superfamily, and lymphotoxin alpha are ligands for herpesvirus entry mediator. Immunity **8:**21-30.

88. **Melikyan, G. B., R. J. Barnard, R. M. Markosyan, J. A. Young, and F. S. Cohen.** 2004. Low pH is required for avian sarcoma and leukosis virus Env-induced hemifusion and fusion pore formation but not for pore growth. Journal of virology **78:**3753-3762.

89. **Mendelsohn, C. L., E. Wimmer, and V. R. Racaniello.** 1989. Cellular receptor for poliovirus: molecular cloning, nucleotide sequence, and expression of a new member of the immunoglobulin superfamily. Cell **56:**855-865.

90. **Mettenleiter, T. C.** 2002. Herpesvirus assembly and egress. Journal of virology **76:**1537-1547.

91. **Miller, C. S., and R. J. Danaher.** 2008. Asymptomatic shedding of herpes simplex virus (HSV) in the oral cavity. Oral Surg Oral Med Oral Pathol Oral Radiol Endod **105:**43-50.

92. **Milne, R. S., A. V. Nicola, J. C. Whitbeck, R. J. Eisenberg, and G. H. Cohen.** 2005. Glycoprotein D receptor-dependent, low-pH-independent endocytic entry of herpes simplex virus type 1. J Virol **79:**6655-6663.

93. **Mitchell, B. M., D. C. Bloom, R. J. Cohrs, D. H. Gilden, and P. G. Kennedy.** 2003. Herpes simplex virus-1 and varicella-zoster virus latency in ganglia. J Neurovirol **9:**194-204.

94. **Mizoguchi, A., H. Nakanishi, K. Kimura, K. Matsubara, K. Ozaki-Kuroda, T. Katata, T. Honda, Y. Kiyohara, K. Heo, M. Higashi, T. Tsutsumi, S. Sonoda, C. Ide, and Y. Takai.** 2002. Nectin: an adhesion molecule involved in formation of synapses. J Cell Biol **156:**555-565.

95. **Modis, Y., S. Ogata, D. Clements, and S. C. Harrison.** 2003. A ligand-binding pocket in the dengue virus envelope glycoprotein. Proc Natl Acad Sci U S A **100:**6986-6991.

96. **Modis, Y., S. Ogata, D. Clements, and S. C. Harrison.** 2004. Structure of the dengue virus envelope protein after membrane fusion. Nature **427:**313-319.

97. **Montgomery, R. I., M. S. Warner, B. J. Lum, and P. G. Spear.** 1996. Herpes simplex virus-1 entry into cells mediated by a novel member of the TNF/NGF receptor family. Cell **87:**427-436.

98. **Moyer, C. L., and G. R. Nemerow.** 2011. Viral weapons of membrane destruction: variable modes of membrane penetration by non-enveloped viruses. Curr Opin Virol **1:**44-49.

99. **Nicola, A. V., A. M. McEvoy, and S. E. Straus.** 2003. Roles for endocytosis and low pH in herpes simplex virus entry into HeLa and Chinese hamster ovary cells. Journal of virology **77:**5324-5332.

100. **Nunberg, J. H., and J. York.** 2012. The curious case of arenavirus entry, and its inhibition. Viruses **4:**83-101.

101. **O'Donnell, C. D., M. Kovacs, J. Akhtar, T. Valyi-Nagy, and D. Shukla.** 2010. Expanding the role of 3-O sulfated heparan sulfate in herpes simplex virus type-1 entry. Virology **397:**389-398.

102. **Pellett, P. E., K. G. Kousoulas, L. Pereira, and B. Roizman.** 1985. Anatomy of the herpes simplex virus 1 strain F glycoprotein B gene: primary sequence and predicted protein structure of the wild type and of monoclonal antibody-resistant mutants. J Virol **53:**243-253.

103. **Peng, T., M. Ponce-de-Leon, H. Jiang, G. Dubin, J. M. Lubinski, R. J. Eisenberg, and G. H. Cohen.** 1998. The gH-gL complex of herpes simplex virus

(HSV) stimulates neutralizing antibody and protects mice against HSV type 1 challenge. Journal of virology **72:**65-72.

104. **Pereira, L., M. Ali, K. Kousoulas, B. Huo, and T. Banks.** 1989. Domain structure of herpes simplex virus 1 glycoprotein B: neutralizing epitopes map in regions of continuous and discontinuous residues. Virology **172:**11-24.

105. **Pertel, P. E., A. Fridberg, M. L. Parish, and P. G. Spear.** 2001. Cell fusion induced by herpes simplex virus glycoproteins gB, gD, and gH-gL requires a gD receptor but not necessarily heparan sulfate. Virology **279:**313-324.

106. **Poppers, J., M. Mulvey, D. Khoo, and I. Mohr.** 2000. Inhibition of PKR activation by the proline-rich RNA binding domain of the herpes simplex virus type 1 Us11 protein. Journal of virology **74:**11215-11221.

107. **Posavad, C. M., J. J. Newton, and K. L. Rosenthal.** 1994. Infection and inhibition of human cytotoxic T lymphocytes by herpes simplex virus. Journal of virology **68:**4072-4074.

108. **Rasile, L., K. Ghosh, K. Raviprakash, and H. P. Ghosh.** 1993. Effects of deletions in the carboxy-terminal hydrophobic region of herpes simplex virus glycoprotein gB on intracellular transport and membrane anchoring. Journal of virology **67:**4856-4866.

109. **Rice, S. A., M. C. Long, V. Lam, P. A. Schaffer, and C. A. Spencer.** 1995. Herpes simplex virus immediate-early protein ICP22 is required for viral modification of host RNA polymerase II and establishment of the normal viral transcription program. Journal of virology **69:**5550-5559.

110. **Roche, S., A. A. Albertini, J. Lepault, S. Bressanelli, and Y. Gaudin.** 2008. Structures of vesicular stomatitis virus glycoprotein: membrane fusion revisited. Cellular and molecular life sciences : CMLS **65:**1716-1728.

111. **Roche, S., S. Bressanelli, F. A. Rey, and Y. Gaudin.** 2006. Crystal structure of the low-pH form of the vesicular stomatitis virus glycoprotein G. Science **313:**187-191.

112. **Roche, S., and Y. Gaudin.** 2002. Characterization of the equilibrium between the native and fusion-inactive conformation of rabies virus glycoprotein indicates that the fusion complex is made of several trimers. Virology **297:**128-135.

113. **Roche, S., F. A. Rey, Y. Gaudin, and S. Bressanelli.** 2007. Structure of the prefusion form of the vesicular stomatitis virus glycoprotein G. Science **315:**843-848.

114. **Roussel, A., J. Lescar, M. C. Vaney, G. Wengler, and F. A. Rey.** 2006. Structure and interactions at the viral surface of the envelope protein E1 of Semliki Forest virus. Structure **14:**75-86.

115. **Salzwedel, K., J. T. West, and E. Hunter.** 1999. A conserved tryptophan-rich motif in the membrane-proximal region of the human immunodeficiency virus type 1 gp41 ectodomain is important for Env-mediated fusion and virus infectivity. Journal of virology **73:**2469-2480.

116. **Sedy, J. R., M. Gavrieli, K. G. Potter, M. A. Hurchla, R. C. Lindsley, K. Hildner, S. Scheu, K. Pfeffer, C. F. Ware, T. L. Murphy, and K. M. Murphy.**

2005. B and T lymphocyte attenuator regulates T cell activation through interaction with herpesvirus entry mediator. Nat Immunol **6:**90-98.

117. **Shelly, S. S., T. M. Cairns, J. C. Whitbeck, H. Lou, C. Krummenacher, G. H. Cohen, and R. J. Eisenberg.** 2012. The Membrane-Proximal Region (MPR) of Herpes Simplex Virus gB Regulates Association of the Fusion Loops with Lipid Membranes. MBio **3**.

118. **Shukla, D., J. Liu, P. Blaiklock, N. W. Shworak, X. Bai, J. D. Esko, G. H. Cohen, R. J. Eisenberg, R. D. Rosenberg, and P. G. Spear.** 1999. A novel role for 3-O-sulfated heparan sulfate in herpes simplex virus 1 entry. Cell **99:**13-22.

119. **Simpson, S. A., M. D. Manchak, E. J. Hager, C. Krummenacher, J. C. Whitbeck, M. J. Levin, C. R. Freed, C. L. Wilcox, G. H. Cohen, R. J. Eisenberg, and L. I. Pizer.** 2005. Nectin-1/HveC Mediates herpes simplex virus type 1 entry into primary human sensory neurons and fibroblasts. J Neurovirol **11:**208-218.

120. **Skehel, J. J., and D. C. Wiley.** 2000. Receptor binding and membrane fusion in virus entry: the influenza hemagglutinin. Annu Rev Biochem **69:**531-569.

121. **Spear, P. G.** 2004. Herpes simplex virus: receptors and ligands for cell entry. Cell Microbiol **6:**401-410.

122. **Spear, P. G., R. J. Eisenberg, and G. H. Cohen.** 2000. Three classes of cell surface receptors for alphaherpesvirus entry. Virology **275:**1-8.

123. **Spear, P. G., M. T. Shieh, B. C. Herold, D. WuDunn, and T. I. Koshy.** 1992. Heparan sulfate glycosaminoglycans as primary cell surface receptors for herpes simplex virus. Adv Exp Med Biol **313:**341-353.

124. **Stampfer, S. D., H. Lou, G. H. Cohen, R. J. Eisenberg, and E. E. Heldwein.** 2010. Structural basis of local, pH-dependent conformational changes in glycoprotein B from herpes simplex virus type 1. J Virol **84:**12924-12933.

125. **Stannard, L. M., A. O. Fuller, and P. G. Spear.** 1987. Herpes simplex virus glycoproteins associated with different morphological entities projecting from the virion envelope. J Gen Virol **68 (Pt 3):**715-725.

126. **Stern, S., M. Tanaka, and W. Herr.** 1989. The Oct-1 homoeodomain directs formation of a multiprotein-DNA complex with the HSV transactivator VP16. Nature **341:**624-630.

127. **Steven, A. C., and P. G. Spear.** 2006. Biochemistry. Viral glycoproteins and an evolutionary conundrum. Science **313:**177-178.

128. **Stiles, K. M., J. C. Whitbeck, H. Lou, G. H. Cohen, R. J. Eisenberg, and C. Krummenacher.** 2010. Herpes simplex virus glycoprotein D interferes with binding of herpesvirus entry mediator to its ligands through downregulation and direct competition. J Virol **84:**11646-11660.

129. **Suarez, T., W. R. Gallaher, A. Agirre, F. M. Goni, and J. L. Nieva.** 2000. Membrane interface-interacting sequences within the ectodomain of the human immunodeficiency virus type 1 envelope glycoprotein: putative role during viral fusion. J Virol **74:**8038-8047.

130. **Takai, Y., and H. Nakanishi.** 2003. Nectin and afadin: novel organizers of intercellular junctions. J Cell Sci **116:**17-27.

131. **Taylor, T. J., M. A. Brockman, E. E. McNamee, and D. M. Knipe.** 2002. Herpes simplex virus. Front Biosci **7:**d752-764.

132. **Timbury, M. C., A. Theriault, and R. A. Elton.** 1974. A stable syncytial mutant of herpes simplex type 2 virus. J Gen Virol **23:**219-224.

133. **Tiwari, V., C. Clement, D. Xu, T. Valyi-Nagy, B. Y. Yue, J. Liu, and D. Shukla.** 2006. Role for 3-O-sulfated heparan sulfate as the receptor for herpes simplex virus type 1 entry into primary human corneal fibroblasts. Journal of virology **80:**8970-8980.

134. **Tiwari, V., S. Y. Shukla, B. Y. Yue, and D. Shukla.** 2007. Herpes simplex virus type 2 entry into cultured human corneal fibroblasts is mediated by herpesvirus entry mediator. J Gen Virol **88:**2106-2110.

135. **Tomishima, M. J., G. A. Smith, and L. W. Enquist.** 2001. Sorting and transport of alpha herpesviruses in axons. Traffic **2:**429-436.

136. **Tong, S., F. Yi, A. Martin, Q. Yao, M. Li, and R. W. Compans.** 2001. Three membrane-proximal amino acids in the human parainfluenza type 2 (HPIV 2) F protein are critical for fusogenic activity. Virology **280:**52-61.

137. **Tsai, B.** 2007. Penetration of nonenveloped viruses into the cytoplasm. Annu Rev Cell Dev Biol **23:**23-43.

138. **Turner, A., B. Bruun, T. Minson, and H. Browne.** 1998. Glycoproteins gB, gD, and gHgL of herpes simplex virus type 1 are necessary and sufficient to mediate

membrane fusion in a Cos cell transfection system. Journal of virology **72:**873-875.

139. **Tuthill, T. J., E. Groppelli, J. M. Hogle, and D. J. Rowlands.** 2010. Picornaviruses. Curr Top Microbiol Immunol **343:**43-89.

140. **Vittone, V., E. Diefenbach, D. Triffett, M. W. Douglas, A. L. Cunningham, and R. J. Diefenbach.** 2005. Determination of interactions between tegument proteins of herpes simplex virus type 1. Journal of virology **79:**9566-9571.

141. **Vlazny, D. A., A. Kwong, and N. Frenkel.** 1982. Site-specific cleavage/packaging of herpes simplex virus DNA and the selective maturation of nucleocapsids containing full-length viral DNA. Proc Natl Acad Sci U S A **79:**1423-1427.

142. **Wanas, E., S. Efler, K. Ghosh, and H. P. Ghosh.** 1999. Mutations in the conserved carboxy-terminal hydrophobic region of glycoprotein gB affect infectivity of herpes simplex virus. J Gen Virol **80 (Pt 12):**3189-3198.

143. **Ward, P. L., and B. Roizman.** 1994. Herpes simplex genes: the blueprint of a successful human pathogen. Trends Genet **10:**267-274.

144. **Westhoff, G. L., S. E. Little, and A. B. Caughey.** 2011. Herpes simplex virus and pregnancy: a review of the management of antenatal and peripartum herpes infections. Obstet Gynecol Surv **66:**629-638.

145. **White, J. M., S. E. Delos, M. Brecher, and K. Schornberg.** 2008. Structures and mechanisms of viral membrane fusion proteins: multiple variations on a common theme. Crit Rev Biochem Mol Biol **43:**189-219.

146. **Wilson, I. A., J. J. Skehel, and D. C. Wiley.** 1981. Structure of the haemagglutinin membrane glycoprotein of influenza virus at 3 A resolution. Nature **289:**366-373.

147. **Wittels, M., and P. G. Spear.** 1991. Penetration of cells by herpes simplex virus does not require a low pH-dependent endocytic pathway. Virus Res **18:**271-290.

148. **Xu, F., M. R. Sternberg, B. J. Kottiri, G. M. McQuillan, F. K. Lee, A. J. Nahmias, S. M. Berman, and L. E. Markowitz.** 2006. Trends in herpes simplex virus type 1 and type 2 seroprevalence in the United States. Jama **296:**964-973.

149. **Zheng, Z., E. Maidji, S. Tugizov, and L. Pereira.** 1996. Mutations in the carboxyl-terminal hydrophobic sequence of human cytomegalovirus glycoprotein B alter transport and protein chaperone binding. J Virol **70:**8029-8040.

150. **Zhou, J., and G. W. Blissard.** 2008. Identification of a GP64 subdomain involved in receptor binding by budded virions of the baculovirus Autographica californica multicapsid nucleopolyhedrovirus. J Virol **82:**4449-4460.

151. **Zhou, J., R. E. Dutch, and R. A. Lamb.** 1997. Proper spacing between heptad repeat B and the transmembrane domain boundary of the paramyxovirus SV5 F protein is critical for biological activity. Virology **239:**327-339.

152. **Zhou, Z. H., M. Dougherty, J. Jakana, J. He, F. J. Rixon, and W. Chiu.** 2000. Seeing the herpesvirus capsid at 8.5 A. Science **288:**877-880.

CHAPTER 2

The membrane proximal region (MPR) of herpes simplex virus gB regulates association of the fusion loops with lipid membranes

This chapter appeared as the published article "The membrane-proximal region (MPR) of Herpes Simplex Virus gB regulates association of the fusion loops with lipid membranes" by S. S. Shelly, T. M. Cairns, J. C. Whitbeck, H. Lou, C. Krummenacher, G. H. Cohen, and R. J. Eisenberg. MBio. 2012 Nov 20; 3(6).

ABSTRACT

Glycoprotein B (gB), gD, and gH/gL constitute the fusion machinery of herpes simplex virus (HSV). Prior studies indicated that fusion occurs in a stepwise fashion whereby the gD/receptor complex activates the entire process, while gH/gL regulates the fusion reaction carried out by gB. Trimeric gB is a class III fusion protein. Its ectodomain of 773 amino acids contains a membrane proximal region (MPR, residues 731-773) and two fusion loops (FL) per protomer. We hypothesized that the highly hydrophobic MPR interacts with the FLs, thereby masking them on virions until fusion begins. To test this hypothesis, we made a series of deletion, truncation, and point mutants of the gB MPR. Although the full-length deletion mutants were expressed in transfected cells, they were not transported to the cell surface, suggesting that removal of even small stretches of the MPR was highly detrimental to gB folding. To circumvent this limitation, we used a baculovirus expression system to generate four soluble proteins, each lacking the transmembrane region and cytoplasmic tail. All retained the FLs as well as decreasing portions of the MPR [gB(773t), gB(759t), gB(749t), gB(739t)]. Despite the presence of the FLs, all were compromised in their ability to bind liposomes as compared to the control, gB(730t), which lacks the MPR. We conclude that residues 731-739 are sufficient to mask the FLs, thereby preventing liposome association. Importantly, mutation of two aromatic residues (F732, F738) to alanine restored the ability of gB(739t) to bind liposomes. Our data suggest that the MPR is important for modulating the association of gB FLs with target membranes.

INTRODUCTION

Herpes simplex virus (HSV) has four envelope glycoproteins that are essential for virus entry into cells: gD, gH, gL, and gB. All herpesviruses use a combination of gB and the heterodimer gH/gL to carry out fusion (9, 14, 16, 30, 41, 42); these three proteins are considered the core fusion machinery. For HSV, an additional protein, gD, is part of this machinery. Our current model of HSV fusion starts with the binding of gD to one of its receptors, likely transmitting a signal to gH/gL, which in turn acts upon gB to trigger fusion (3). HSV-1 gB is a 904 amino acid type I membrane glycoprotein whose crystal structure identifies it as a class III fusion protein (23). Although there is no primary sequence conservation, HSV-1 gB shares a high degree of structural homology with other class III fusion proteins including vesicular stomatitis virus (VSV) G (46), baculovirus gp64 (26), and Epstein-Barr virus (EBV) gB (5). According to ultrastructural data (5, 23, 26, 46), these presumed post-fusion conformations show that all are homotrimers with a long central coiled coil structure reminiscent of class I fusion proteins. Yet, all have internal bipartite fusion loops (FLs) which are similar to the single internal FL of class II fusion proteins (14, 28, 31, 55). Single point mutations within either of the gB fusion loops caused loss of cell-cell fusion and failure of soluble gB to associate with membranes (20, 21).

For VSV G, ultrastructural data are available for both pre- and post-fusion forms (46, 47) and indicate that the FLs are situated near the transmembrane region and are close to the viral membrane in both forms. For the fusion loops to start and end in this position, it is presumed that an intermediate step occurs where the fusion loops reposition

to the top of gB to interact with the cellular membrane. Then, as gB changes conformation to its post-fusion form, it pulls the viral and cellular membranes close together to facilitate lipid mixing. The prevailing concept is that these hydrophobic loops would be masked on the virus surface prior to fusion activation to avoid premature or otherwise unwanted interactions that may be detrimental to virus infectivity.

The form of HSV gB used for crystallization ended at amino acid 730, leaving the fusion loop region exposed (23). Residues downstream of amino acid 730 were initially excluded for crystallization trials due to their elevated hydrophobicity, which could impede crystal formation. These downstream residues (731-773) constitute the gB membrane proximal region (MPR) (10, 23, 40, 43). The structure of the MPR remains unknown for any of the class III fusion proteins but it seems likely to be in close proximity to the FLs (Figure 2-1A).

MPRs provide essential functions in different types of fusion proteins. Mutations within the MPRs of the fusion proteins for HIV (50), paramyxoviruses (57, 64), VSV (24), and baculovirus (34) abolish fusion but do not affect cell surface protein expression. MPRs are characteristically rich in aromatic residues (W, Y, F) (56) that have been proposed to bridge the gap between the aqueous and hydrophobic environments present at the lipid interface (29). These aromatic residues could also act in concert (synergistically) with fusion peptides/loops to destabilize membranes and promote lipid mixing (25, 56). Indeed, aromatic residues are also vital in FL function; it is presumed that their side chains, along with their carbon backbones, are inserted into the target membrane (37, 44, 46). Interestingly, the MPR of baculovirus gp64 does not contain any

aromatic residues, but its bulky leucine residues appear critical for cell-cell fusion (34). MPRs might also act as flexible tethers to help fusion proteins become properly positioned between two lipid bilayers, as described for VSV G (45).

Several studies of gB from different herpesviruses highlight the functional importance of its MPR. Most gB MPR mutants are defective in protein folding and cell surface expression (35, 43, 58, 62), making it difficult to assess its functional role. However, the few HSV gB MPR mutants that are expressed on the cell surface are impaired in cell-cell fusion or virus entry (35, 58).

Previously, we suggested that the MPR could mask the hydrophobic FLs in the pre-fusion state (21) in a way that would be analogous to how the FLs of class II fusion proteins are masked at the dimer interface (18, 48, 61). Our goal here was to carry out a systematic analysis of the MPR. We first made a series of MPR deletion mutants in this region in full-length gB and expressed each mutant in mammalian cells. Unfortunately, none of these mutants were efficiently transported to the cell surface, a defect previously reported for other gB MPR deletions (43). We next constructed recombinant baculoviruses to express C-terminal gB truncation mutants, containing various lengths of the MPR. Despite the presence of the fusion loops, all of the proteins containing portions of the MPR were compromised in their ability to bind liposomes as compared to the MPR-less gB(730t), including gB(739t), which contains only nine MPR residues. However, mutation of two aromatic residues in gB(739t) to alanine (F732A/F738A) restored the ability of this protein to bind liposomes. Thus, our data are consistent with a

critical role for the MPR in regulating exposure of the gB fusion loops thereby preventing premature association with lipid.

MATERIALS AND METHODS

Cells. Mouse B78H1 melanoma cells engineered to express the gD receptor nectin-1 (C10 cells) were grown in Dulbecco's modified Eagle medium (DMEM) supplemented with 5% fetal bovine serum (FBS) and 500 μg/ml of G418. Chinese hamster ovary (CHO-K1) cells were grown in Ham's F-12 medium containing 10% FBS. CHO-K1 and C10 cells were kindly provided by P. G. Spear. Sf9 (*Spodoptera frugiperda*) cells were grown in Sf900II serum-free medium (Gibco).

Antibodies. Rabbit polyclonal antibodies (PAb) R68 and R69 were raised against full-length gB1 purified from infected cells as previously described (19). gB-specific monoclonal antibodies (MAbs) SS55 and DL16 were characterized previously and recognize discontinuous (conformation-dependent) epitopes and are trimer-specific (6).

Plasmids. Full-length gB constructs containing deletions within the MPR, pSS1000 [gBD(730-747)], pSS1001 [gBD(748-773)] pSS1002 [gBD(730-739)], pSS1003 [gBD(735-744)], pSS1004 [gBD(740-749)], pSS1005 [gBD(750-759)], pSS1008 [gBD(765-773)], were created using the QuikChange XL site-directed mutagenesis kit (Stratagene Cloning Systems) as described previously (11). QuikChange primers were designed to "loop out" unwanted residues during amplification of template pPEP98

(containing the full-length gB gene from KOS, a gift of P. Spear) (42) and were as follows (deletion between underlined nucleotides, only forward primers shown): pSS1000, 5'-CATCCACGCCGACGCCAACGCCGCGGTCGGCAAGGTGGTGATGGGC; pSS1001, 5'-CGAGGGGATGGGCGACCTGGGGCGCCCCTTTGGGGCGCTGGCCGTGGG; pSS1002, 5'-CACGCCGACGCCAACGCCGAGGGGATGGGCGACCTG; pSS1003, 5'-GCCGCCATGTTCGCGGGCCTGGGGCGCGCGGTCGGC; pSS1004, 5'-GGCCTGGGCGCGTTCTTCGGCAAGGTGGTGATGGGC; pSS1005, 5'-GACCTGGGGCGCGCGGTCGTGGTATCGGCCGTGTCG; and pSS1008, 5'-GGCGGCGTGGTATCGGCCGTGCCCTTTGGGGCGCTGGCC. All deletions were confirmed by sequencing the gB gene. Plasmids for expression of full-length HSV glycoproteins (pPEP99, pPEP100, pPEP101) and those needed in the cell-cell fusion assay (pCAGGS/MCS, pT7EMCLuc, pCAGT7) were gifts of P. G. Spear (39, 42).

Production and purification of soluble HSV glycoproteins. To construct a baculovirus vector expressing the MPR-containing gB ectodomain, we PCR-amplified residues 526-773 of gB1 from template pKBXX (containing the gB gene from KOS, a gift of S. Person) using primers 5′-CGGCTGCAGTTTACGTACAA (PstI site underlined) and 5′-CGCGAGTTCAATTGGACATGAAGGAGGACAC (EcoRI site underlined). This fragment was cloned into PstI-EcoRI digested pCW289 (7) to generate pLH633 [gB(773t)]. Other truncations of gB1 were generated from template pLH633 by

QuikChange mutagenesis, generating stop codons (underlined) at residues 740 (primer 5′-GGCCTGGGCGCGTTCTTCTGAATTCGGTACCGACTCTGC), 750 (primer 5′-GACCTGGGGCGCGCGGTCTGAATTCGGTACCGACTCTGC), 760 (primer 5′-GATGGGCATCGTGGGCGGCTGAATTCGGTACCGACTCTGC). The resulting constructs were named pSS1010 [gB(739t)], pSS1013 [gB(749t)], and pSS1015 [gB(759t)], respectively. A double point mutant, gB-F732/738A(739t) (pSS1023), was generated from template pSS1010 by QuikChange using primer 5′-GCCAACGCCGCCATGGCCGCGGGCCTGGGC and 5′-GCGGGCCTGGGCGCGGCCTTCGAGGGGATGGGC (substitutions underlined) to sequentially add first F732A and then F738A to the coding sequence. All mutations were verified by sequencing the entire gB gene. Recombinant baculoviruses were generated as previously described (53). The resulting soluble gB proteins were purified with a DL16 immunosorbent column (7). Soluble gB-W174R(730t) was described previously (20). Soluble gD(306t) was purified from baculovirus-infected insect cells as detailed elsewhere (49, 53).

Western blotting. Purified, soluble proteins were mixed with an equal volume of 2X sample buffer containing either no reducing agent and 0.2% SDS ("native" conditions) or 200mM dithiothreitol and 2% SDS ("denaturing" conditions) (13). Proteins from denatured samples were also boiled for 5 min before electrophoresis. For full-length proteins, **C10** cells were grown on 6-well plates and transfected with the desired plasmids according to the GenePORTER protocol (Gene Therapy Systems, Inc.). At 24-48 h post-

transfection, cells were lysed in 200 mL of lysis buffer (10 mM Tris (pH 8), 150 mM NaCl, 10 mM EDTA, 1% NP-40, 0.5% deoxycholic acid), 5 mL of which was used for electrophoresis (denaturing conditions). All proteins were resolved by polyacrylamide gel electrophoresis and transferred to nitrocellulose for Western blotting.

Fusion assay. To detect cell-cell fusion, we used a previously described luciferase reporter assay (32, 39, 42). Briefly, CHO-K1 cells were grown in 24-well plates and transfected with plasmids encoding T7 RNA polymerase (pCAGT7), gD (pPEP99), gH (pPEP100), and gL (pPEP101) and either wild-type gB (pPEP98), mutant gB, or empty vector (pCAGGS/MCS). To prepare receptor-expressing cells, CHO-K1 cells growing in six-well plates were transfected with a plasmid encoding the firefly luciferase gene under control of the T7 promoter (pT7EMCLuc) and a plasmid encoding HVEM (pSC386). Six hours post-transfection, receptor-expressing cells were trypsinized and added to the glycoprotein-expressing cells. At 18h post-cocultivation, cells were washed with PBS, lysed in reporter lysis buffer (Promega), and frozen. Finally, the extracts were thawed and mixed with 100 µl of luciferase substrate (Promega) and immediately assayed for light output by luminometry.

CELISA. To detect gB cell surface expression, we used a modification of a cell-based enzyme-linked immunosorbent assay (CELISA). CHO-K1 cells growing in 96-well plates were transfected with pCAGT7, pPEP99, pPEP100, pPEP101, and a plasmid encoding either wild-type gB (pPEP98), mutant gB, or empty vector (pCAGGS/MCS).

Forty nanograms of each plasmid/well and 0.5 µl of Lipofectamine 2000 (Invitrogen) were used. Cells were exposed to the DNA-Lipofectamine 2000 mixture for 5 h, after which the mixture was replaced with growth medium. Cells were grown overnight, fixed in 3% paraformaldehyde, and rinsed with PBS. Cells were then incubated for 1 h with PAb R68 diluted in 3% bovine serum albumin-PBS and incubated for 30 min with goat anti-rabbit antibodies coupled to horseradish peroxidase. Cells were rinsed with 20 mM citrate buffer (pH 4.5), incubated with peroxidase substrate (Moss, Inc.), and the absorbance at 405 nm was recorded using a microtiter plate reader. The absorbance values of cells transfected with the empty vector pCAGGS/MCS was subtracted and data were normalized to WT gB.

Liposome flotation assay. Liposome flotation assay conditions were adapted from previously described methods (15, 20, 27). Liposomes were purchased from Encapsula Nanosciences (Nashville, TN) at a size of 400 nm, containing a 1.7:1 molar ratio of soy-phosphatidylcholine to cholesterol. Briefly, purified soluble gB (1 µg), liposomes (25 µg), 1x protease inhibitor cocktail (Roche), and 15 µl of 200 mM sodium citrate were combined and the final reaction volume was adjusted to 50 µl with PBS. Protein-liposome mixtures were then incubated at 37°C for 1 h. To eliminate unwanted electrostatic protein-lipid associations, mixtures were incubated with 1 M KCl for 15 min at 37°C before being loaded at the bottom of a sucrose gradient. Mixtures were adjusted to 40% sucrose in a final volume of 500 µl and overlaid with 4 ml of 25% sucrose-PBS and 500 µl of 5% sucrose-PBS. The gradients were centrifuged for 3 h in a Beckman

SW55Ti rotor at 246,000 x *g* at 4°C. Seven equal fractions (approximately 700 µl each) were collected, starting from the top of the gradient. Dot blotting onto nitrocellulose was performed using 225 µL per fraction and probed with the anti-gB PAb R68.

Surface plasmon resonance (biosensor) experiments to detect gB-liposome binding. Surface plasmon resonance (SPR) experiments were performed using a Biacore 3000 or Biacore X100 optical biosensor (GE Healthcare, Biacore Life Sciences) at 25°C. Filtered and degassed HBS-N buffer (10 mM HEPES pH 7.4, 150 mM NaCl) was used in all liposome association experiments. We used an L1 sensor chip (Biacore) as it has a hydrophobic surface capable of binding liposomes. Liposomes were purchased from Encapsula Nanosciences (Nashville, TN) at a size of 400 nm, containing a 1.7:1 molar ratio of soy-phosphatidylcholine to cholesterol. To prepare the chip surface for liposome binding, it was washed sequentially with 20 µl of 1% octyl-β-D-glucopyranoside, 20 µl of 0.5% SDS, 10 µl of 1% octyl-β-D-glucopyranoside, and 10 µl of 30% ethanol. Liposomes (1 mM, diluted in HBS-N) were injected until the chip was saturated, giving a signal of approximately 8500 response units (RU). Once bound, the liposomes remained on the chip and there was no appreciable dissociation (no measurable off-rate). Purified soluble proteins diluted in HBS-N buffer were then individually injected at various concentrations (achieved by dilution in HBS-N buffer) at a flow rate of 5 mL/min. After injection of the soluble protein was complete (typically 20 mL for 240 s), the RU was recorded and used to determine the level of protein binding. After each protein injection the surface preparation protocol was performed to remove protein and liposomes from the

chip, regenerating the surface to the RU baseline.

Gel filtration/ size exclusion chromatography. Size exclusion chromatography of gB (52) was performed on a AKTApurifier equipped with a Superdex S200 (24 mL) column (GE Healthcare) equilibrated with phosphate-buffered saline. The Superdex column was calibrated by using thyroglobulin (669 kDa), ferritin (440 kDa), aldolase (158 kDa), conalbumin (75 kDa), ovalbumin (43 kDa), carbonic anhydrase (29 kDa), ribonuclease A (14 kDa), and aprotinin (6 kDa); blue dextran was used to determine the void volume (GE Healthcare). For each sample, 5 mL of each fraction was separated by SDS-PAGE and the high molecular weight, trimeric, and monomeric forms of gB were visualized by Western blotting with an anti-gB PAb (R68). Fractions that contained mostly trimers/monomers were pooled and tested by SPR for liposome binding.

RESULTS

The crystal structure of HSV-1 gB (Figure 2-1A) was solved using a soluble form of gB truncated at amino acid 730 (gB730t) (23) to avoid the hydrophobic membrane proximal residues (730-773) just upstream of the transmembrane region (TMR) that might impair crystal formation (10, 40). The form of HSV gB used for crystallization ended at amino acid 730, leaving the fusion loop region exposed (23). Residues downstream of amino acid 730 were initially excluded for crystallization trials due to their elevated hydrophobicity, which could impede crystal formation. We hypothesized that these 43 amino acids, constituting the membrane proximal region (MPR) of gB,

obscure the fusion loops and prevent them from interacting with a target membrane until gB is "activated" for fusion (21). We assumed that these residues are in close proximity to the fusion loops based on the gB crystal structure (Figure 2-1A, yellow).

MPR deletions impair HSV gB transport. To determine if the MPR regulated the ability of the fusion loops to associate with membranes, we first constructed seven MPR deletion mutants (within the context of full-length gB) (Figure 2-1B). The N-terminal half of the MPR was deleted in gBD(730-747) and the C-terminal half was deleted in gBD(748-773). The remaining mutants contained smaller deletions spanning the MPR: gBD(730-739), gBD(735-744), gBD(740-749), gBD(750-759), and gBD(765-773). All mutants were efficiently expressed in B78-C10 cells, as seen by Western blots of total cell lysates (Figure 2-2A). However, when intact transfected cells were tested by CELISA, all of the deletion mutants were poorly expressed (<30% that of gB-WT) on the cell surface, indicating that although the mutants were expressed they were inefficiently transported to the cell surface (Figure 2-2B, black bars). Consequently, none were able to function in a cell-cell fusion assay (Figure 2-2B, gray bars). Thus, as seen in other studies (43, 62), deletion of even small sections of the gB MPR has a negative impact on proper protein folding and transport.

Construction of soluble, MPR-containing gBs. To characterize the biochemical properties of the gB MPR, we created and purified a series of soluble gB ectodomains (no TMR or endodomain) that lack portions of the MPR. We previously characterized the gB

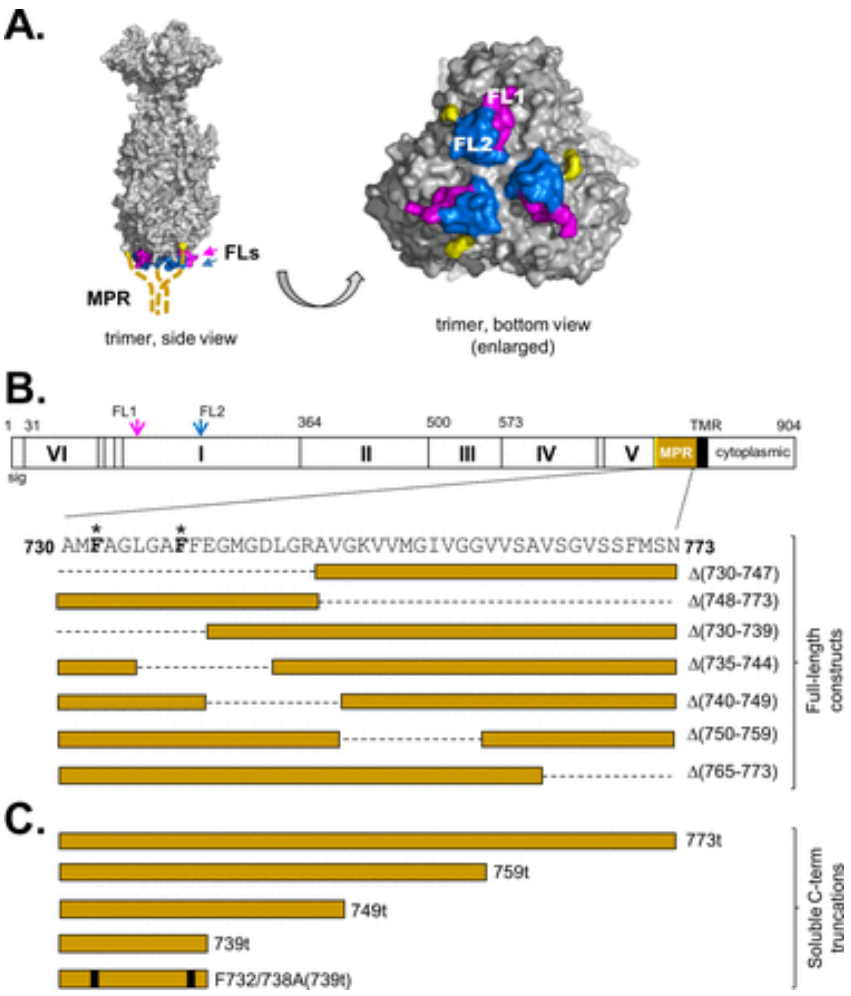

Figure 2-1. (A) Surface representation of the gB trimer. Residues of FL1 (from all 3 monomers) are shown in pink while those of FL2 are shown in blue. The C-termini of the solved gB monomers are highlighted (yellow). The unsolved MPRs (amino acids 730-773) of each protomer are represented as dashed, tan lines emanating from the gB monomer C-termini. FL1 and FL2 of one protomer are labeled in the bottom view of the trimer. (B) Stick figure of a gB protomer, showing its structural domains (Roman

numerals). FL1 and FL2 are indicated with arrows, colored as in (A). Amino acid numbers are shown along the top. The MPR is highlighted in tan and its residues are in expanded view below. Residues that were mutated in this study are highlighted in bold and starred. Deletion mutants are designated as boxes and aligned below the MPR amino acids, with a dashed line indicating deleted residues in the full-length protein. (C) Stick representation of the soluble C-terminal truncation mutants generated in this study. The point mutations F732A and F738A are indicated as black bars. Sig, signal sequence. TMR, transmembrane region.

ectodomain gB(730t), lacking all of the MPR, and found that it remains oligomeric, retains all of its major epitopes, and associates with liposomes (12, 20, 23). Here, we compared it with both soluble forms of gB bearing partial MPRs [gB(759t), gB(749t), gB(739t)] and a complete ectodomain containing the full MPR, gB(773t) (Figure 2-1C). All were expressed and secreted into the supernatant of baculovirus-infected cells (Figure 2-3A). When the proteins were examined on a non-denaturing gel, all contained both monomeric and trimeric forms of gB (Figure 2-3A, bottom panel). Although all of the truncated proteins were recognized by MAbs with trimer-specific, conformation-dependent epitopes (DL16, SS55), indicative of proper protein folding, gB(759t) appeared to react less well (Figure 2-3B). All MPR-containing gBs also retained their ability to react with MAbs with epitopes in each functional region (data not shown).

Presence of the MPR affects binding of soluble gB to liposomes.

(i) Analysis by liposome flotation. We previously observed that the MPR-less soluble gB(730t) interacts *in vitro* with liposomes when the two are mixed (12, 20), presumably recapitulating the interaction of the gB fusion loops with the cell membrane during virus-cell fusion. Initially, we used the liposome flotation assay to assess whether the MPR, or portions of it, interfered with this interaction. Purified soluble proteins were individually incubated with liposomes (phosphatidylcholine-cholesterol) at 37^{o}C. Each protein-liposome mixture was then adjusted to 40% sucrose, layered beneath a sucrose step gradient and centrifuged to allow the liposomes and any associated proteins to float to the top, while proteins that failed to bind liposomes would remain at the bottom of the

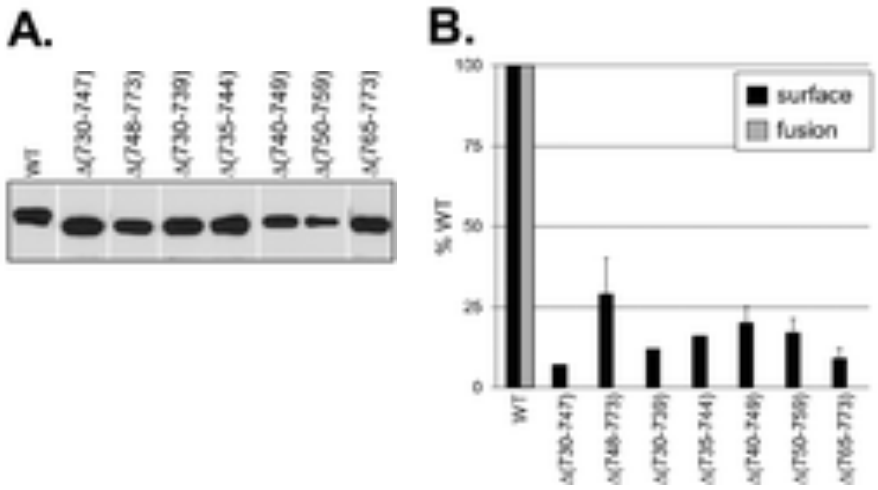

Figure 2-2. Characterization of gB MPR deletion mutants. (A) Full-length MPR mutants were expressed in mammalian cells and total cell extracts were analyzed by denaturing Western blot. Blots were probed with the anti-gB PAb R68. (B) Protein surface expression as detected by CELISA (black bars). Transfected CHO-K1 cells were fixed with 3% paraformaldehyde, then incubated with the anti-gB PAb R69 and GAM-HRP. Cells transfected with empty vector DNA were used as a negative control, and this value was subtracted from the other experimental samples. Quantitative cell-cell fusion assay (gray bars) was performed with co-cultivation of target CHOK1 cells (expressing the luciferase protein and the HSV receptor HVEM) with effector CHO cells (expressing T7 polymerase, gD, gH and gL, plus either WT gB, mutant gB, or empty vector DNA). Cell extracts were tested for light production 18 h later. Percent WT was calculated as follows: for CELISA = (sample absorbance / WT absorbance) x 100; for fusion assay = (relative light units (RLU) of test sample/ RLU of WT) x 100.

gradient. The liposome-containing (top) fractions were analyzed by dot blot using a polyclonal anti-gB antibody for visualization (Figure 2-3C). As previously observed (20), gB(730t) was not detected in the upper fractions in the absence of liposomes, but floated to the top of the gradient in their presence. In the case of the MPR-containing gBs, the ability to co-associate with liposomes decreased markedly. The data shown in Figure 2-3C suggests there might be a small difference in binding between gB(739t) and gB(773t) but this type of analysis is not quantitative. Therefore, we turned to surface plasmon resonance (SPR, biosensor) to get a more accurate measurement of liposome binding (8).

(ii) Analysis by SPR/biosensor. Liposome are able to bind to the lipophilic L1 chip of the Biacore instrument, which detects mass changes by SPR (1). In this assay, liposomes were first injected and flowed across an L1 chip surface and liposome binding, i.e. the mass change due to binding, was detected as an increase in response units (RU) (Figure 2-4A). Approximately 8500 RU of liposomes were sufficient to saturate each flowcell of the chip and this amount was used in each experiment. Next, each gB protein was added and allowed to flow across the chip for 240 s. An increase in RU was indicative of protein binding to the immobilized liposomes. It is this second response curve (gB-liposome binding, Figure 2-4A, framed) that is shown in Figs. 4B-E. To set up the appropriate binding conditions for our proteins, we first compared gB(730t), known to bind liposomes in a flotation assay, to both the fusion loop mutant gB-W174R(730t) and to gD(306t), two proteins which do not bind liposomes (20). As expected, gB(730t)

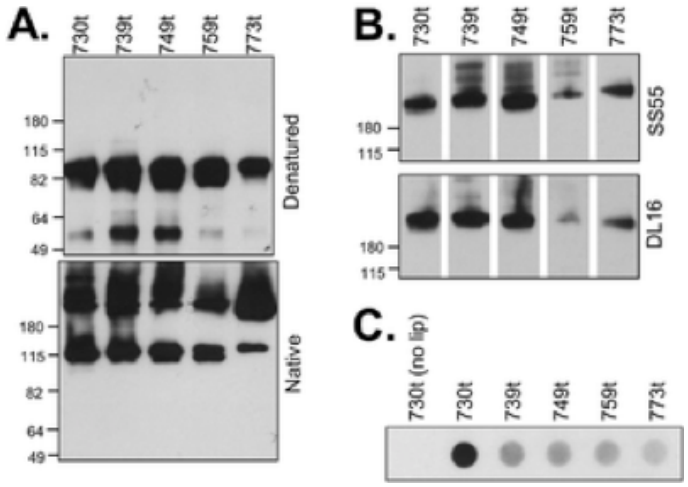

Figure 2-3. Soluble gB MPR-containing proteins are expressed and folded correctly. (A) Four gB mutants (739t, 749t, 759t, 773t) were cloned and expressed in a baculovirus expression system as secreted forms each truncated after the indicated amino acid. Proteins were detected with the PAb R69 and visualized by denaturing (top panel) or "native" (bottom panel) Western blot. (B) Reactivity of gB MPR-containing proteins with the conformation-dependent MAbs SS55 (top panel) or DL16 (bottom panel) via "native" Western blot. Molecular weight standards are shown on the left in kilodaultons for both (A) and (B). (C) Liposome flotation assay. Purified soluble glycoproteins were incubated with liposomes for 1 h at 37^{o}C. Samples were then adjusted to 1M KCl, incubated for an additional 15 min and then layered beneath a discontinuous 5-40% sucrose gradient, centrifuged for 3 h, and then fractionated. The top, liposome-containing fraction was analyzed by dot blot with the PAb R68.

readily bound to the immobilized liposomes, as indicated by the increase in RU, while gB-W174R(730t) and gD(306t) did not (Figure 2-4B). Furthermore, gB(730t) bound to liposomes in a dose-dependent manner, showing an increase in RU from 0.08 mM to 5 mM of protein (Figure 2-4C). Thus, we demonstrated that biosensor analysis yields reproducible and quantitative data on membrane binding by soluble glycoproteins.

The liposome binding capacity of the MPR-containing gB forms was then analyzed within the same range of protein concentrations as used for gB(730t). We found that gB(773t), which contains the complete MPR, bound to liposomes in a dose-dependent manner, albeit at a much lower level than seen for gB(730t) (compare Figure 2-4C and 2-4D). Although, curve-fitting for kinetic analysis (1) was not possible with our data sets, possibly due to complications associated with liposome binding. None of the MPR-containing gB truncations bound to liposomes as well as gB(730t), although all exhibited a low level of measurable binding (Figure 2-4E), especially when compared to the two negative controls (Figure 2-4B). Of importance, we detected no significant differences in gB-liposome binding between proteins containing portions of or the complete MPR [gB(739t), gB(749t), gB(759t), or gB(773t)]. Upon averaging the maximum binding from several experiments (i.e. after two minutes of injection of 0.16 mM gB) we determined that gB(739t) bound to liposomes at a level that was 35% of that of gB(730t), gB(749t) 38%, gB(759t) 29%, and gB(773t) 46% (Figure 2-4F). In comparison, the negative control gB-W174R(730t) bound at 18% that of gB(730t). The data show that the presence of the first nine amino acids of the MPR (residues 731-739) are sufficient to significantly diminish the association of gB with liposomes.

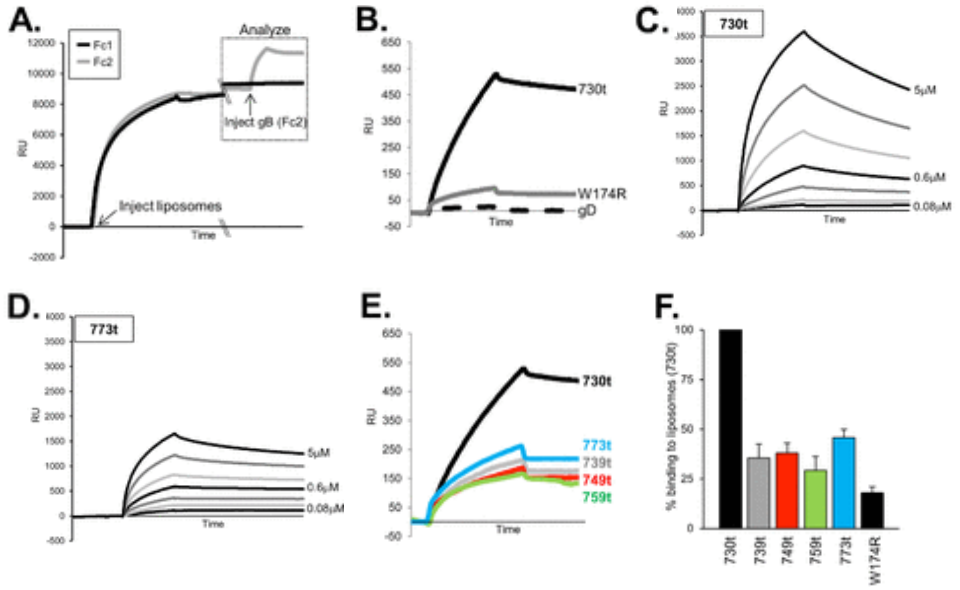

Figure 2-4. Liposome binding assay, biosensor analysis. (A) Liposomes are injected and flowed across flowcell (Fc) 1 and Fc2, with binding at saturation [~8500 RU (response units)]. Soluble gB(730t) is then injected across Fc2 at 5 mL/min for 240 s and binding to liposomes is measured as an increase in RU; this portion of the graph (boxed) is shown and analyzed in subsequent figures. A double-slash denotes a break in the x-axis (no injections were performed during that time period). (B) Response curve showing binding of control proteins gB(730t) (positive control), fusion loop mutant gB-W174R(730t) (negative control), and soluble gD (negative control). Two-fold serial dilutions of gB(730t) (C) or gB(773t) (D) were injected across the liposome-coated flow cell at 10 µl/min for 2 minutes to evaluate ligand-liposome association. After each injection the surface preparation protocol was performed to remove protein and liposomes from the chip, regenerating the surface to the RU baseline. (E) Each soluble

protein (156 nM) was flowed across an L1 chip containing immobilized liposomes as described in (A). Flow rate was 5 mL/min. (F) Bar graph representation of gB-liposome binding via biosensor. The graph displays an average of at least 3 separate experiments, with samples presented as percent binding of gB(730t) (set at 100%). Error bars represent percent error.

The decrease in liposome binding is not due to aggregation of the MPR mutants.

Our data suggest that the MPR specifically obscures the fusion loops and prevents their interaction with lipids; however, another possibility is that the hydrophobic character of the MPR promotes gB aggregation, possibly obscuring the fusion loops non-specifically and preventing binding to membranes/lipids. To address this issue, we used gel filtration to separate out any high molecular weight (HMW, i.e., aggregated) gB species from those fractions predominantly containing gB trimers (Figure 2-5, left panels). We then tested the pooled trimeric fractions for liposome binding using SPR (Figure 2-5, right panels). Each protein was chromatographed by size exclusion on a sepharose column as previously described (52). Multiple fractions were obtained and evaluated by Western blotting and a representative group of data is shown in Figure 2-5. The bulk of gB(730t) eluted in the trimeric fractions (boxed in Figure 2-5A) and much less was found in the earlier, HMW fractions. In contrast, the bulk of the MPR-containing gBs (represented by gB(749t) in Figure 2-5B) was in the HMW fractions (Figure 2-5B and data not shown). For each protein, the trimeric fractions were pooled and equal concentrations of protein were injected over the liposome-L1 chip. As expected, the trimeric pool of gB(730t) bound well to liposomes (Figure 2-5A, right panel). Importantly, the trimeric pools of MPR-containing gBs were unable to bind liposomes, as exemplified by gB(749t) (Figure 2-5B). Indeed, the modest binding of unfractionated gB(749t) was substantially reduced by removal of the HMW material, suggesting that its binding was due to non-specific association of aggregated material. Together, our results indicate that aggregation of MPR-containing gB does not prevent liposome binding, but instead indicate that MPR-

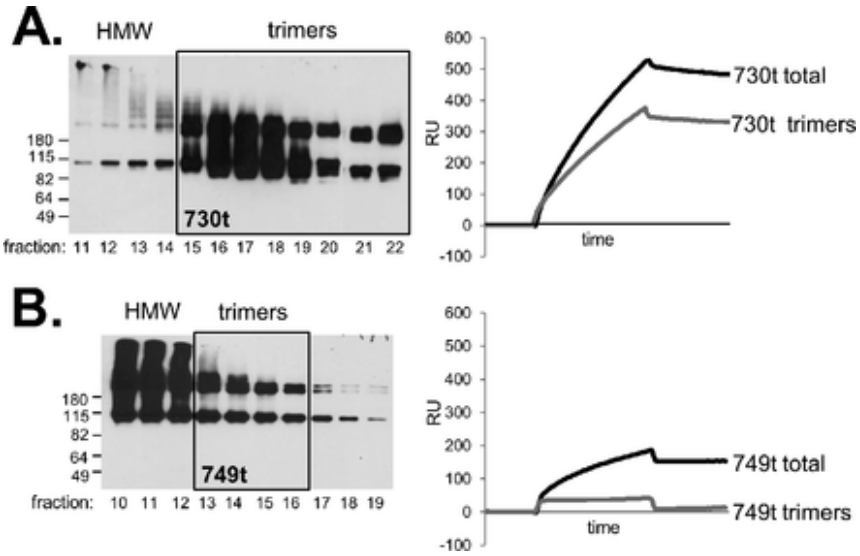

Figure 2-5. Gel filtration/size exclusion chromatography of (A) gB(730t) and (B) gB(773t). Fractions containing mostly trimeric (boxed in the Western blot) species were tested via biosensor for liposome binding at 156nM gB for 240 s. Fractions containing high molecular weight species (HMW, samples to the right of the box on the Western blot) were excluded from study. "Total" refers to the gB sample before it underwent gel filtration.

containing gB trimers are specifically compromised in their liposome-binding ability as compared to gB(730t), presumably due to the FLs being obscured by the MPR.

A double point mutation within the MPR restores gB-liposome binding. Because mutants such as gB-W174R(730t) do not bind liposomes (Figure 2-4B), it is clear that association of gB(730t) with lipid membranes occurs via its fusion loops (20). Here we have shown that the first nine residues of the MPR are sufficient to reduce this binding (Figure 2-4E-F). Among residues 731-739 (MFAGLGAFF) there are four hydrophobic amino acids: F732, L735, F738, and F739. These residues could stabilize the MPR and through their side chains possibly form contacts with the fusion loops or surrounding residues. To address the role of these nine residues, we selected F732 and F738, as based on our model they were most likely to form such contacts (Figure 2-6A), and mutated them to alanine, creating a double point mutant within the context of gB(739t), gB-F732/738A(739t) (Figure 2-1C). We predicted that this mutant would prevent putative interactions between the MPR and the underlying residues of the fusion loops (modeled in Figure 2-6A) and therefore might improve gB-liposome binding in the context of gB(739t). The mutant protein was recognized by MAbs against conformation-dependent epitopes, indicating that it was properly folded (Figure 2-6B). Unlike its parent protein gB(739t), very few HMW species were observed when gB-F732/738A(739t) was analyzed by gel filtration (Figure 2-6C). Interestingly, biosensor analysis revealed that

gB-F732/738A(739t) bound liposomes much better than gB(739t) and nearly as well as gB(730t) (Figure 2-6D). These data suggest that the phenylalanine mutations compromise the ability of the MPR to shield the fusion loops, permitting their exposure and subsequent association with lipid membranes.

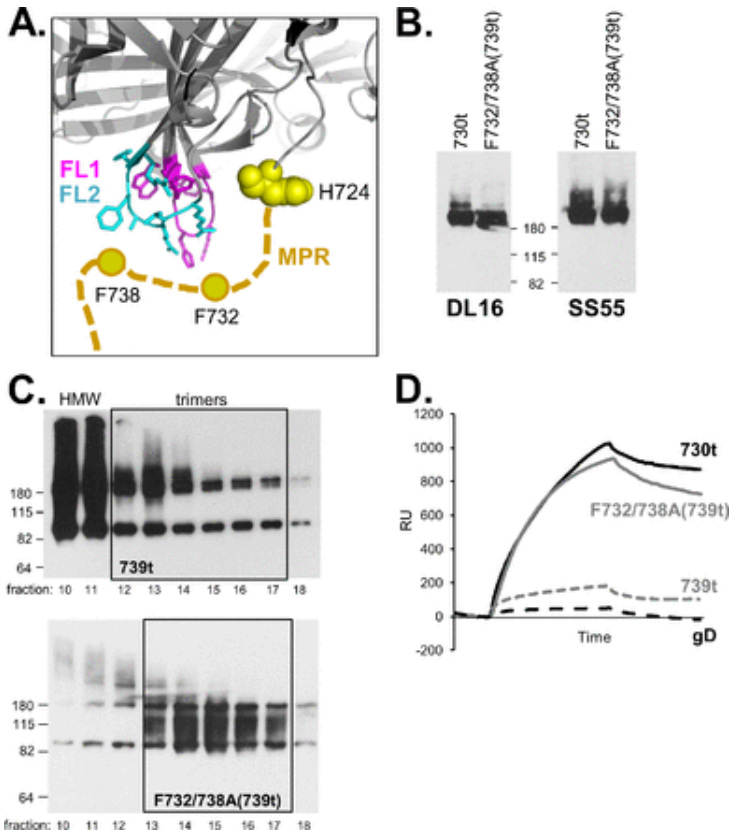

Figure 2-6. (A) Model of a possible interaction between the gB fusion loops and MPR. The gB trimer is rendered in cartoon form in gray, focusing on the fusion loops (FL1 pink, FL2 blue) and C-terminus of one of the protomers (H724, yellow spheres). Side-chains of both fusion loops are shown. The MPR is depicted as a gold dashed line, with the aromatic residues F732 and F738 represented as circles. (B) Native Western blot of soluble gB proteins, probed with the indicated MAbs. Molecular weight standards are shown between the two blots in kilodaultons. (C) Native Western blot of gel filtration fractions as described in Figure 2-5. (D) gB-liposome binding assay (biosensor analysis) as described in Figure 2-4A. Soluble gB(730t) served as the positive control and soluble gD as the negative control.

DISCUSSION

Both class I and class II viral fusion proteins have their fusion peptides/loops buried inside the molecule in the pre-fusion form (59). Here, we suggest that for the class III fusion protein HSV gB, the MPR serves this role. Soluble gB ectodomains containing various lengths of the MPR were all reduced in liposome binding as compared to the MPR-less gB(730t); this included gB(739t), which contains only nine MPR residues. Mutation of two phenylalanine residues to alanine (F732A/F738A) in the gB(739t) MPR sequence restored the ability of this protein to bind liposomes. We believe that substitution of alanine residues for F732 and F738 disrupts the association of the MPR with the fusion loops, thereby allowing the fusion loops to be unimpeded and now able to bind lipid membranes. Our data are consistent with a role for the MPR in regulating the lipid association capability of the gB fusion loops.

Use of biosensor to evaluate gB-liposome binding. To study gB-liposome interactions, we used SPR/biosensor in addition to our previously described liposome flotation assay (12, 20). SPR has been used in the HIV field to dissect antibody-MPR (of the viral fusion protein gp41)-liposome binding (reviewed in (22)). Here we have applied it to the HSV fusion protein, gB. Since liposomes remain as individual vesicles when bound to an L1 sensor chip (2), as they do with liposome flotation, the two assays should be in agreement to measure protein-liposome interactions. Measuring liposome binding by SPR has several advantages over the standard flotation assay. First, it is far easier and faster to measure binding, as multiple samples can be analyzed on a single chip.

Moreover, SPR allows for real-time measurement of gB-liposome binding whereas the flotation assay relies on a secondary observation (antibody binding on a dot or Western blot) taking place approximately 6 hours after the proteins and liposomes are co-incubated. The quantitative nature of the biosensor also allowed us to compare percent binding of each experimental sample to wild type [in this case, MPR-containing gBs, gB fusion loop mutants, or gD to gB(730t)].

The HSV gB MPR is sensitive to mutation. Unlike the MPRs of other fusion proteins (24, 34, 50, 57, 64), the MPR of gB is particularly sensitive to deletion (43) (Figure 2-2). While our data point to MPR residues 731-739 as having a role in modulating fusion, the remainder of the MPR remains essential at the very least for protein folding and transport; this may be due to hydrophobic residues in the FLs or the MPR being recognized by ER chaperones, leading to ER retention. While deletions within the gB MPR are detrimental in the context of full-length proteins, deletion of the MPR in soluble gB ectodomains does not affect protein expression in our baculovirus system (nor does inclusion of the MPR). Although the soluble gB ectodomain is believed to be in a post-fusion form, we are hypothesizing that the MPR functions as a fusion loop "mask" even when gB is in a pre-fusion form prior to fusion. In fact, a pre-fusion structure of VSV G (47) and model of EBV gB (5) suggest that structural domain I, which contains the fusion loops, remains in the same relative conformation both pre- and post-fusion, suggesting that this strategy is sound. In further support, the FLs remain in close proximity to the ectodomain C-terminus (and therefore MPR) in both pre- and post-fusion forms.

Previously characterized MPR point mutants in full-length HSV-1 gB were found to be complementation-defective for gB-null virus and exhibited a slower rate of entry, although two of the four mutants characterized were also defective in protein trafficking (58). None of these point mutants were within residues 731-739, which we have defined as having an effect on liposome binding. In additional experiments, we found that separate mutation of F732A or F738A (in the context of full-length gB) had no effect on cell surface expression yet each had a negative effect on cell-cell fusion (data not shown). This result is in accordance with our data from the soluble gB-F732/738A double mutant. We predict that the decrease in cell-cell fusion would be explained by premature "triggering" of the FL, due to disruption of important MPR contacts required to maintain gB in a pre-fusion form. It is of note that gB residue F738 is conserved in all alphaherpesviruses (23, 58).

Role of the MPR in other viruses. MPR mutations in both VSV G (24) and baculovirus gp64 (34) abolish fusion but do not affect cell surface protein expression, indicative of a role for the MPR in the function of these proteins. In the VSV G, the amino acids upstream of the TMR in the linear sequence are modeled as "stretching" from the top of the protein structure (crown) down to the transmembrane region in the post-fusion structure (46), and this region is hypothesized to act as a flexible tether for positioning of the fusion protein between the viral and cellular lipid bilayers (45). Unlike the gB fusion loops, those of baculovirus gp64 are hypothesized to have a second role, in virus-cell attachment (26, 63). Therefore, one would expect the triggering of gp64 fusion loops

would occur earlier in the pathway (to facilitate virus-cell attachment) than for gB (to initiate virus-cell fusion), leaving the MPRs of gp64 and gB to perhaps serve different functions.

How might the gB MPR and FLs work together? There are several hypotheses on what triggers gB activation, thereby exposing the fusion loops and promoting fusion of the virus and cell membranes (59). A low pH, "histidine switch" model has been proposed for gp64 (33) and was also tested for HSV gB by Heldwein and colleagues (54), who found that only one of the two fusion loops (FL2, containing H263) changed conformation at low pH; the bulk of the soluble gB(730t) remained unchanged in structure. Although this work was done on soluble gB (thought to be in the post-fusion conformation), it fits with a pre-fusion model of EBV gB which predicts that domain I (containing the FLs) retains its fold between pre- and post-fusion forms (5). Therefore, we suggest that the change in FL2 in response to low pH is sufficient to disengage the FLs from the MPR and expose them to lipids. Indeed, when gB(739t) was incubated at pH 5, its ability to bind liposomes increased to 68% that of gB(730t) (data not shown). However, we need to keep in mind that HSV gB also functions at neutral pH in certain cell types (17, 36, 38, 60) and activation may occur through gHgL-gB interactions (3, 4), and perhaps even the gB cytoplasmic tail (51). Regardless of these possibilities, our data highlight the importance of the MPR in regulating exposure of the gB fusion loops and suggest they play a critical role in maintaining gB in an inactive form, i.e. unable to insert its fusion loops into a target membrane until it is triggered to execute virus-cell fusion.

REFERENCES

1. 2007. Biacore X-100 Handbook, AC ed. General Electric Company.
2. **Anderluh, G., M. Besenicar, A. Kladnik, J. H. Lakey, and P. Macek.** 2005. Properties of nonfused liposomes immobilized on an L1 Biacore chip and their permeabilization by a eukaryotic pore-forming toxin. Analytical biochemistry **344:**43-52.
3. **Atanasiu, D., W. T. Saw, G. H. Cohen, and R. J. Eisenberg.** 2010. Cascade of events governing cell-cell fusion induced by herpes simplex virus glycoproteins gD, gH/gL, and gB. J Virol **84:**12292-12299.
4. **Atanasiu, D., J. C. Whitbeck, M. P. de Leon, H. Lou, B. P. Hannah, G. H. Cohen, and R. J. Eisenberg.** 2010. Bimolecular complementation defines functional regions of herpes simplex virus gB that are involved with gH/gL as a necessary step leading to cell fusion. J Virol **84:**3825-3834.
5. **Backovic, M., R. Longnecker, and T. S. Jardetzky.** 2009. Structure of a trimeric variant of the Epstein-Barr virus glycoprotein B. Proc Natl Acad Sci U S A **106:**2880-2885.
6. **Bender, F. C., M. Samanta, E. E. Heldwein, M. P. de Leon, E. Bilman, H. Lou, J. C. Whitbeck, R. J. Eisenberg, and G. H. Cohen.** 2007. Antigenic and mutational analyses of herpes simplex virus glycoprotein B reveal four functional regions. J Virol **81:**3827-3841.

7. **Bender, F. C., J. C. Whitbeck, M. Ponce de Leon, H. Lou, R. J. Eisenberg, and G. H. Cohen.** 2003. Specific association of glycoprotein B with lipid rafts during herpes simplex virus entry. J Virol **77:**9542-9552.

8. **Besenicar, M., P. Macek, J. H. Lakey, and G. Anderluh.** 2006. Surface plasmon resonance in protein-membrane interactions. Chemistry and physics of lipids **141:**169-178.

9. **Browne, H., B. Bruun, and T. Minson.** 2001. Plasma membrane requirements for cell fusion induced by herpes simplex virus type 1 glycoproteins gB, gD, gH and gL. J Gen Virol **82:**1419-1422.

10. **Bzik, D. J., B. A. Fox, N. A. DeLuca, and S. Person.** 1984. Nucleotide sequence specifying the glycoprotein gene, gB, of herpes simplex virus type 1. Virology **133:**301-314.

11. **Cairns, T. M., L. S. Friedman, H. Lou, J. C. Whitbeck, M. S. Shaner, G. H. Cohen, and R. J. Eisenberg.** 2007. N-terminal mutants of herpes simplex virus type 2 gH are transported without gL but require gL for function. J Virol **81:**5102-5111.

12. **Cairns, T. M., J. C. Whitbeck, H. Lou, E. E. Heldwein, T. K. Chowdary, R. J. Eisenberg, and G. H. Cohen.** 2011. Capturing the herpes simplex virus core fusion complex (gB-gH/gL) in an acidic environment. J Virol **85:**6175-6184.

13. **Cohen, G. H., V. J. Isola, J. Kuhns, P. W. Berman, and R. J. Eisenberg.** 1986. Localization of discontinuous epitopes of herpes simplex virus glycoprotein D:

use of a nondenaturing ("native" gel) system of polyacrylamide gel electrophoresis coupled with Western blotting. J Virol **60:**157-166.

14. **Connolly, S. A., J. O. Jackson, T. S. Jardetzky, and R. Longnecker.** 2011. Fusing structure and function: a structural view of the herpesvirus entry machinery. Nat Rev Microbiol **9:**369-381.

15. **Doms, R. W., A. Helenius, and J. White.** 1985. Membrane fusion activity of the influenza virus hemagglutinin. The low pH-induced conformational change. J Biol Chem **260:**2973-2981.

16. **Eisenberg, R. J., D. Atanasiu, T. M. Cairns, J. R. Gallagher, C. Krummenacher, and G. H. Cohen.** 2012. Herpes virus fusion and entry: a story with many characters. Viruses **4:**800-832.

17. **Fuller, A. O., and P. G. Spear.** 1987. Anti-glycoprotein D antibodies that permit adsorption but block infection by herpes simplex virus 1 prevent virion-cell fusion at the cell surface. Proc Natl Acad Sci U S A **84:**5454-5458.

18. **Gibbons, D. L., M. C. Vaney, A. Roussel, A. Vigouroux, B. Reilly, J. Lepault, M. Kielian, and F. A. Rey.** 2004. Conformational change and protein-protein interactions of the fusion protein of Semliki Forest virus. Nature **427:**320-325.

19. **Handler, C. G., R. J. Eisenberg, and G. H. Cohen.** 1996. Oligomeric structure of glycoproteins in herpes simplex virus type 1. J Virol **70:**6067-6070.

20. **Hannah, B. P., T. M. Cairns, F. C. Bender, J. C. Whitbeck, H. Lou, R. J. Eisenberg, and G. H. Cohen.** 2009. Herpes simplex virus glycoprotein B associates with target membranes via its fusion loops. J Virol **83:**6825-6836.

21. **Hannah, B. P., E. E. Heldwein, F. C. Bender, G. H. Cohen, and R. J. Eisenberg.** 2007. Mutational evidence of internal fusion loops in herpes simplex virus glycoprotein B. J Virol **81:**4858-4865.

22. **Hearty, S., P. J. Conroy, B. V. Ayyar, B. Byrne, and R. O'Kennedy.** 2010. Surface plasmon resonance for vaccine design and efficacy studies: recent applications and future trends. Expert review of vaccines **9:**645-664.

23. **Heldwein, E. E., H. Lou, F. C. Bender, G. H. Cohen, R. J. Eisenberg, and S. C. Harrison.** 2006. Crystal structure of glycoprotein B from herpes simplex virus 1. Science **313:**217-220.

24. **Jeetendra, E., K. Ghosh, D. Odell, J. Li, H. P. Ghosh, and M. A. Whitt.** 2003. The membrane-proximal region of vesicular stomatitis virus glycoprotein G ectodomain is critical for fusion and virus infectivity. J Virol **77:**12807-12818.

25. **Jeetendra, E., C. S. Robison, L. M. Albritton, and M. A. Whitt.** 2002. The membrane-proximal domain of vesicular stomatitis virus G protein functions as a membrane fusion potentiator and can induce hemifusion. J Virol **76:**12300-12311.

26. **Kadlec, J., S. Loureiro, N. G. Abrescia, D. I. Stuart, and I. M. Jones.** 2008. The postfusion structure of baculovirus gp64 supports a unified view of viral fusion machines. Nat Struct Mol Biol **15:**1024-1030.

27. **Kielian, M., M. R. Klimjack, S. Ghosh, and W. A. Duffus.** 1996. Mechanisms of mutations inhibiting fusion and infection by Semliki Forest virus. J Cell Biol **134:**863-872.

28. **Kielian, M., and F. A. Rey.** 2006. Virus membrane-fusion proteins: more than one way to make a hairpin. Nat Rev Microbiol **4:**67-76.

29. **Killian, J. A., and G. von Heijne.** 2000. How proteins adapt to a membrane-water interface. Trends Biochem Sci **25:**429-434.

30. **Kinzler, E. R., and T. Compton.** 2005. Characterization of human cytomegalovirus glycoprotein-induced cell-cell fusion. J Virol **79:**7827-7837.

31. **Lamb, R. A., R. G. Paterson, and T. S. Jardetzky.** 2006. Paramyxovirus membrane fusion: lessons from the F and HN atomic structures. Virology **344:**30-37.

32. **Lazear, E., A. Carfi, J. C. Whitbeck, T. M. Cairns, C. Krummenacher, G. H. Cohen, and R. J. Eisenberg.** 2008. Engineered disulfide bonds in herpes simplex virus type 1 gD separate receptor binding from fusion initiation and viral entry. J Virol **82:**700-709.

33. **Li, Z., and G. W. Blissard.** 2011. Autographa californica multiple nucleopolyhedrovirus GP64 protein: roles of histidine residues in triggering membrane fusion and fusion pore expansion. J Virol **85:**12492-12504.

34. **Li, Z., and G. W. Blissard.** 2009. The pre-transmembrane domain of the Autographa californica multicapsid nucleopolyhedrovirus GP64 protein is critical for membrane fusion and virus infectivity. J Virol **83:**10993-11004.

35. **Lin, E., and P. G. Spear.** 2007. Random linker-insertion mutagenesis to identify functional domains of herpes simplex virus type 1 glycoprotein B. Proc Natl Acad Sci U S A **104:**13140-13145.

36. **Milne, R. S., A. V. Nicola, J. C. Whitbeck, R. J. Eisenberg, and G. H. Cohen.** 2005. Glycoprotein D receptor-dependent, low-pH-independent endocytic entry of herpes simplex virus type 1. J Virol **79:**6655-6663.

37. **Modis, Y., S. Ogata, D. Clements, and S. C. Harrison.** 2004. Structure of the dengue virus envelope protein after membrane fusion. Nature **427:**313-319.

38. **Nicola, A. V., A. M. McEvoy, and S. E. Straus.** 2003. Roles for endocytosis and low pH in herpes simplex virus entry into HeLa and Chinese hamster ovary cells. J Virol **77:**5324-5332.

39. **Okuma, K., M. Nakamura, S. Nakano, Y. Niho, and Y. Matsuura.** 1999. Host range of human T-cell leukemia virus type I analyzed by a cell fusion-dependent reporter gene activation assay. Virology **254:**235-244.

40. **Pellett, P. E., K. G. Kousoulas, L. Pereira, and B. Roizman.** 1985. Anatomy of the herpes simplex virus 1 strain F glycoprotein B gene: primary sequence and predicted protein structure of the wild type and of monoclonal antibody-resistant mutants. J Virol **53:**243-253.

41. **Pertel, P. E.** 2002. Human herpesvirus 8 glycoprotein B (gB), gH, and gL can mediate cell fusion. J Virol **76:**4390-4400.

42. **Pertel, P. E., A. Fridberg, M. L. Parish, and P. G. Spear.** 2001. Cell fusion induced by herpes simplex virus glycoproteins gB, gD, and gH-gL requires a gD receptor but not necessarily heparan sulfate. Virology **279:**313-324.

43. **Rasile, L., K. Ghosh, K. Raviprakash, and H. P. Ghosh.** 1993. Effects of deletions in the carboxy-terminal hydrophobic region of herpes simplex virus

glycoprotein gB on intracellular transport and membrane anchoring. J Virol **67:**4856-4866.

44. **Rey, F. A., F. X. Heinz, C. Mandl, C. Kunz, and S. C. Harrison.** 1995. The envelope glycoprotein from tick-borne encephalitis virus at 2 A resolution. Nature **375:**291-298.

45. **Roche, S., A. A. Albertini, J. Lepault, S. Bressanelli, and Y. Gaudin.** 2008. Structures of vesicular stomatitis virus glycoprotein: membrane fusion revisited. Cell Mol Life Sci **65:**1716-1728.

46. **Roche, S., S. Bressanelli, F. A. Rey, and Y. Gaudin.** 2006. Crystal structure of the low-pH form of the vesicular stomatitis virus glycoprotein G. Science **313:**187-191.

47. **Roche, S., F. A. Rey, Y. Gaudin, and S. Bressanelli.** 2007. Structure of the prefusion form of the vesicular stomatitis virus glycoprotein G. Science **315:**843-848.

48. **Roussel, A., J. Lescar, M. C. Vaney, G. Wengler, and F. A. Rey.** 2006. Structure and interactions at the viral surface of the envelope protein E1 of Semliki Forest virus. Structure **14:**75-86.

49. **Rux, A. H., S. H. Willis, A. V. Nicola, W. Hou, C. Peng, H. Lou, G. H. Cohen, and R. J. Eisenberg.** 1998. Functional region IV of glycoprotein D from herpes simplex virus modulates glycoprotein binding to the herpesvirus entry mediator. J Virol **72:**7091-7098.

50. **Salzwedel, K., J. T. West, and E. Hunter.** 1999. A conserved tryptophan-rich motif in the membrane-proximal region of the human immunodeficiency virus type 1 gp41 ectodomain is important for Env-mediated fusion and virus infectivity. J Virol **73:**2469-2480.

51. **Silverman, J. L., N. G. Greene, D. S. King, and E. E. Heldwein.** 2012. Membrane requirement for the folding of the HSV-1 gB cytodomain suggests a unique mechanism of fusion regulation. J Virol.

52. **Silverman, J. L., S. Sharma, T. M. Cairns, and E. E. Heldwein.** 2010. Fusion-deficient insertion mutants of herpes simplex virus type 1 glycoprotein B adopt the trimeric postfusion conformation. J Virol **84:**2001-2012.

53. **Sisk, W. P., J. D. Bradley, R. J. Leipold, A. M. Stoltzfus, M. Ponce de Leon, M. Hilf, C. Peng, G. H. Cohen, and R. J. Eisenberg.** 1994. High-level expression and purification of secreted forms of herpes simplex virus type 1 glycoprotein gD synthesized by baculovirus-infected insect cells. J Virol **68:**766-775.

54. **Stampfer, S. D., H. Lou, G. H. Cohen, R. J. Eisenberg, and E. E. Heldwein.** 2010. Structural basis of local, pH-dependent conformational changes in glycoprotein B from herpes simplex virus type 1. J Virol **84:**12924-12933.

55. **Steven, A. C., and P. G. Spear.** 2006. Biochemistry. Viral glycoproteins and an evolutionary conundrum. Science **313:**177-178.

56. **Suarez, T., W. R. Gallaher, A. Agirre, F. M. Goni, and J. L. Nieva.** 2000. Membrane interface-interacting sequences within the ectodomain of the human

immunodeficiency virus type 1 envelope glycoprotein: putative role during viral fusion. J Virol **74:**8038-8047.

57. **Tong, S., F. Yi, A. Martin, Q. Yao, M. Li, and R. W. Compans.** 2001. Three membrane-proximal amino acids in the human parainfluenza type 2 (HPIV 2) F protein are critical for fusogenic activity. Virology **280:**52-61.

58. **Wanas, E., S. Efler, K. Ghosh, and H. P. Ghosh.** 1999. Mutations in the conserved carboxy-terminal hydrophobic region of glycoprotein gB affect infectivity of herpes simplex virus. J Gen Virol **80 (Pt 12):**3189-3198.

59. **White, J. M., S. E. Delos, M. Brecher, and K. Schornberg.** 2008. Structures and mechanisms of viral membrane fusion proteins: multiple variations on a common theme. Critical reviews in biochemistry and molecular biology **43:**189-219.

60. **Wittels, M., and P. G. Spear.** 1991. Penetration of cells by herpes simplex virus does not require a low pH-dependent endocytic pathway. Virus Res **18:**271-290.

61. **Zhang, Y., W. Zhang, S. Ogata, D. Clements, J. H. Strauss, T. S. Baker, R. J. Kuhn, and M. G. Rossmann.** 2004. Conformational changes of the flavivirus E glycoprotein. Structure **12:**1607-1618.

62. **Zheng, Z., E. Maidji, S. Tugizov, and L. Pereira.** 1996. Mutations in the carboxyl-terminal hydrophobic sequence of human cytomegalovirus glycoprotein B alter transport and protein chaperone binding. J Virol **70:**8029-8040.

63. **Zhou, J., and G. W. Blissard.** 2008. Identification of a GP64 subdomain involved in receptor binding by budded virions of the baculovirus Autographica californica multicapsid nucleopolyhedrovirus. J Virol **82:**4449-4460.

64. **Zhou, J., R. E. Dutch, and R. A. Lamb.** 1997. Proper spacing between heptad repeat B and the transmembrane domain boundary of the paramyxovirus SV5 F protein is critical for biological activity. Virology **239:**327-339.

CHAPTER 3

GENERAL DISCUSSION

HSV entry is a highly regulated process that requires four viral glycoproteins; gD, gH/gL heterodimer, and gB (8, 11). The crystal structures of these core fusion components have been solved and provide detailed information about their structure and function, but much work still needs to be completed to fully understand the HSV entry process (4, 5, 12, 14). The gB MPR was not included in the crystallized gB construct [gB(730t)], so its structural organization is not known (12). In this thesis I investigated the role of the gB MPR in the function and regulation of fusion.

As described in Chapter 2, using a series of gB deletions, truncations, and point mutations we found that the presence of as few as nine MPR residues [gB(739t)] resulted in a decrease in gB's ability to associate with liposomes. We also found mutation of two aromatic residues in gB(739t) to alanine (F732A/F738A) restored liposome binding. In comparison, MPR-less gB [gB(730t)] bound liposomes well via its fusion loops as was observed in our lab's previous work (10). These data are consistent with a critical role for the MPR in regulating exposure of the gB fusion loops, thereby preventing premature association with lipid.

Analysis of the gB ectodomain crystal structure suggests it represents the post-fusion form of the fusion protein based on structural homology with the VSV G post-fusion structure (12, 17-19). Interestingly, in the VSV G pre-fusion and post-fusion structures the FL containing domain undergoes little intra-domain conformational rearrangement. In both the pre-fusion and post-fusion structures the VSV G fusion loops

remain exposed and appear accessible to interact with membranes while the entire domain maintains its overall structure (17-19). Given the structural homology between post-fusion structures of the class III fusion proteins VSV G and HSV gB, we hypothesized that VSV G could be used to model and predict the HSV gB pre-fusion structure. A similar approach was used to create a hypothetical model of pre-fusion EBV gB, but this model has not yet been verified by a pre-fusion EBV gB crystal structure (3). A hypothetical HSV gB pre-fusion organizational model was proposed by John Gallagher and J. Charles Whitbeck in our laboratory (Figure 3-1A). This model predicts the general conformational changes from HSV gB pre-fusion to post-fusion through a pre-hairpin intermediate (Figure 3-1).

The class III fusion protein VSV G's pre-fusion structure revealed exposed fusion loops (19). We hypothesize that HSV gB, and as noted in the previously published model of EBV gB, pre-fusion structures are similar to VSVG, and they will also have exposed fusion loops (3, 17, 19, 22). This is in contrast with the internally buried fusion peptides/loops of class I and class II fusion proteins.

Our proposed pre-fusion gB model lacks the MPR (Figure 3-1A), as the gB post-fusion structure does, but we hypothesized in chapter 2 that the HSV MPR functions to "mask" the fusion loops from premature exposure to membrane (Figure 2-6A). MPR masking of the gB FLs adds another potential layer of regulation to already the complex HSV entry process.

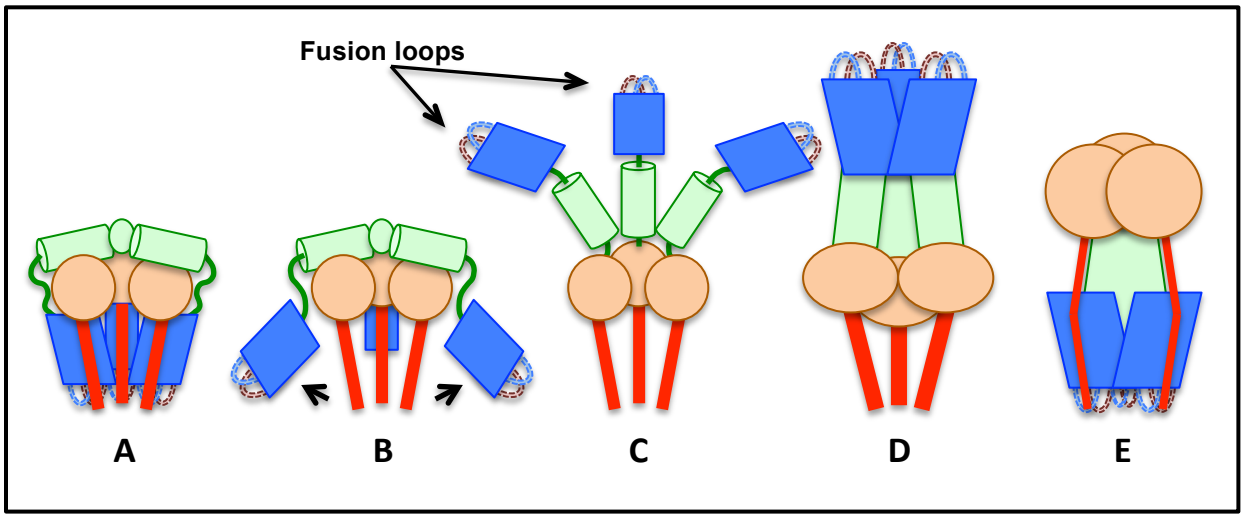

Figure 3-1. Model of conformational changes predicted to occur between the pre-fusion and the post-fusion forms of HSV gB. (A) Shows the pre-fusion form of gB modeled after the published pre-fusion form of VSV G. (B) and (C) depict changes predicted to occur as structural domain 1 (blue; including the fusion loops) disengages from the MPR (not shown) and extends toward the target (host) cell membrane. Arrows indicate direction of movement. (D) shows the fully extended (pre-hairpin) intermediate. Here the fusion loops are predicted to insert into the target membrane. (E) represents the post-fusion structure of gB based on the published crystal structure. Figure provided by John Gallagher and J. Charles Whitbeck.

Regulation of the gB transition from pre-fusion to post-fusion resulting in membrane fusion must require an activation trigger leading to FL exposure. In chapter 2 we suggest a low pH "histidine" switch model as described by Stampfer et al. (21) resulting in a shift in FL2 disengaging the MPR and exposing the FL for membrane interaction. This low pH model is attractive due to the FL2 conformational change noted above, but it does not fit all HSV entry situations. Since HSV does not require low pH to enter all cell types, as described in the introduction, another mechanism is needed for gB activation. The interaction between gB and gH/gL could serve to induce a conformational change in gB that releases the MPR from the FL allowing cellular membrane binding and initiation of fusion reaction (1, 2).

After gB activation and FL exposure the predicted conformational changes proceed from the pre-fusion form through an extended pre-hairpin intermediate to folds to the solved post-fusion gB structure pulling the viral and cellular membranes together (Figure 3-1). Our proposal includes global rearrangements of the gB domains in relation to each other and few changes within domains themselves. Interestingly, in response to low pH the class II fusion protein TBEV E also undergoes large movements of domains, but few conformational changes occur within the individual domains during transition from a dimeric state to a trimeric post-fusion state. Many conclusions can be drawn through analysis of our biochemical assays, functional assays, and comparative fusion protein analysis. Ultimately, HSV gB's ability to facilitate membrane fusion will be best understood by evaluation of a pre-fusion structure, and hopefully intermediate structures as well.

Future directions

In this thesis the role of the MPR has been investigated to provide insight into the regulation and exposure of gB FLs. Not surprisingly this work has generated many new questions. To answer these questions a continuation of the detailed analysis of the interaction between the MPR and the FLs is needed. Using our biochemical and functional assays in combination with an expanded array of MPR and FL mutations we may be able to further identify key interactions between the MPR and FLs. The further refinement of the gB MPR interaction with the FLs may reveal important steps in the regulation of gB-membrane interactions and fusion mechanism.

Arguably the greatest future insight into gB function would be delivered by the capture of a pre-fusion structure. Inclusion of the MPR into this structure would be ideal, but give the high hydrophobicity that prompted the MPRs exclusion from the post-fusion structure its inclusion is unlikely (12). Lacking global gB structural data we could build more modestly on our MPR structural knowledge using long peptides encompassing the MPR sequence for crystallization and structural analysis as was performed for HIV-1 gp41 MPER (15, 20). Using a variety of techniques including circular dichroism, cryo-electron microscopy, SPR we may determine further details of the gB MPR structure and function by analyzing a MPR peptide.

To continue the investigation of gB in the absence of a pre-fusion structure we have initiated the development of a series of polyclonal antibodies to the gB MPR and FLs. These reagent could provide a wealth of information about the accessibility and

functional interactions between the FLs and MPR during the fusion process. Few neutralizing antibodies to viral fusion loops/peptides have been identified, but several reports in Dengue virus and related flaviviruses have identified a neutralizing antibody that maps to their fusion peptides (6, 7). We have preliminary data that support the successful development of a polyclonal antibody to the HSV FLs (data not shown).

Similarly, MPR specific antibodies have rarely been reported. In the HIV-1 gp41 neutralizing antibodies that map to the MPER (membrane proximal external region) have been identified in several patients. Analysis of these neutralizing antibodies has expanded the understanding of gp41s role in fusion and lipid interaction (9, 13, 16). Development of an antibody against the HSV gB-MPR could provide a wealth of information leading to a better understanding of the MPRs interaction, structure, and function.

Finally, future analysis of FLs and MPR needs to be evaluated in context of the entire HSV entry complex. Given HSV's requirement for four glycoproteins gD, gH/gL, and gB, for both entry and virus-induced cell fusion, the continued dissection of this mechanism will be a continuing challenge. Ultimately, the detailed structural and functional understanding of HSV entry will have long-range implications contributing to the framework for future therapeutics and vaccine development across the herpesvirus families.

REFERENCES

1. **Atanasiu, D., W. T. Saw, G. H. Cohen, and R. J. Eisenberg.** 2010. Cascade of events governing cell-cell fusion induced by herpes simplex virus glycoproteins gD, gH/gL, and gB. J Virol **84:**12292-12299.
2. **Atanasiu, D., J. C. Whitbeck, M. P. de Leon, H. Lou, B. P. Hannah, G. H. Cohen, and R. J. Eisenberg.** 2010. Bimolecular complementation defines functional regions of herpes simplex virus gB that are involved with gH/gL as a necessary step leading to cell fusion. J Virol **84:**3825-3834.
3. **Backovic, M., R. Longnecker, and T. S. Jardetzky.** 2009. Structure of a trimeric variant of the Epstein-Barr virus glycoprotein B. Proc Natl Acad Sci U S A **106:**2880-2885.
4. **Carfi, A., H. Gong, H. Lou, S. H. Willis, G. H. Cohen, R. J. Eisenberg, and D. C. Wiley.** 2002. Crystallization and preliminary diffraction studies of the ectodomain of the envelope glycoprotein D from herpes simplex virus 1 alone and in complex with the ectodomain of the human receptor HveA. Acta Crystallogr D Biol Crystallogr **58:**836-838.
5. **Chowdary, T. K., T. M. Cairns, D. Atanasiu, G. H. Cohen, R. J. Eisenberg, and E. E. Heldwein.** 2010. Crystal structure of the conserved herpesvirus fusion regulator complex gH-gL. Nature structural & molecular biology **17:**882-888.
6. **Costin, J. M., E. Zaitseva, K. M. Kahle, C. O. Nicholson, D. K. Rowe, A. S. Graham, L. E. Bazzone, G. Hogancamp, M. Figueroa Sierra, R. H. Fong, S. T. Yang, L. Lin, J. E. Robinson, B. J. Doranz, L. V. Chernomordik, S. F.**

Michael, J. S. Schieffelin, and S. Isern. 2013. Mechanistic study of broadly neutralizing human monoclonal antibodies against dengue virus that target the fusion loop. Journal of virology **87:**52-66.

7. **Deng, Y. Q., J. X. Dai, G. H. Ji, T. Jiang, H. J. Wang, H. O. Yang, W. L. Tan, R. Liu, M. Yu, B. X. Ge, Q. Y. Zhu, E. D. Qin, Y. J. Guo, and C. F. Qin.** 2011. A broadly flavivirus cross-neutralizing monoclonal antibody that recognizes a novel epitope within the fusion loop of E protein. PLoS One **6:**e16059.

8. **Eisenberg, R. J., D. Atanasiu, T. M. Cairns, J. R. Gallagher, C. Krummenacher, and G. H. Cohen.** 2012. Herpes virus fusion and entry: a story with many characters. Viruses **4:**800-832.

9. **Frey, G., J. Chen, S. Rits-Volloch, M. M. Freeman, S. Zolla-Pazner, and B. Chen.** 2010. Distinct conformational states of HIV-1 gp41 are recognized by neutralizing and non-neutralizing antibodies. Nature structural & molecular biology **17:**1486-1491.

10. **Hannah, B. P., T. M. Cairns, F. C. Bender, J. C. Whitbeck, H. Lou, R. J. Eisenberg, and G. H. Cohen.** 2009. Herpes simplex virus glycoprotein B associates with target membranes via its fusion loops. J Virol **83:**6825-6836.

11. **Heldwein, E. E., and C. Krummenacher.** 2008. Entry of herpesviruses into mammalian cells. Cell Mol Life Sci **65:**1653-1668.

12. **Heldwein, E. E., H. Lou, F. C. Bender, G. H. Cohen, R. J. Eisenberg, and S. C. Harrison.** 2006. Crystal structure of glycoprotein B from herpes simplex virus 1. Science **313:**217-220.

13. **Huarte, N., A. Araujo, R. Arranz, M. Lorizate, H. Quendler, R. Kunert, J. M. Valpuesta, and J. L. Nieva.** 2012. Recognition of Membrane-Bound Fusion-Peptide/MPER Complexes by the HIV-1 Neutralizing 2F5 Antibody: Implications for Anti-2F5 Immunogenicity. PLoS One **7:**e52740.

14. **Krummenacher, C., V. M. Supekar, J. C. Whitbeck, E. Lazear, S. A. Connolly, R. J. Eisenberg, G. H. Cohen, D. C. Wiley, and A. Carfi.** 2005. Structure of unliganded HSV gD reveals a mechanism for receptor-mediated activation of virus entry. Embo J **24:**4144-4153.

15. **Liu, J., Y. Deng, A. K. Dey, J. P. Moore, and M. Lu.** 2009. Structure of the HIV-1 gp41 membrane-proximal ectodomain region in a putative prefusion conformation. Biochemistry **48:**2915-2923.

16. **Montero, M., N. E. van Houten, X. Wang, and J. K. Scott.** 2008. The membrane-proximal external region of the human immunodeficiency virus type 1 envelope: dominant site of antibody neutralization and target for vaccine design. Microbiol Mol Biol Rev **72:**54-84, table of contents.

17. **Roche, S., A. A. Albertini, J. Lepault, S. Bressanelli, and Y. Gaudin.** 2008. Structures of vesicular stomatitis virus glycoprotein: membrane fusion revisited. Cellular and molecular life sciences : CMLS **65:**1716-1728.

18. **Roche, S., S. Bressanelli, F. A. Rey, and Y. Gaudin.** 2006. Crystal structure of the low-pH form of the vesicular stomatitis virus glycoprotein G. Science **313:**187-191.

19. **Roche, S., F. A. Rey, Y. Gaudin, and S. Bressanelli.** 2007. Structure of the prefusion form of the vesicular stomatitis virus glycoprotein G. Science **315:**843-848.

20. **Shi, W., J. Bohon, D. P. Han, H. Habte, Y. Qin, M. W. Cho, and M. R. Chance.** 2010. Structural characterization of HIV gp41 with the membrane-proximal external region. The Journal of biological chemistry **285:**24290-24298.

21. **Stampfer, S. D., H. Lou, G. H. Cohen, R. J. Eisenberg, and E. E. Heldwein.** 2010. Structural basis of local, pH-dependent conformational changes in glycoprotein B from herpes simplex virus type 1. J Virol **84:**12924-12933.

22. **White, J. M., S. E. Delos, M. Brecher, and K. Schornberg.** 2008. Structures and mechanisms of viral membrane fusion proteins: multiple variations on a common theme. Crit Rev Biochem Mol Biol **43:**189-219.

APPENDIX

Autophagy is an essential component of *Drosophila* immunity against vesicular stomatitis virus

Reprinted from Publication Immunity, 30(4), S. S. Shelly, N. Lukinova, S. Bambina, A. Berman, S. Cherry, Autophagy is an essential component of Drosphila immunity against vesicular stomatitis virus, 588-598, Copyright (2009), with permission from Elsevier.

ABSTRACT

Intrinsic innate immune mechanisms are the first line of defense against pathogens and exist to control infection autonomously in infected cells. Here, we showed that autophagy, an intrinsic mechanism that can degrade cytoplasmic components, played a direct antiviral role against the mammalian viral pathogen vesicular stomatitis virus (VSV) in the model organism *Drosphila*. We found that the surface glycoprotein, VSV-G, was likely the pathogen-associated molecular pattern (PAMP) that initiated this cell-autonomous response. Once activated, autophagy decreased viral replication, and repression of autophagy led to increased viral replication and pathogenesis in cells and animals. Lastly, we showed that the antiviral response was controlled by the phosphatidylinositol 3-kinase (PI3K)-Akt-signaling pathway, which normally regulates autophagy in response to nutrient availability. Altogether, these data uncover an intrinsic antiviral program that links viral recognition to the evolutionarily conserved nutrient-signaling and autophagy pathways.

INTRODUCTION

Detection and clearance of viruses by the innate immune system relies on several distinct and essential pathways that are evolutionarily conserved (18). Extracellular virions are recognized via Toll-like receptors present on the cell surface and within endolysosomal compartments. These receptors were first identified in *Drosphila* and are now recognized as the canonical pathogen recognition system in all metazoans (53). Cytoplasmic pattern recognition receptors, originally identified in plants (36), also act as intracellular pathogen detectors. Yet another intracellular pattern recognition system responsible for the degradation of viral dsRNA genomes or replication intermediates is the RNA interference (RNAi) pathway (31). Recently, autophagy, another ancient and conserved intracellular pathway, has also been implicated in innate immunity and pathogen destruction ((16), (21), (30), (34), (39) and (44)).

Autophagy was first genetically characterized in yeast as a response to starvation and is the process by which cells degrade cytoplasmic components, including organelles for recycling ((23), (24), (25) and (38)). Macroautophagy, which will be referred to as autophagy throughout this article, occurs through the de novo formation of double-membraned vesicles called autophagosomes that envelop cytoplasmic regions, which mature and grow, and subsequently fuse with the lysosome for degradation of the internalized cytoplasmic contents. Autophagy is involved in a plethora of processes, including the removal of damaged organelles and intracellular protein aggregates, turnover of long-lived proteins, and cell death (37). Autophagy is required both for normal development and survival from nutrient depravation. For these processes, it has

been shown that autophagy is controlled by the phosphatidylinositol 3-kinase (PI3K)-Akt-signaling pathway. Activation of the signaling pathway inhibits autophagy, whereas the loss of signaling through this cascade relieves the negative repression of target of rapamycin (TOR) kinase on Atg1, an essential upstream component of the autophagy pathway (51). Therefore, there is a direct link between nutrient availability and autophagy.

In mammalian systems, autophagy was recently shown to be important in innate immune defense against intracellular pathogens (30). Studies on bacterial pathogens have revealed that some bacteria are cleared from the cytoplasm by autophagy ((2), (16), (33), (39), (40) and (50)). There have also been studies implicating autophagy in antiviral defense. For example, many viruses can be observed inside of autophagic compartments, including herpes simplex virus 1 (HSV-1) and Sindbis virus ((49) and (52)). Moreover, data suggest that beclin 1 (the human homolog of Atg6), perhaps via autophagy, restricts viral encephalitis induced by both HSV-1 and Sindbis ((32) and (41)). In plants, autophagy prevents the spread of cell death during the hypersensitive response, which restricts viral replication (34). However, it has not been established that autophagy itself is sufficient to control the replication of these viruses or whether there are other facets of activated pathways, such as cell death, that are affecting viral growth. Given the potentially critical role of autophagy in defending from infection and the fact that little is known about intrinsic antiviral mechanisms, we set out to determine whether autophagy can directly control viral replication in the genetically tractable organism *Drosphila* melanogaster. *Drosphila* has no acquired immune system, relying only on innate systems

to combat pathogens ((10) and (28)). This simplified immune system allows us to test the role of innate factors in isolation. Here, we showed that autophagy controlled vesicular stomatitis virus (VSV) replication in both cultured *Drosphila* cells and adult flies. VSV infection via the surface glycoprotein was sensed by flies, and this, in turn, activated autophagy independently of viral replication. Increased autophagic activity was mediated by repression of the nutrient-signaling cascade, which alleviated repression of autophagy, activating the antiviral program. This pathway was critical to the control of viruses because the loss of autophagy converts a nonpathogenic VSV infection into a lethal one.

MATERIALS AND METHODS

Cells, antibodies, and reagents. *Drosphila* S2 cells were grown and maintained as described in Schneider's media supplemented with 10% FBS (JRH), penicillin/streptomycin, and glutamine (9). BHK21 cells were maintained in DMEM/10% FBS (Sigma), penicilin/streptomycin, and glutamine. Antibodies were obtained from the following sources: anti-GFP (Invitrogen; different lots have different background bands), anti-tubulin (Sigma), anti-VSVG (gift from R. Doms), anti-VSVM (gift from D. Lyles and R. Hardy),and anti-phospho-Akt and anti-total Akt (Cell Signaling). Polyclonal rabbit Anti-Atg8 was generated against peptide (FDKRRAEGDKIRRKYPDR) and affinity purified by ProSci. Fluorescently labeled secondary antibodies were obtained from Jackson Immunochemicals, and other secondary antibodies were obtained from Amersham. Additional chemicals were obtained from Sigma.

Virus and viral components. VSV-eGFP (a kind gift from J. Rose) was grown in BHK cells as described (43). VSV was UV inactivated as described (17). Viral RNPs were purified as described (15), and the viral RNA was purified from the RNP with Trizol following the manufacturer's protocol. To generate VSV-G VPs, we transfected 293Ts with pVSV-G (Invitrogen) by using Fugene HD following the manufacturer's protocol. Supernatant was clarified, ultracentrifuged through a 20% sucrose cushion, and resuspended in PBS.

RNAi and infections. dsRNAs for RNAi were generated and used for RNAi for 3 days as described (8). Amplicons used are described at http://flyrnai.org. Cells were passaged into serum-free media supplemented with dsRNA at 250 ng/20,000 cells. After 1 hr, complete media was added. After 3 days, cells were infected with the indicated viral inoculum and assayed at the indicated time point postinfection.

Immunofluorescence. Cells were processed for immunofluorescence as previously described. In brief, cells were fixed in 4% formaldehyde/PBS, washed in PBS/0.1% Triton X-100 (PBST) twice, and blocked in 2% BSA/PBST. Primary antibody was diluted in block and incubated overnight at 4°C. Cells were washed three times in PBST and incubated in secondary antibody for 1 hr at room temperature. Cells were counterstained with Hoechst 33342 (Sigma) and imaged with an automated microscope (ImageXpress Micro). Three wells per treatment and three sites per well were collected.

Quantitation was performed with automated image analysis software (MetaXpress). Experiments were performed at least three times.

Drosphila S2* cells were transfected with pMT-Gal4 and UAS-GFP-LC3 by using Effectene (QIAGEN) per the manufacturer's protocol. After 2 days, the cells were induced with 500 uM CuSO4, and 24 hr later, the cells were either infected or uninfected at an MOI = 30 or transfected with Flag-RAN along with viral RNA or RNP. After 20 hr, the cells were fixed, counterstained with Hoechst 33342, and processed for fluorescence microscopy. More than 150 cells per treatment were counted for each experiment.

Hemocytes of the indicated genotype were obtained by dissection of third-instar larvae in complete Schneider's media. Fifteen larvae were pooled for each of two independent experiments. Cells were either uninfected or infected with VSV (MOI = 30), fixed and stained with Hoechst 33342, and imaged on an inverted scope (Leica).

For Lysotracker staining of adult flies, we dissected their abdomens in complete media, treated them with 100 nM Lysotracker Red counterstained with Hoechst 33342 for 10 min at room temp, and mounted them in complete media. The dissected fat bodies were imaged on an inverted scope (Leica). Three animals per genotype were imaged for each of three independent experiments.

Immunoblotting, Northern blots, and titers. Cell or flies were collected at the time points indicated. The cells or flies were lysed in radioimmunoprecipitation assay (RIPA) buffer supplemented with a protease inhibitor cocktail (Boehringer). Samples were separated by 10% SDS-PAGE and blotted as previously described (9). For northern blot

analysis, cells or flies were lysed, and total RNA was extracted with Trizol (Invitrogen) according to the manufacturer. Ten micrograms of total RNA was run on a 1% gel and transferred to Hybond N+ nylon, and a radiolabeled probe was generated from the indicated gene. Experiments were performed at least three times independently. For titering, cells were collected, freeze thawed, and titered on BHK21 cells. Flies were crushed in DMEM/10% FBS and titered on BHK21 cells.

Electron microscopy. Cells were pretreated with the indicated dsRNA for 3 days where indicated. Next, the cells were infected at an MOI = 5 for 20 hr and fixed in 2% PFA/2% glutaraldehyde in 0.1 M sodium cacodylate buffer (pH 7.4) for 1 hr at room temperature, postfixed in 2% osmium tetroxide in 0.1 M sodium cacodylate, and enbloc stained with 2% aqueous uranyl acetate in maleate buffer (pH 5.2) for 30 min at room temperature. After dehydration in a graded ethanol series, cells were removed from the dish in propyleneoxide embedded in Epon 812. Ultrathin sections (~70 nm) were mounted on mesh copper grids, stained with 2% uranyl acetate in acetone followed by bismuth subnitrite, and examined in a FEI-Tecnai T12 electron microscope; digital images were collected with Gatan CCD camera at a primary magnification of 2100×. The number of intracellular organelles was measured by randomly counting at least 20 cells per treatment per experiment. At least two independent experiments were performed for each comparison. Data were analyzed and plotted by using R (http://www.R-project.org). Significance was assessed with a Wilcoxon test.

Adult infections. All flies were obtained from the Bloomington stock center unless stated otherwise and were maintained on standard medium at room temperature. Flies carrying UAS-Atg12IR or UAS-Atg7IR (gift of T. Neufeld) or UAS-Atg18IR (VDRC) were crossed to Actin-GAL4/+ flies at room temperature. Flies wild-type (w1118), UAS-PTEN, UAS-Δp60 (gift of M. Birnbaum), or UAS-Akt IR (VDRC) were crossed to heat shock GAL4. Heat shock PTEN flies were crossed to Atg1 heterozygous flies (Atg1[00305]). On the day of injection, the progeny were heat shocked at 37°C for 1 hour and shocked every 2 days throughout the experiment. The 4- to 7-day-old adults of the stated genotypes were inoculated with VSV-GFP as previously described (9). Groups of at least 20 flies were challenged for mortality studies, and a log-rank test was used to determine significance. Insulin (1 mg/ml) was injected in the presence or absence of VSV-GFP. Flies were processed at the indicated time point postinfection. Flies carrying UAS-eGFP-huLC3 were crossed to Hemolectin-Gal4 to drive expression in hemocytes ((14) and (46)).

RESULTS

VSV infection of Drosphila cells. We first characterized infection of *Drosphila* cells with VSV. VSV is the prototypical member of the nonsegmented negative sense RNA virus family and is transmitted to cattle by insects ((29) and (42)). This virus infects and spreads between arthropods and mammals yet is controlled by the immune system of each, resulting in little mortality in either host. To study mechanisms of defense against

this virus, we challenged *Drosphila* S2 cells with VSV that expresses a GFP reporter (VSV-GFP) upon successful replication (43).

We found that VSV-GFP replicates in *Drosphila* cells in a dose-dependent manner. New viral antigens were detected by 20 hr after infection as measured by GFP production as well as the production of the viral glycoprotein VSV-G (Figure A-1A) (8). We also monitored viral replication with immunoblot analysis to detect the production of viral antigens. Whole-cell lysates from cells infected with increasing multiplicities of infection (MOI) were examined with an antibody against GFP or VSV-M (Figure A-1B). Thus, we can monitor a dose-dependent increase in viral infection with both assays.

We also determined whether VSV productively infects *Drosphila* cells. To this end, we monitored the production of new viral progeny. Cells were infected with increasing amounts of virus, and 24 hr after infection, the amount of virus produced was measured by plaque assay on mammalian cells, demonstrating a full replication cycle in *Drosphila* cells (Figure A-1C). Thus, VSV productively infects *Drosphila* cells, generating virus that is infectious to mammalian cells.

Autophagy controls viral infection in cultured cells. *Drosphila* has homologs of 11 yeast autophagy-related genes, and many of these have been confirmed to be required for autophagy in flies during development or starvation (48). To test whether loss of the autophagy pathway affects viral replication in tissue culture cells, we generated dsRNAs against three of these highly conserved genes previously shown to be involved in autophagy in flies (Atg5, Atg8a, and Atg18) (48). Three different genes were tested in

order to rule out off-target effects of the dsRNAs, as well as to confirm that effects observed are due to the autophagy pathway rather than an unrelated pathway or process affected by any individual RNAi reagent. To deplete the proteins, we treated cells with dsRNA for 3 days and then challenged the cells with VSV-GFP. We used automated imaging and analysis to monitor infection. With this assay, we observed a substantial increase in the percentage of infected cells by knocking down each autophagy-related gene (Figure A-2A). Semiquantitative RT-PCR and RT-qPCR were used to demonstrate that treatment with dsRNAs leads to a depletion of the cognate mRNA (Figure A-S1). The increase in viral replication measure by fluorescence was verified biochemically; cells were depleted for Atg5, Atg8a, or Atg18, infected with VSV, and probed by immunoblot for GFP (Figure A-2B). We observed an increase in the amount of GFP in the autophagy-related RNA-depleted cells.

To further validate that the autophagy pathway as a whole is required for the phenotype, we tested additional conserved autophagy genes including Atg1, Atg2, Atg4, Atg6, Atg7, Atg8b, or Atg9. Cells were treated with the indicated dsRNA for 3 days and then infected with VSV. By using microscopy and automated image analyses, we quantified the percentage of infected cells across four independent experiments and normalized the infection to untreated cells. When compared to the nontargeting control dsRNA (β-gal), we observed a significant increase in VSV infection upon depletion of autophagy genes (Figure A-2C). We also found a similar increase in viral titers produced in cells depleted for autophagy genes (Figure A-2D). Altogether, these data demonstrate that autophagy

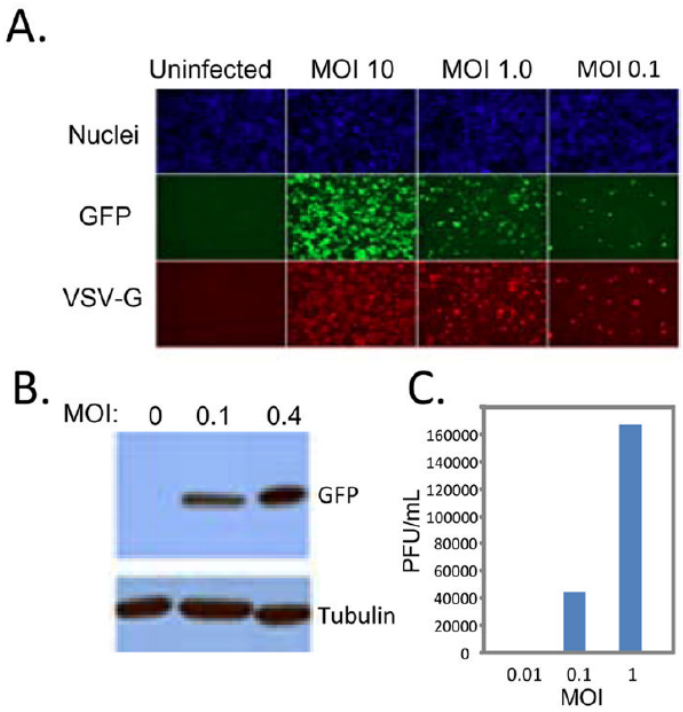

Figure A-1. VSV infects *Drosphila* cells. (A) Schneider cells were infected with VSV-GFP at the indicated multiplicity of infection (MOI) for 20 hr. Cells were processed for immunofluorescence and imaged with an automated microscope (ImagXpress Micro). Infected cells express GFP and the viral glycoprotein VSV-G and are counterstained with Hoechst 33342 to observe nuclei. (B) Viral antigen production at the indicated MOI at 24 hr after infection was measured by immunoblot against the virally produced antigen GFP or the cellular control tubulin. These data show a representative experiment; similar findings were made in at least three repetitions. (C) Viral titers from cells infected with the indicated MOI of VSV at 24 hr postinfection. These data show a representative experiment; similar findings were made in at least two repetitions.

controls viral replication, consistent with its playing an antiviral role in cultured cells.

VSV infection activates autophagy in cultured cells. The finding that autophagy inhibits VSV replication suggests that autophagy might be induced by VSV infection of cells. Autophagy is routinely monitored by three assays: electron microscopy, fluorescent GFP-LC3 punctae, or as lipidated LC3 by immunoblot (22). We first monitored autophagy by electron microscopy. This approach allows identification of intracellular organelles and structures and shows that virally induced compartments are of autophagic origin. Double-membrane vesicles that contain cytoplasmic components or degrading organelles such as mitochondria are not known to arise by any other mechanism. Therefore, we performed electron microscopy analysis on both VSV-infected and uninfected S2 cells (Figure A-3A). Higher-magnification images show double-membrane vesicles with cytoplasmic contents or membranous contents (degrading mitochondria) indicative of autophagic compartments (Figure A-3B). Upon quantification of autophagic bodies, we found a > 2.5-fold increase in the number of autophagosomes in the infected cells (Figure A-3C).

To verify that the VSV-induced vesicular structures we observed were indeed autophagic in origin, we tested whether Atg5 depletion by RNAi could prevent their induction. Indeed, we found that loss of Atg5 inhibited the induction of these autophagic compartments as measured by electron microscopy (Figure A-3D). Altogether, these data suggest that viral infection induces autophagy, which, in turn, attenuates viral replication.

Given that VSV infection activates autophagy, there were two possible viral inducers: incoming virions and viral replication products. To test whether virus replication is required, we challenged cells with either replication-competent or UV-inactivated virus and measured the effect on autophagy by using electron microscopy. UV-inactivated virus binds cells, undergoes endocytosis, and fuses within the endolysosomal compartment (11). The core, released into the cytoplasm, is replication incompetent. We verified that the UV-inactivated virus was indeed replication defective by fluorescence microscopy (Figure A-S2). By using electron microscopy, we found that both replication-competent and UV-inactivated VSV induce autophagic vesicles (Figure A-3C). Indeed, quantification reveals that UV-inactivated virus induces the formation of autophagic bodies to a similar extent as replication-competent virus. This suggests that the incoming virus presents the cells with a pre-existing molecule (perhaps a pathogen-associated molecular pattern [PAMP]) that is sufficient to activate the antiviral program.

During autophagy, cytosolic LC3 (LC3-I) is conjugated on its carboxyl terminus with phosphatidylethanolamine, forming lipidated LC3 (LC3-II), which localizes to the autophagic membrane. The amount of LC3-II correlates with the number of autophagosomes and can be monitored by immunoblot (22). In *Drosphila*, there are two LC3 homologs that are 95% similar, Atg8a and Atg8b. We developed an antibody that recognized the C terminus of both homologs because treatment of cells with dsRNA against Atg8 (dsRNA has overlap with both targets) completely abolished the signal (Figure A-3E). In addition, we observed an increase in the production of Atg8-II

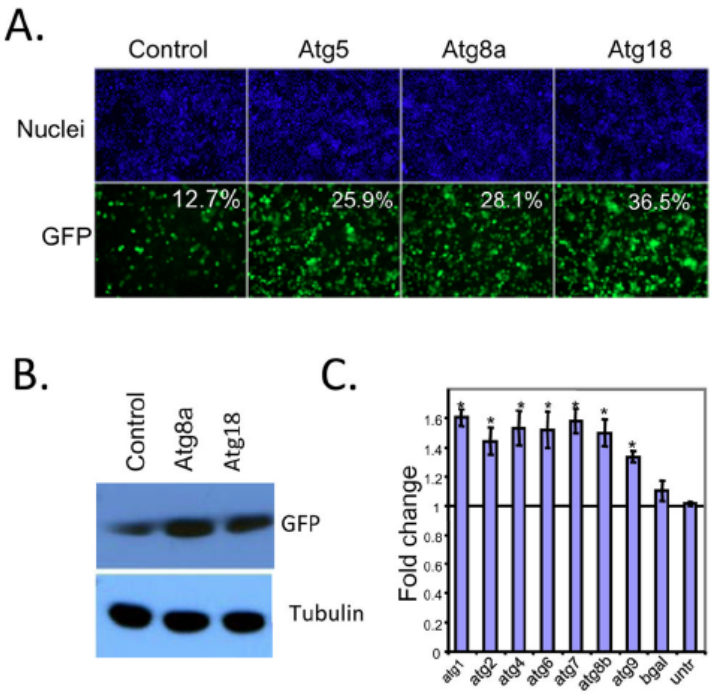

Figure A-2. Autophagy is antiviral in *Drosphila* cells. (A) S2 cells were pretreated with dsRNA against control dsRNA (luciferase) or the autophagy genes Atg5, Atg8a, or Atg18 for 3 days and then infected (MOI = 1) for 20 hr and processed for immunofluoresence and imaged as above. Infected cells express GFP, and the percent infection is calculated with automated image analysis (MetaXpress) from three wells, with three sites per well. Loss of autophagy genes significantly increases VSV infection ($p < 0.05$). (B) Depletion of autophagy genes increases the production of viral antigens by immunoblot. Cells pretreated with the indicated dsRNAs were infected (MOI = 0.1) and processed for immunoblot at 24 hr after infection. Viral antigens were measured by anti-GFP and normalized to the control protein tubulin. These data show representative experiments; similar findings were made in at least three repetitions. (C) Depletion of additional

autophagy genes by RNAi leads to an increase in the percent infection as compared to control dsRNA. Mean ± SD are shown for four independent experiments as the fold effect compared to control dsRNA (MOI = 0.1–0.25, 24 hr postinfection); *p < 0.05, Student's t test. (D) Viral titers of cells pretreated with the indicated dsRNAs at 48 hr postinfection with an MOI = 0.1. Data are presented as the mean ± SD fold change from control treatment of four averaged experiments; *p < 0.01, Student's t test.

upon starvation, validating our antibody (Figure A-3F). Next, we tested whether infection with wild-type or UV-inactivated virus induced the production of Atg8-II. Indeed, we observed marked induction of Atg8-II upon treatment with both replication-competent and replication-incompetent virus (Figure A-3F).

VSV induces autophagy as measured by GFP-LC3 punctae formation. To further study the role of autophagy in VSV infection, we took advantage of an assay that depends on the translocation of the autophagosome protein LC3 (Atg8) from the cytosol (diffuse distribution) to newly formed autophagosomes, which appear as bright cytoplasmic punctae (20). GFP-LC3 is an autophagosome-specific membrane marker detected in punctae upon autophagosomes induction in both mammalian and *Drosphila* systems ((46), (48) and (57)). This assay allows us to monitor the induction of autophagy cell by cell. We expressed this GFP-tagged LC3 (GFP-LC3) in cultured cells and found that there is diffuse cytoplasmic staining (Figure A-4A). However, upon infection with either wild-type or UV-inactivated virus, we observed a significant increase in the percentage of punctae-containing cells (Figure A-4B). Moreover, we found that there was also an increase in the number of punctae per cell upon infection with either wild-type or UV-inactivated VSV (Figure A-4C). Lastly, we tested whether the activation of autophagy was cell autonomous. To this end, cells expressing GFP-LC3 were uninfected, infected, or infected at a multiplicity of infection such that 30% of the cells were VSV-M+. Next, we quantified the percentage of cells with punctae that were either VSV+ or VSV−. We found that only the infected cells had an increase in GFP-LC3 punctae (Figure A-4D).

Together, the combination of electron microscopy, the induction of Atg8-II, and GFP-LC3 punctae formation shows that VSV infection, in the absence of viral replication, led to a robust, cell-autonomous increase in autophagy in *Drosphila* cells.

The viral glycoprotein, VSV-G, induces autophagy. The VSV virion is largely composed of: the viral RNA genome; the proteins that are bound to the viral RNA that makes up the RNA-nucleoprotein complex (RNP); matrix proteins associated with the nucleocapsid; and the membrane-bound surface envelope spike glycoprotein that extends from the viral membrane. We set out to determine which component of the virion is the PAMP that is recognized by *Drosphila* cells, leading to the induction of antiviral autophagy. To this end, we purified virions from which we isolated the RNP and the viral RNA (15). Because VSV is a negative-strand RNA virus, the naked nucleic acid is not capable of initiating an infection in the absence of the viral proteins that make up the RNP (VSV proteins: N, P, and L). We verified that the purified RNA was nonfunctional and that the RNP was functional by cotransfection with a reporter to mark the transfected cells (Figure A-S3A). We tested whether cells transfected with the viral RNA or RNP induced autophagy as measured by GFP-LC3 punctae formation and found that neither PAMP induced autophagy with this assay (Figures A-4E and A-4F).

Next, we set out to test whether the viral glycoprotein VSV-G could induce autophagy. To purify VSV-G-containing vesicular particles (VPs) devoid of any other viral component, we either mock transfected or transfected 293T cells with VSV-G. VSV-G alone is sufficient to induce blebbing and the formation of VPs that are

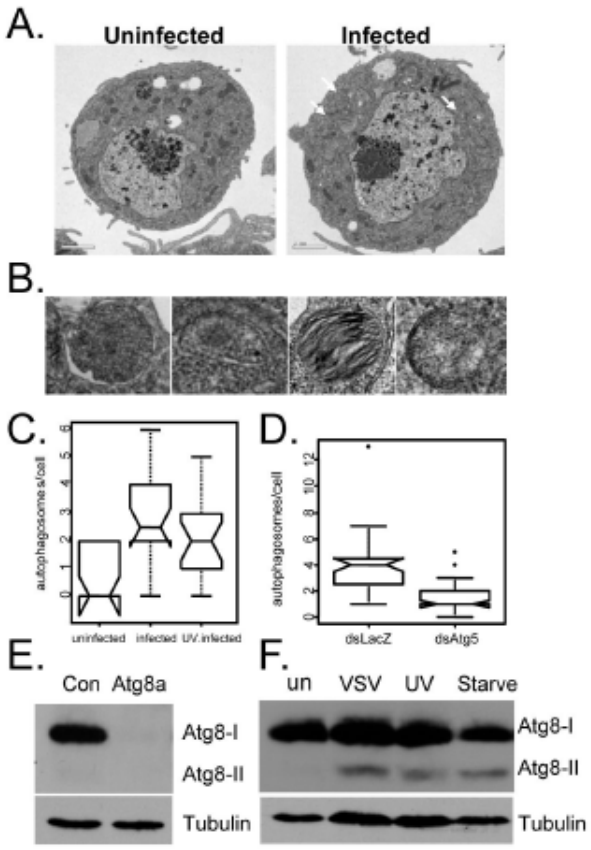

Figure A-3. VSV infection activates autophagy independent of replication. (A) VSV infection induces autophagosome formation as measured by electron microscopy. Representative images are shown for cells that are either uninfected or infected at an MOI = 5 at 20 hr after infection. (B) Higher-magnification images of autophagosomes in VSV-infected cells. (C) Active and UV-inactivated virus induce autophagic vesicles. Cells were infected with UV-inactivated VSV-GFP as above. Autophagic bodies were counted for at least 20 cells from each treatment and presented as a notched box plot. The horizontal dark line represents the median for each category. The box represents the interquartile range, and the whiskers encompass the most extreme data values. The

notches represent a confidence interval for the median, and nonoverlapping notches indicate different medians at the 5% significance level. There is a significant difference between uninfected and infected or UV-virus infected (∗p = 9.0e−5 and p = 3.7e−3, Wilcoxon test), respectively. However, there is no significant difference in the number of autophagosomes per cell between infected and UV-virus infected (p = 0.22, Wilcoxon test). (D) The induction of autophagic vesicles by VSV is Atg5 dependent. S2 cells were pretreated with either control (LacZ) or Atg5 dsRNA for 3 days and infected with VSV-GFP at an MOI = 5 for 20 hr. Autophagic bodies were counted for 35 cells from each treatment and presented as a notched box plot as described in (C). There is a significant difference between control and Atg5-depleted cells (∗p = 1.2e−07, Wilcoxon test). These findings were observed in at least two independent experiments. (E) Immunoblot analysis of cells treated with control dsRNA or dsRNA against Atg8 (Atg8a and Atg8b). Atg8 is observed in resting cells (Atg8-I, ~16 kD). (F) A smaller form of Atg8 is induced in cells that are serum starved or cells that are infected with VSV or UV-inactivated VSV (Atg8-II, ~14 kD). These data show representative experiments; similar findings were made in at least three repetitions.

infectious and have no other viral component ((1) and (45)). We purified the VPs and found that only the VPs from the VSV-G-transfected cells carry VSV-G by immunoblot (data not shown) and that *Drosphila* cells treated with the VSV-G VPs, but not the preparation from mock-transfected cells, were positive for VSV-G by immunofluorescence (Figure A-S3B). Next, we challenged cells expressing GFP-LC3 with the purified blebs and found that treatment of cells with VSV-G+ VPs was sufficient to induce LC3-GFP+ punctae (Figure A-4G). Taken together, our data suggest that VSV-G is the PAMP that is recognized by *Drosphila* cells.

VSV infection induces autophagy both in primary cells and in adult flies. We extended our findings to primary cells by taking advantage of transgenic animals that express GFP-LC3 in larval hemocytes. Hemocytes are the *Drosphila* phagocytic macrophage-like cell type from which S2 cells are derived. We used the Gal4-UAS system, in which transgenes under the control of Gal4 transcription factor-binding sites (UAS sites) can be induced by Gal4 expression (5). This allows us to drive expression of the autophagosome marker GFP-LC3 with a specific hemocyte promoter, hemolectin. Third-instar larval hemocytes expressing GFP-LC3 (hemolectin-Gal4, UAS-GFP-LC3) were isolated and challenged with VSV ex vivo. In uninfected primary hemocytes, there is diffuse, low GFP-LC3 expression (Figure A-5A). In contrast, by 2 hr after infection, the hemocytes show bright GFP-positive punctae indicative of autophagosome induction (Figures A-5A and A-5B). This time point is prior to the initiation of viral replication,

further supporting the hypothesis that a preformed component of the virus, rather than replicating virus, is recognized by cells to induce autophagy.

To further demonstrate that infection induces autophagy in vivo, we infected adult flies with VSV-GFP and monitored autophagy with Lysotracker staining, a marker for acidified compartments that has been extensively used in flies ((4), (7) and (19)). With this assay, we found that VSV infection (GFP expression) leads to an increase in autophagy (Lysotracker+) in vivo (Figure A-5C). Moreover, this induction is again cell autonomous; only GFP+ cells were Lysotracker+. These data show that both *Drosphila* cells and animals respond to VSV infection by inducing an autophagic program.

Autophagy plays an antiviral role in adult flies. To determine whether autophagy also plays an innate antiviral role in the adult organism in vivo, we characterized viral infection of adult flies by challenging them with VSV and monitored infection. We found that VSV infection is nonpathogenic in adult flies as measured by mortality postinfection (Figure A-6A). We next set out to determine whether depletion of autophagy genes alters the susceptibility of flies to infection. Mutant flies were generated in vivo by driving expression of transgenes bearing long hairpin double-stranded RNA constructs targeting specific autophagy genes in vivo, leading to loss-of-function phenotypes. We crossed control and transgenic flies with hairpin transgenes against Atg18 (UAS-Atg18 IR), previously shown to be required for starvation-induced autophagy in flies, to actin-GAL4, resulting in high levels of ubiquitous transgene expression (48). We validated that

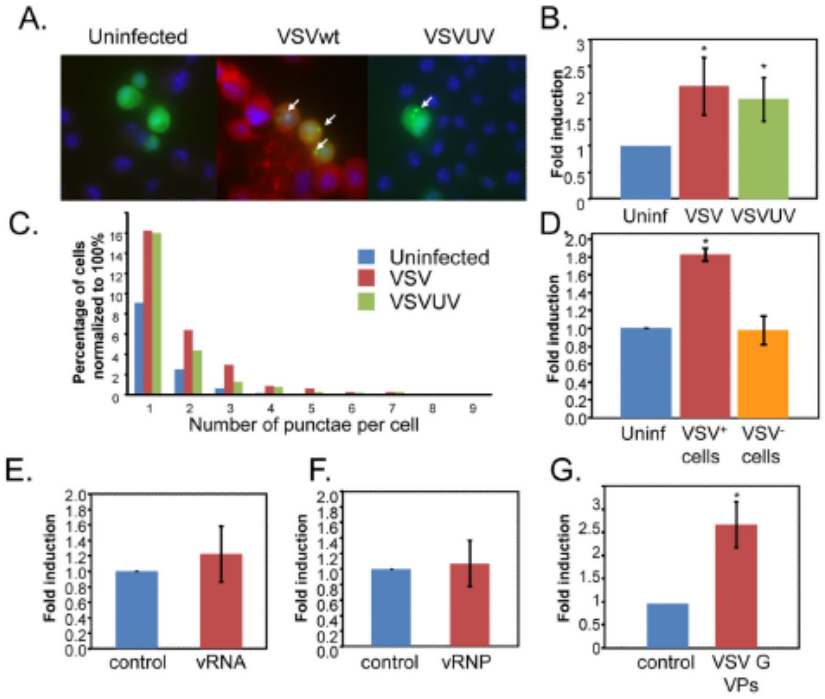

Figure A-4. VSV infection induces autophagy in *Drosphila* cells. VSV induces autophagosomes as measured by LC3 relocalization. (A) *Drosphila* cells were transfected with a GFP-LC3 reporter (green). Cells were either uninfected or infected with wild-type VSV or UV-inactivated VSV for 24 hr, fixed, and probed with anti-VSVM (red) and Hoechst 33342 (blue). A representative image is shown. Arrows indicate GFP-LC3+ punctae. (B) The percentage of cells with punctae was counted for five experiments, and fold change was graphed for cells that were uninfected (blue) or cells that were infected with wild-type VSV (red) or UV-inactivated VSV (green). Error bars represent SD. ∗p < 0.01, Student's t test. (C) The number of punctae per cell normalized to 100% for each treatment (n > 150 for each condition) quantified postinfection with either VSV or UV-inactivated VSV. (D) The induction of GFP-LC3 punctae is cell autonomous. The

percentage of cells with punctae was counted for three experiments, and fold change was graphed for cells that were either uninfected (blue), infected (red), or uninfected in a well in which 30% of the cells were infected (orange). Error bars represent SD. ∗$p < 0.01$, Student's t test. (E) The percentage of punctae+ cells transfected with control (red) or viral RNA (blue) was counted for three experiments, and fold change was graphed. Error bars represent SD. (F) The percentage of punctae+ cells transfected with control (red) or viral RNP (blue) was counted for three experiments, and fold change was graphed. Error bars represent SD. (G) The percentage of punctae+ cells infected with control (red) or VSV-G+ VPs (blue) was counted for three experiments, and fold change was graphed. Error bars represent SD. ∗$p < 0.01$, Student's t test.

Atg18 is indeed depleted in these flies by semiquantitative RT-PCR and RT-qPCR (Figure A-S1). Whereas UAS-Atg18 IR singly transgenic flies and flies expressing a control dsRNA (Figure A-S4) were resistant to VSV-induced lethality, actin-GAL4>UAS-Atg18 IR doubly transgenic flies that were depleted for Atg18 became sensitive to infection and succumbed to the virus (Figure A-6A). Flies depleted for Atg18 had a normal life span and were not more sensitive to infection with *Drosphila* C virus (Figure A-S4). Together, this shows that the altered pathology of the autophagy mutant is specific and that this pathway is protective against VSV infection.

We also found that the increased mortality correlates with increased viral replication in flies. At all time points after infection, there was a marked increase in the amounts of VSV antigen production, as measured by immunoblot (Figure A-6B), and increased virus production by plaque assay (Figure A-6C). Taken together, our data suggest that loss of autophagy in adult flies leads to increased viral replication, leading to mortality from an otherwise nonlethal infection.

To verify that our data for Atg18 is due to an effect on autophagy and not another role for Atg18, we tested whether depletion of additional autophagy genes Atg7 or Atg12, which were previously shown to be required for starvation-induced autophagy in flies, also affects viral replication (48). We found that there was a significant increase in the amount of VSV RNA replication in animals depleted for Atg18 (Figure A-6D), Atg7 (Figure A-6E), or Atg12 (Figure A-6F) as measured by RNA blot. We also monitored viral replication by immunoblot analysis of the virus-encoded GFP and again

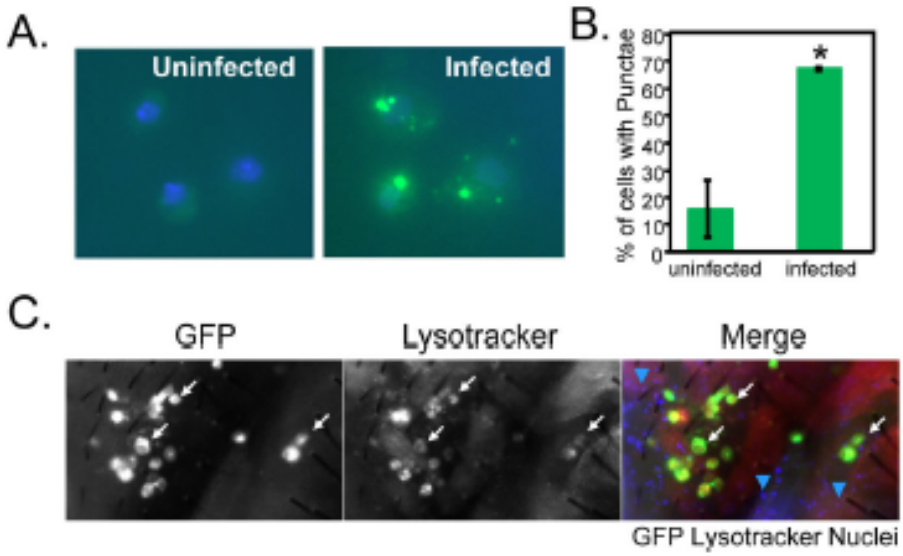

Figure A-5. VSV infection induces autophagy in primary cells and in adult flies. (A) Primary hemocytes expressing GFP-LC3 (Hml-gal4>UAS-eGFP-huLC3, green) were either uninfected or infected ex vivo for 2 hr and then fixed and stained with Hoechst 33342 to visualize nuclei (blue) by fluorescence microscopy. A representative image is shown. (B) The percentage of cells with punctae was counted ($n > 40$ for each condition). Error bars represent the range of two independent experiments. Increased punctae formation is observed in the infected cells. $*p < 0.001$, chi-square test in each experiment. (C) Adult wild-type flies were infected with VSV-GFP for 3 days. The flies were monitored for infection (GFP+) and autophagy (Lysotracker+) and were counterstained with Hoechst 33342 to observe the nuclei. There is increased Lysotracker staining in the infected cells in vivo in the animal. White arrows indicate that cells that

are Lysotracker+ are also GFP+. Blue arrows (merged image) show that the GFP− cells throughout the tissue are not Lysotracker+. These data show representative experiments; similar findings were made in at least three repetitions.

observed a significant increase in viral growth in flies depleted for the autophagy genes Atg7 and Atg12 (Figure A-S5). We also validated that RNAi itself does not impact viral replication by expressing a control dsRNA against the β-galactosidase gene and found that there was no effect on viral growth (data not shown). Next, we determined whether loss of Atg7 also had an effect on survival postchallenge with VSV. Indeed, we found that, whereas UAS-Atg7 IR singly transgenic flies were resistant to VSV-induced lethality, actin- GAL4>UAS-Atg7 IR doubly transgenic flies were more sensitive to infection, although it takes longer to succumb to the infection (Figure A-S4).
Lastly, we tested whether loss of Atg18 had an effect on hemocyte numbers or functionality. To monitor this phagocytic cell type, we injected flies that were either wild-type or depleted for Atg18 with fluorescent beads that are efficiently phagocytosed by hemocytes, allowing for the number and activity of this cell type to be monitored (12). We found that there was no difference in the number of hemocytes or the level of phagocytic activity in the hemocytes of adult flies depleted for Atg18 (Figure A-S6). Taken together, we demonstrate that autophagy is induced by infection, inhibits VSV replication, and prevents viral pathogenesis in animals.

Nutrient signaling controls autophagy during viral infection in animals. Given that autophagy is induced by infection, we were interested in determining which signaling pathway might control this antiviral response. The PI3K-Akt pathway has been previously shown to regulate autophagy during development and starvation. Therefore, we tested whether this pathway also senses VSV infection in vivo. In resting cells,

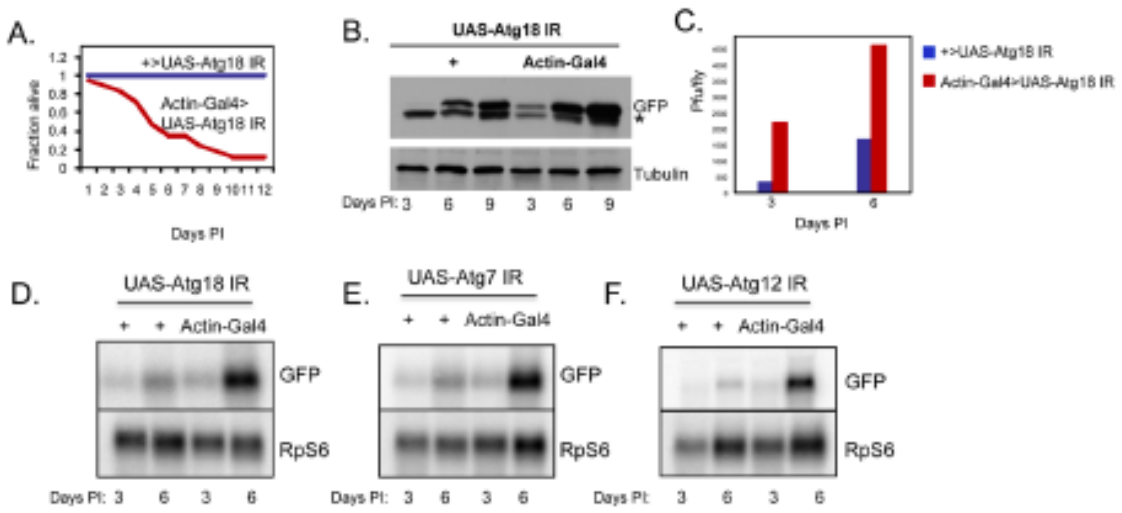

Figure A-6. Autophagy is antiviral in adult flies. (A) Adult flies expressing ubiquitous and high amounts of dsRNA against Atg18 (Actin-Gal4>UAS-Atg18IR) or sibling controls (+>UAS-Atg18IR) were challenged with 104 plaque-forming units (pfu) VSV, and morbidity was monitored as a function of time after infection. Log-rank test reveals that loss of Atg18 significantly increases susceptibility ($p < 0.001$). A representative experiment is shown; similar findings were made in at least three experiments. (B) Adult flies expressing ubiquitous and high amounts of dsRNA against Atg18 (Actin-Gal4>UAS-Atg18IR) or their sibling controls (+>UAS-Atg18IR) were challenged with VSV and monitored over time for viral replication, as measured by immunoblot against virally produced GFP, and normalized to a cellular control protein. Asterisk indicates a nonspecific band. (C) Adult flies expressing ubiquitous and high amounts of dsRNA against Atg18 (Actin-Gal4>UAS-Atg18IR, black bars) or their sibling controls (+>UAS-

Atg18IR, white bars) were challenged with VSV and monitored over time for viral replication as measured by viral titers. (D) Adult flies expressing ubiquitous and high amounts of dsRNA against Atg18 (Actin-Gal4>UAS-Atg18IR) or their sibling controls (+>UAS-Atg18IR) were challenged with VSV and monitored over time for viral replication as measured by RNA blot. (E) Adult flies expressing ubiquitous and high amounts of dsRNA against Atg7 (Actin-Gal4>UAS-Atg7IR) or their respective sibling controls (+>UAS-Atg7IR) were challenged with VSV and monitored over time for viral replication as measured by RNA blot. (F) Adult flies expressing ubiquitous and high amounts of dsRNA against Atg12 (Actin-Gal4>UAS-Atg12IR) or their respective sibling controls (+>UAS-Atg12IR) were challenged with VSV and monitored over time for viral replication as measured by RNA blot.

autophagy is repressed, at least in part, by the PI3K-signaling pathway. Akt, a key kinase in this pathway, has been demonstrated to control autophagy via activation of the TOR kinase (35). TOR is a global cell regulator that responds to nutritional conditions and represses autophagy via Atg1 ((27) and (47)). Inhibiting this pathway either by decreased inputs from extracellular ligands or by overexpression of negative regulators leads to decreased signaling and increased autophagy ((46) and (48)).

To modulate this pathway and test whether the PI3K-Akt pathway controls VSV-induced autophagy, we took advantage of a well-studied negative regulator, PTEN. PTEN is a phosphatase that blocks PI3K signaling by dephosphorylating PI(3,4,5)P3 (55). Overexpression of this factor leads to an increase in autophagy in the larval fat body ((3) and (48)). We overexpressed this gene in transgenic animals with a heat shock Gal4 driver and found that there was no effect on fly viability (data not shown). We tested whether PTEN also controls autophagy in the adult fat body by using Lysotracker, a standard assay in *Drosphila* ((4), (7) and (19)). With this assay, we found that overexpression of PTEN induces autophagy in fat bodies of well-fed adults (Figure A-S7).

We then challenged flies overexpressing PTEN and thus undergoing constitutive autophagy with VSV and monitored viral replication. We observed a decrease in viral protein production compared to controls by immunoblot analysis (Figure A-7A). To further dissect the role of PI3K signaling in the control of VSV infection, we tested whether inhibition of the pathway with a different negative regulator also blocks

infection. We took advantage of a deleted form of p60, the adaptor that couples the insulin receptor to the catalytic subunit of PI3K, Dp110 (6). This deletion mutant, Δp60, is a variant that lacks the Dp110-binding domain, which, when overexpressed, inhibits the PI3K-Akt-signaling pathway similarly to the overexpressed PTEN, thereby leading to an increase in autophagy (48). By using the same heat shock GAL4 overexpression system to drive expression of Δp60, we also observed a decrease in VSV replication as measured by immunoblot (Figure A-7A). Together, these data indicate that inhibition of the PI3K-Akt pathway, which, in turn, activates autophagy, also inhibits VSV replication, suggesting that this pathway plays an important role in the antiviral response.

To verify that the increase in VSV replication observed upon inhibition of the PI3K-Akt pathway is indeed due to activation of autophagy and not another pathway regulated by this signaling cascade, we performed epistasis analysis. Atg1, a conserved serine-threonine-specific protein kinase, is a crucial component of the autophagy machinery and a key regulator of autophagy. Loss of Atg1 blocks autophagy, whereas overexpression leads to an increase in autophagy in flies ((48) and (47)). Therefore, it is a limiting component of this pathway. First, we tested whether loss of one copy of Atg1 had an effect on infection and found that this had no effect on VSV levels (Figure A-S8). Next, we performed the epistasis analysis in a sensitized background by crossing flies carrying a heat shock promoter driving expression of PTEN (heat shock PTEN) to flies that were heterozygous for Atg1. This allowed us to compare flies that overexpressed PTEN and had two copies of Atg1 to flies that were heterozygous for Atg1. We expected that the decreased viral replication mediated by overexpression of PTEN would be

attenuated in animals that had reduced Atg1 levels. We challenged these siblings and found that removing one copy of Atg1 relieves the PTEN-mediated repression of VSV replication (Figure A-7B). This experiment demonstrates that the effect of PTEN on VSV is mediated by an increase in autophagy.

The previous experiments relied on overexpression phenotypes; therefore, we tested whether we observed a similar dependence on nutrient signaling by using a loss-of-function strategy. Loss of Akt signaling is predicted to activate autophagy and inhibit VSV replication. To this end, we tested whether loss of Akt by RNAi, by using a previously validated transgene, would result in decreased viral replication (54). We found that depletion of Akt by RNAi led to a decrease in VSV replication as measured by immunoblot (Figure A-7C).

Together, these data suggest that infection by VSV is sensed by flies, leading to a decrease in PI3K/Akt signaling, which increases autophagy and inhibits viral replication. However, these data do not show whether infection itself modulates this signaling pathway. A prediction is that VSV infection is sensed by the fly, leading to the repression of PI3K/Akt signaling to activate the antiviral autophagy program. We set out to test this hypothesis by monitoring signaling during infection. One method to monitor signaling through this pathway is to measure the levels of phosphorylation of Akt by immunoblot. We challenged the flies with VSV and compared the amounts of phospho-Akt to flies that were uninfected. We observed a substantial decrease in amounts of phospho-Akt in VSV-infected animals (Figure A-7D). In contrast, total Akt protein remained constant. Thus, VSV infection leads to an inhibition of Akt signaling in animals.

DISCUSSION

Although autophagy has been implicated in diverse processes, both normal and pathogenic, a role in controlling viral replication has been difficult to demonstrate directly in vivo and is complicated by differing requirements by distinct pathogens. With a new model system, we found that autophagy plays an important antiviral role against VSV in tissue culture cells as well as in adult flies. By modulating the pathway in vivo—either inhibiting it with RNAi against components of the autophagic machinery or activating it by repressing the function of upstream members of the PI3K/Akt-signaling pathway—we demonstrate a reciprocal effect on viral replication: activation of autophagy inhibits, and inhibition of autophagy exacerbates infection. Moreover, we showed that infection is sensed by flies and leads to inhibition of the Akt-signaling pathway. This, in turn, leads to activation of the antiviral autophagic program, thereby protecting the animal from an otherwise lethal virus infection.

Furthermore, our data suggest that autophagy is directly activated by VSV infection, most likely via the surface glycoprotein VSV-G, and thus activation does not require viral replication. Although VSV RNA can be recognized by the cytoplasmic sensors in mammals, we showed that VSV RNA was not the sensor for autophagy in flies. Moreover, this class of intracellular sensors has not yet been identified in *Drosphila*. Interestingly, recent work in mammalian systems indicates that VSV-G can also be recognized by TLR4 to activate this class of pattern recognition receptors (PRRs) (13). It has been observed that TLR4 signaling can activate autophagy downstream of

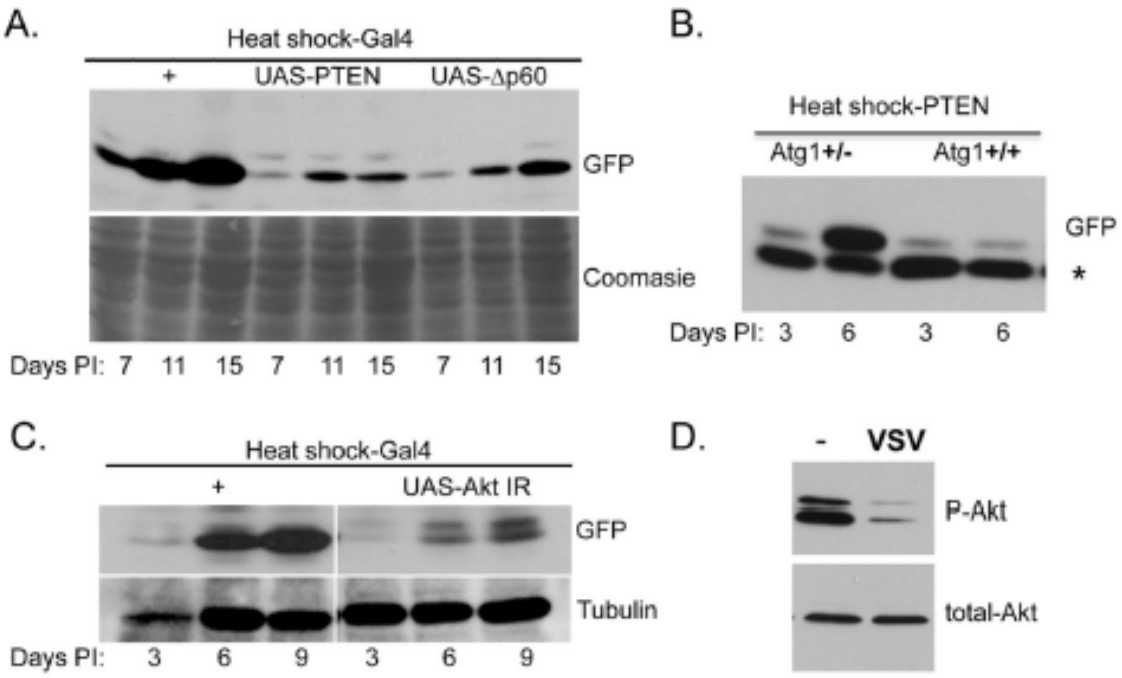

Figure A-7. The PI3K-Akt pathway controls autophagy and viral replication in adult flies. (A) Flies carrying a heat shock-inducible Gal4 were crossed to UAS-PTEN, UAS-Δp60, or control at room temperature. Progeny were collected and heat shocked at 37°C for 1 hr on the day of infection and every 2 days after challenge. Viral replication was monitored over time for viral replication by immunoblot against virally produced GFP and normalized to cellular proteins. (B) Flies carrying a heat shock-inducible PTEN were crossed to flies heterozygous for a mutant Atg1 allele at room temperature. Progeny were collected and heat shocked at 37°C for 1 hr on the day of infection and every 2 days after challenge. Viral replication was monitored over time for viral replication by immunoblot against virally produced GFP and normalized to a cellular control protein. (C) Flies carrying a heat shock-inducible Gal4 were crossed to UAS-Akt IR at room

temperature. Progeny were collected and heat shocked at 37°C for 1 hr on the day of infection and every 2 days after challenge. Viral replication was monitored over time for viral replication by immunoblot against virally produced GFP and normalized to cellular proteins. (D) Flies were injected with insulin in the presence or absence of VSV. Phospho-Akt and Total-Akt were monitored by immunoblot. These data show representative experiments; similar findings were made in at least three repetitions.

the bacterial PAMP LPS, suggesting a link between pattern recognition by TLRs and the cellular antimicrobial response (56). *Drosphila* has nine TLRs, raising the possibility that this VSV-G-dependent viral recognition pathway uses this class of pattern recognition receptors; however, other receptors may be involved. Previous studies found that, in specialized antigen-presenting dendritic cells that are not competent for VSV replication, autophagy is required to present VSV antigens to endosomal TLR7, suggesting that different aspects of the autophagic pathway may modulate viral replication under different conditions or in specialized cell types (26).

Autophagy has been shown to be essential for defense against a variety of pathogens in cell culture. Our studies suggest that VSV-G is recognized by a pattern recognition receptor whose activation leads to inhibition of the PI3K-signaling pathway, increasing autophagy and thereby blocking viral replication. Importantly, this newly identified antiviral pathway may play a role in the control of additional infectious agents. Moreover, it may be fruitful to explore pharmacological modulation of the pathway as a means to inhibit viral replication because there are a number of small molecule modulators that have been developed to regulate the PI3K-Akt-signaling pathway.

ACKNOWLEDGEMENTS

We thank M. Tudor, S. Ross, N. Bonini, J. DiAngelo, and members of the Cherry laboratory for critically reading the manuscript; P. Bates for helpful suggestions; J. Rose for VSV-GFP; T. Neufeld for Atg snapback transgenic flies; J. DiAngelo and M. Birnbaum for Akt pathway transgenic flies; the Vienna *Drosphila* RNAi Center (VDRC)

for Atg18 and Akt snapback transgenic flies; the Bloomington Stock Center for other fly stocks; R. Doms for anti-VSV G antibody; D. Lyles and R. Hardy for anti-VSV M antibody; and N. Shah for technical assistance and electron microscopy support. This work was supported by a training grant T32AI07324 to S.S. and by NIH grants 1R01AI07451 and U54AI057168 to S.C.

REFERENCES

1. **Abe, A., S. T. Chen, A. Miyanohara, and T. Friedmann.** 1998. In vitro cell-free conversion of noninfectious Moloney retrovirus particles to an infectious form by the addition of the vesicular stomatitis virus surrogate envelope G protein. J Virol **72:**6356-6361.
2. **Andrade, R. M., M. Wessendarp, M. J. Gubbels, B. Striepen, and C. S. Subauste.** 2006. CD40 induces macrophage anti-Toxoplasma gondii activity by triggering autophagy-dependent fusion of pathogen-containing vacuoles and lysosomes. J Clin Invest **116:**2366-2377.
3. **Arico, S., A. Petiot, C. Bauvy, P. F. Dubbelhuis, A. J. Meijer, P. Codogno, and E. Ogier-Denis.** 2001. The tumor suppressor PTEN positively regulates macroautophagy by inhibiting the phosphatidylinositol 3-kinase/protein kinase B pathway. J Biol Chem **276:**35243-35246.
4. **Bilen, J., and N. M. Bonini.** 2007. Genome-wide screen for modifiers of ataxin-3 neurodegeneration in Drosophila. PLoS Genet **3:**1950-1964.
5. **Brand, A. H., and N. Perrimon.** 1993. Targeted gene expression as a means of altering cell fates and generating dominant phenotypes. Development **118:**401-415.
6. **Britton, J. S., W. K. Lockwood, L. Li, S. M. Cohen, and B. A. Edgar.** 2002. Drosophila's insulin/PI3-kinase pathway coordinates cellular metabolism with nutritional conditions. Dev Cell **2:**239-249.

7. **Chen, G. C., J. Y. Lee, H. W. Tang, J. Debnath, S. M. Thomas, and J. Settleman.** 2008. Genetic interactions between Drosophila melanogaster Atg1 and paxillin reveal a role for paxillin in autophagosome formation. Autophagy **4:**37-45.

8. **Cherry, S., T. Doukas, S. Armknecht, S. Whelan, H. Wang, P. Sarnow, and N. Perrimon.** 2005. Genome-wide RNAi screen reveals a specific sensitivity of IRES-containing RNA viruses to host translation inhibition. Genes Dev **19:**445-452.

9. **Cherry, S., and N. Perrimon.** 2004. Entry is a rate-limiting step for viral infection in a Drosophila melanogaster model of pathogenesis. Nat Immunol **5:**81-87.

10. **Cherry, S., and N. Silverman.** 2006. Host-pathogen interactions in drosophila: new tricks from an old friend. Nat Immunol **7:**911-917.

11. **Dubovi, E. J., and J. S. Youngner.** 1976. Inhibition of pseudorabies virus replication by vesicular stomatitis virus. II Activity of defective interfering particles. J Virol **18:**534-541.

12. **Elrod-Erickson, M., S. Mishra, and D. Schneider.** 2000. Interactions between the cellular and humoral immune responses in Drosophila. Curr Biol **10:**781-784.

13. **Georgel, P., Z. Jiang, S. Kunz, E. Janssen, J. Mols, K. Hoebe, S. Bahram, M. B. Oldstone, and B. Beutler.** 2007. Vesicular stomatitis virus glycoprotein G activates a specific antiviral Toll-like receptor 4-dependent pathway. Virology **362:**304-313.

14. **Goto, A., T. Kadowaki, and Y. Kitagawa.** 2003. Drosophila hemolectin gene is expressed in embryonic and larval hemocytes and its knock down causes bleeding defects. Dev Biol **264:**582-591.

15. **Gupta, A. K., T. Das, and A. K. Banerjee.** 1995. Casein kinase II is the P protein phosphorylating cellular kinase associated with the ribonucleoprotein complex of purified vesicular stomatitis virus. J Gen Virol **76 (Pt 2):**365-372.

16. **Gutierrez, M. G., S. S. Master, S. B. Singh, G. A. Taylor, M. I. Colombo, and V. Deretic.** 2004. Autophagy is a defense mechanism inhibiting BCG and Mycobacterium tuberculosis survival in infected macrophages. Cell **119:**753-766.

17. **Iwasaki, A.** 2007. Role of autophagy in innate viral recognition. Autophagy **3:**354-356.

18. **Janeway, C. A., Jr., and R. Medzhitov.** 2002. Innate immune recognition. Annu Rev Immunol **20:**197-216.

19. **Juhasz, G., and T. P. Neufeld.** 2006. Autophagy: a forty-year search for a missing membrane source. PLoS Biol **4:**e36.

20. **Kabeya, Y., N. Mizushima, T. Ueno, A. Yamamoto, T. Kirisako, T. Noda, E. Kominami, Y. Ohsumi, and T. Yoshimori.** 2000. LC3, a mammalian homologue of yeast Apg8p, is localized in autophagosome membranes after processing. Embo J **19:**5720-5728.

21. **Kirkegaard, K., M. P. Taylor, and W. T. Jackson.** 2004. Cellular autophagy: surrender, avoidance and subversion by microorganisms. Nat Rev Microbiol **2:**301-314.

22. **Klionsky, D. J., H. Abeliovich, P. Agostinis, D. K. Agrawal, G. Aliev, D. S. Askew, M. Baba, E. H. Baehrecke, B. A. Bahr, A. Ballabio, B. A. Bamber, D. C. Bassham, E. Bergamini, X. Bi, M. Biard-Piechaczyk, J. S. Blum, D. E. Bredesen, J. L. Brodsky, J. H. Brumell, U. T. Brunk, W. Bursch, N. Camougrand, E. Cebollero, F. Cecconi, Y. Chen, L. S. Chin, A. Choi, C. T. Chu, J. Chung, P. G. Clarke, R. S. Clark, S. G. Clarke, C. Clave, J. L. Cleveland, P. Codogno, M. I. Colombo, A. Coto-Montes, J. M. Cregg, A. M. Cuervo, J. Debnath, F. Demarchi, P. B. Dennis, P. A. Dennis, V. Deretic, R. J. Devenish, F. Di Sano, J. F. Dice, M. Difiglia, S. Dinesh-Kumar, C. W. Distelhorst, M. Djavaheri-Mergny, F. C. Dorsey, W. Droge, M. Dron, W. A. Dunn, Jr., M. Duszenko, N. T. Eissa, Z. Elazar, A. Esclatine, E. L. Eskelinen, L. Fesus, K. D. Finley, J. M. Fuentes, J. Fueyo, K. Fujisaki, B. Galliot, F. B. Gao, D. A. Gewirtz, S. B. Gibson, A. Gohla, A. L. Goldberg, R. Gonzalez, C. Gonzalez-Estevez, S. Gorski, R. A. Gottlieb, D. Haussinger, Y. W. He, K. Heidenreich, J. A. Hill, M. Hoyer-Hansen, X. Hu, W. P. Huang, A. Iwasaki, M. Jaattela, W. T. Jackson, X. Jiang, S. Jin, T. Johansen, J. U. Jung, M. Kadowaki, C. Kang, A. Kelekar, D. H. Kessel, J. A. Kiel, H. P. Kim, A. Kimchi, T. J. Kinsella, K. Kiselyov, K. Kitamoto, E. Knecht, et al.** 2008. Guidelines for the use and interpretation of assays for monitoring autophagy in higher eukaryotes. Autophagy **4:**151-175.

23. **Klionsky, D. J., J. M. Cregg, W. A. Dunn, Jr., S. D. Emr, Y. Sakai, I. V. Sandoval, A. Sibirny, S. Subramani, M. Thumm, M. Veenhuis, and Y.**

Ohsumi. 2003. A unified nomenclature for yeast autophagy-related genes. Dev Cell **5:**539-545.

24. **Klionsky, D. J., and Y. Ohsumi.** 1999. Vacuolar import of proteins and organelles from the cytoplasm. Annu Rev Cell Dev Biol **15:**1-32.

25. **Kuma, A., M. Hatano, M. Matsui, A. Yamamoto, H. Nakaya, T. Yoshimori, Y. Ohsumi, T. Tokuhisa, and N. Mizushima.** 2004. The role of autophagy during the early neonatal starvation period. Nature **432:**1032-1036.

26. **Lee, H. K., J. M. Lund, B. Ramanathan, N. Mizushima, and A. Iwasaki.** 2007. Autophagy-dependent viral recognition by plasmacytoid dendritic cells. Science **315:**1398-1401.

27. **Lee, S. B., S. Kim, J. Lee, J. Park, G. Lee, Y. Kim, J. M. Kim, and J. Chung.** 2007. ATG1, an autophagy regulator, inhibits cell growth by negatively regulating S6 kinase. EMBO Rep **8:**360-365.

28. **Lemaitre, B., and J. Hoffmann.** 2007. The host defense of Drosophila melanogaster. Annu Rev Immunol **25:**697-743.

29. **Letchworth, G. J., L. L. Rodriguez, and J. Del cbarrera.** 1999. Vesicular stomatitis. Vet J **157:**239-260.

30. **Levine, B., and V. Deretic.** 2007. Unveiling the roles of autophagy in innate and adaptive immunity. Nat Rev Immunol **7:**767-777.

31. **Li, H. W., and S. W. Ding.** 2005. Antiviral silencing in animals. FEBS Lett **579:**5965-5973.

32. **Liang, X. H., L. K. Kleeman, H. H. Jiang, G. Gordon, J. E. Goldman, G. Berry, B. Herman, and B. Levine.** 1998. Protection against fatal Sindbis virus encephalitis by beclin, a novel Bcl-2-interacting protein. J Virol **72:**8586-8596.

33. **Ling, Y. M., M. H. Shaw, C. Ayala, I. Coppens, G. A. Taylor, D. J. Ferguson, and G. S. Yap.** 2006. Vacuolar and plasma membrane stripping and autophagic elimination of Toxoplasma gondii in primed effector macrophages. J Exp Med **203:**2063-2071.

34. **Liu, Y., M. Schiff, K. Czymmek, Z. Talloczy, B. Levine, and S. P. Dinesh-Kumar.** 2005. Autophagy regulates programmed cell death during the plant innate immune response. Cell **121:**567-577.

35. **Lum, J. J., R. J. DeBerardinis, and C. B. Thompson.** 2005. Autophagy in metazoans: cell survival in the land of plenty. Nat Rev Mol Cell Biol **6:**439-448.

36. **Meylan, E., J. Tschopp, and M. Karin.** 2006. Intracellular pattern recognition receptors in the host response. Nature **442:**39-44.

37. **Mizushima, N., B. Levine, A. M. Cuervo, and D. J. Klionsky.** 2008. Autophagy fights disease through cellular self-digestion. Nature **451:**1069-1075.

38. **Mizushima, N., A. Yamamoto, M. Matsui, T. Yoshimori, and Y. Ohsumi.** 2004. In vivo analysis of autophagy in response to nutrient starvation using transgenic mice expressing a fluorescent autophagosome marker. Mol Biol Cell **15:**1101-1111.

39. **Nakagawa, I., A. Amano, N. Mizushima, A. Yamamoto, H. Yamaguchi, T. Kamimoto, A. Nara, J. Funao, M. Nakata, K. Tsuda, S. Hamada, and T.**

Yoshimori. 2004. Autophagy defends cells against invading group A Streptococcus. Science **306:**1037-1040.

40. **Ogawa, M., T. Yoshimori, T. Suzuki, H. Sagara, N. Mizushima, and C. Sasakawa.** 2005. Escape of intracellular Shigella from autophagy. Science **307:**727-731.

41. **Orvedahl, A., D. Alexander, Z. Talloczy, Q. Sun, Y. Wei, W. Zhang, D. Burns, D. A. Leib, and B. Levine.** 2007. HSV-1 ICP34.5 confers neurovirulence by targeting the Beclin 1 autophagy protein. Cell Host Microbe **1:**23-35.

42. **Palese, P., H. Zheng, O. G. Engelhardt, S. Pleschka, and A. Garcia-Sastre.** 1996. Negative-strand RNA viruses: genetic engineering and applications. Proc Natl Acad Sci U S A **93:**11354-11358.

43. **Ramsburg, E., J. Publicover, L. Buonocore, A. Poholek, M. Robek, A. Palin, and J. K. Rose.** 2005. A vesicular stomatitis virus recombinant expressing granulocyte-macrophage colony-stimulating factor induces enhanced T-cell responses and is highly attenuated for replication in animals. J Virol **79:**15043-15053.

44. **Rich, K. A., C. Burkett, and P. Webster.** 2003. Cytoplasmic bacteria can be targets for autophagy. Cell Microbiol **5:**455-468.

45. **Rolls, M. M., P. Webster, N. H. Balba, and J. K. Rose.** 1994. Novel infectious particles generated by expression of the vesicular stomatitis virus glycoprotein from a self-replicating RNA. Cell **79:**497-506.

46. **Rusten, T. E., K. Lindmo, G. Juhasz, M. Sass, P. O. Seglen, A. Brech, and H. Stenmark.** 2004. Programmed autophagy in the Drosophila fat body is induced by ecdysone through regulation of the PI3K pathway. Dev Cell **7:**179-192.

47. **Scott, R. C., G. Juhasz, and T. P. Neufeld.** 2007. Direct induction of autophagy by Atg1 inhibits cell growth and induces apoptotic cell death. Curr Biol **17:**1-11.

48. **Scott, R. C., O. Schuldiner, and T. P. Neufeld.** 2004. Role and regulation of starvation-induced autophagy in the Drosophila fat body. Dev Cell **7:**167-178.

49. **Seay, M. D., and S. P. Dinesh-Kumar.** 2005. Life after death: are autophagy genes involved in cell death and survival during plant innate immune responses? Autophagy **1:**185-186.

50. **Singh, S. B., A. S. Davis, G. A. Taylor, and V. Deretic.** 2006. Human IRGM induces autophagy to eliminate intracellular mycobacteria. Science **313:**1438-1441.

51. **Stephan, J. S., and P. K. Herman.** 2006. The regulation of autophagy in eukaryotic cells: do all roads pass through Atg1? Autophagy **2:**146-148.

52. **Talloczy, Z., H. W. t. Virgin, and B. Levine.** 2006. PKR-dependent autophagic degradation of herpes simplex virus type 1. Autophagy **2:**24-29.

53. **Uematsu, S., and S. Akira.** 2006. Toll-like receptors and innate immunity. J Mol Med (Berl) **84:**712-725.

54. **Wang, B., J. Goode, J. Best, J. Meltzer, P. E. Schilman, J. Chen, D. Garza, J. B. Thomas, and M. Montminy.** 2008. The insulin-regulated CREB coactivator TORC promotes stress resistance in Drosophila. Cell Metab **7:**434-444.

55. **Wullschleger, S., R. Loewith, and M. N. Hall.** 2006. TOR signaling in growth and metabolism. Cell **124:**471-484.

56. **Xu, Y., C. Jagannath, X. D. Liu, A. Sharafkhaneh, K. E. Kolodziejska, and N. T. Eissa.** 2007. Toll-like receptor 4 is a sensor for autophagy associated with innate immunity. Immunity **27:**135-144.

57. **Yano, T., S. Mita, H. Ohmori, Y. Oshima, Y. Fujimoto, R. Ueda, H. Takada, W. E. Goldman, K. Fukase, N. Silverman, T. Yoshimori, and S. Kurata.** 2008. Autophagic control of listeria through intracellular innate immune recognition in drosophila. Nat Immunol **9:**908-916.

SUPPLEMENTAL DATA

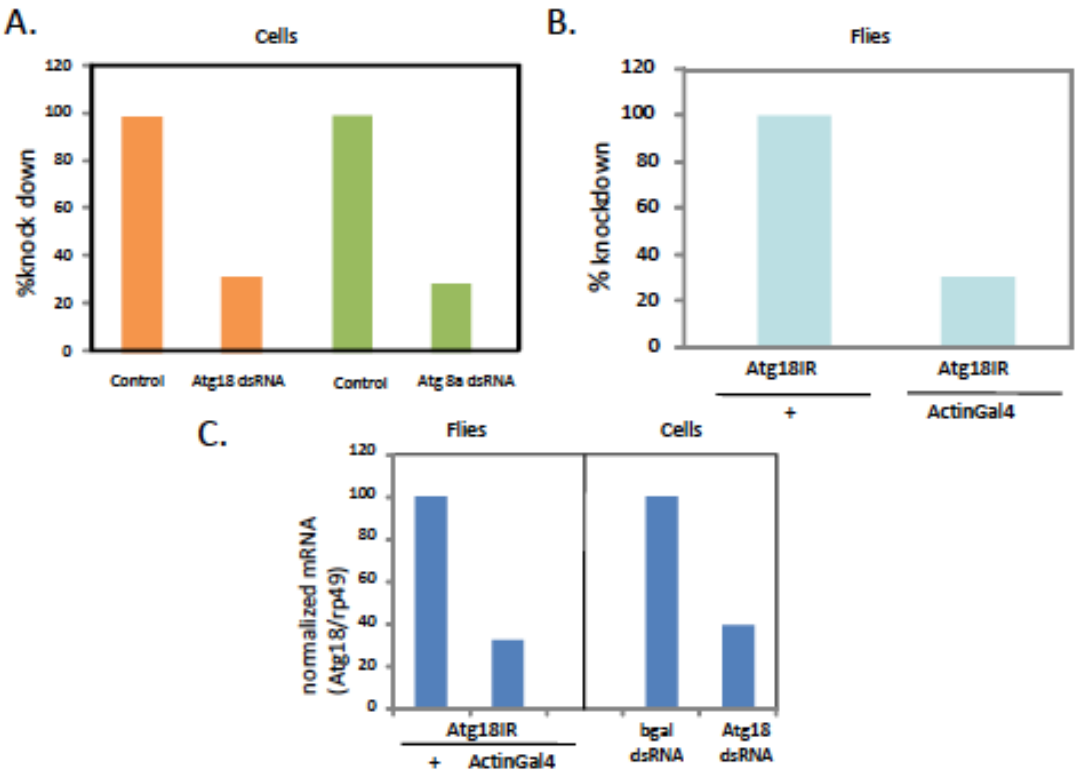

Figure A-S1. dsRNA against autophagy genes is efficacious both in cells and flies as measured either by semiquantitative RT-PCR or RT-qPCR. (A) >75% depletion of the cognate message as measured by semi-quantitative RT-PCR against Atg18 (orange) or Atg8a (green) normalized to a cellular control (clathrin heavy chain). Control dsRNA treated samples are set to 100%. (B) Semi-quantitative RT-PCR against Atg18 normalized to control (clathrin heavy chain). Adult flies expressing ubiquitous and high level dsRNA against Atg18 (Actin-Gal4; UAS-Atg18IR) were compared to sibling controls (+; UAS-Atg18IR) which were set to 100%. C. RT-qPCR against Atg18

normalized to control (rp49) in adult flies as in B. or in cells pre-treated with the indicated dsRNAs.

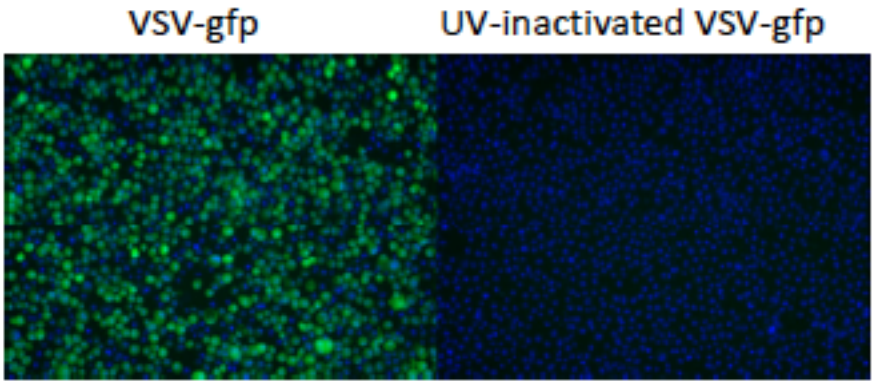

Figure A-S2. Schneider Cells Were Infected with VSV-GFP (MOI=9) or UV-Inactivated VSV-GFP (Equivalent Volume) for 20 Hours. Cells were processed for immunofluorescence and imaged using an automated microscope (ImagXpress Micro). There were no Gfp+ cells in the UV inactivated sample.

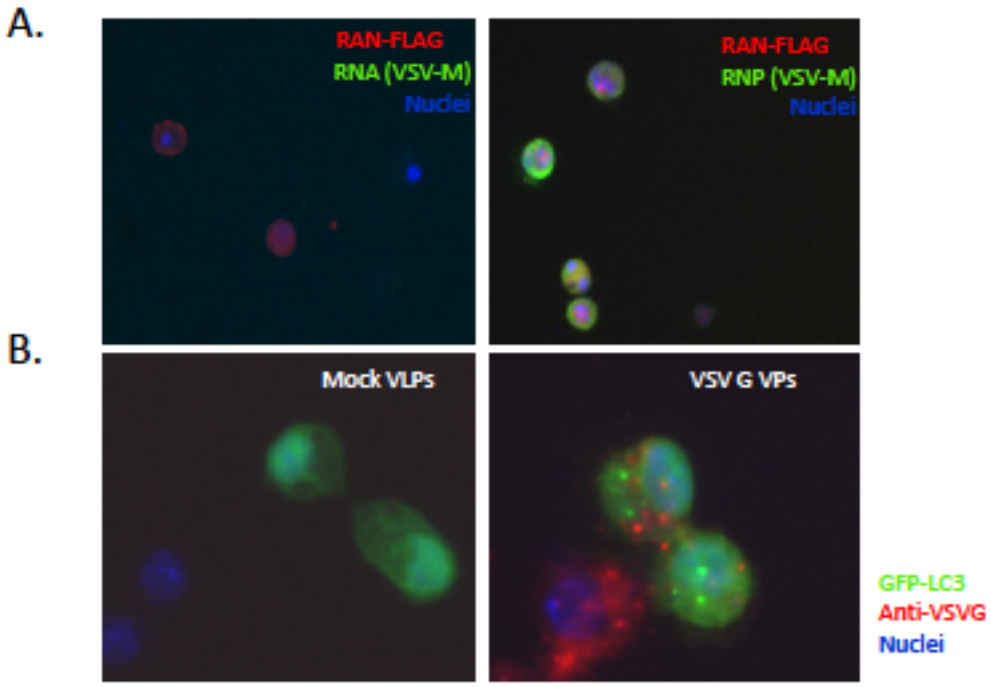

Figure A-S3. Purified viral components reveal that VSV G is the PAMP. (A) Purified VSV RNP but not VSV RNA is infectious when transfected into cells. Schneider cells were co-transfected with Flag-tagged RAN and either VSV RNA (left) or VSV RNP (right). Cells were processed for immunofluorescence with anti-FLAG (red), anti-VSV M (green) and nuclei (blue) and imaged. There were no VSV-M+ cells in the viral RNA transfected sample while >95% of the Flag+ (transfected) cells were VSV-M+. (B) Cells treated with VPs from VSV G transfected 293s but not blebs from mock-transfected cells are VSV G+ and induce GFP-LC3 punctae. Cells were transfected with GFP-LC3 and then treated with VPs and processed for fluorescence with GFP-LC3 (green), anti-VSV G (red) and nuclei (blue).

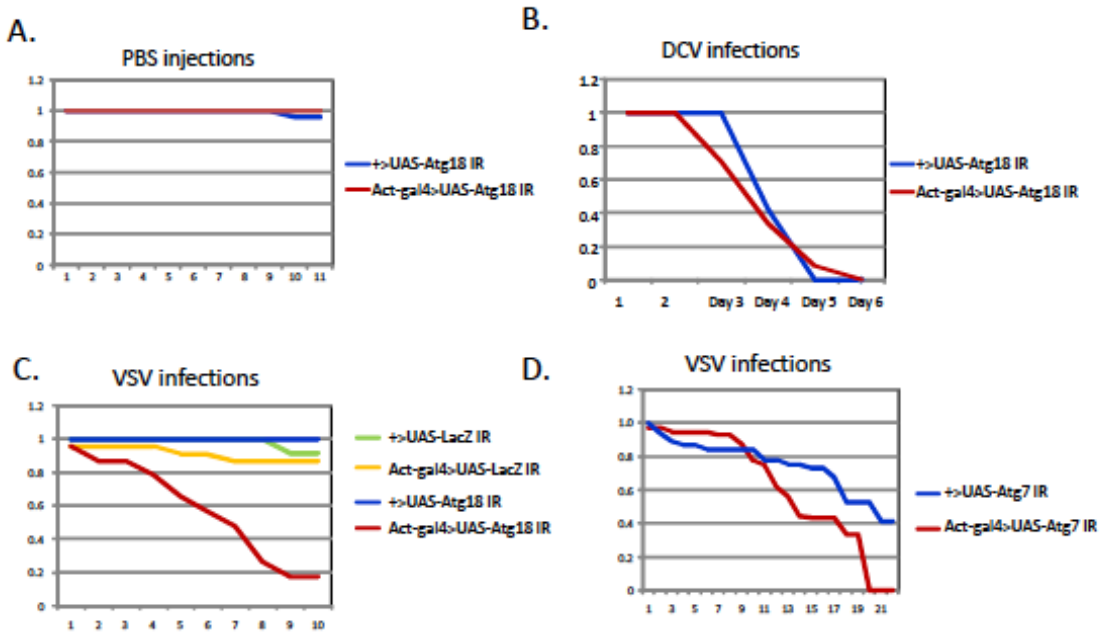

Figure A-S4. Depletion of autophagy in adult flies specifically impairs VSV susceptibility. Flies of the indicated genotypes were challenged with (A) PBS or (B) *Drosphila* C Virus (DCV) or (C) VSV. (D) VSV and monitored daily for mortality. Log rank test reveals that loss of Atg7 significantly increases susceptibility ($p<0.05$). A representative experiment is shown. Each challenge was repeated at least three times.

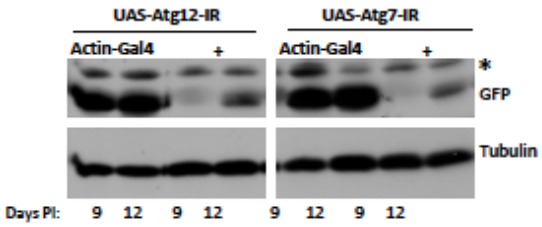

Figure A-S5. Autophagy controls VSV but not DCV infection in adult flies.

Adult flies expressing ubiquitous and high-level dsRNA against either Atg12 (Actin-Gal4; UASAtg12IR) or Atg7 (Actin-Gal4; UAS-Atg7IR) or their respective sibling controls (+; UASAtg12IR or +; UAS-Atg7IR) were challenged with VSV and monitored over time for viral replication as measured by immunoblot against virally produced GFP and normalized to a cellular control protein. There is a significant increase in VSV replication in flies depleted for autophagy genes measured by protein production. * indicates nonspecific background band.

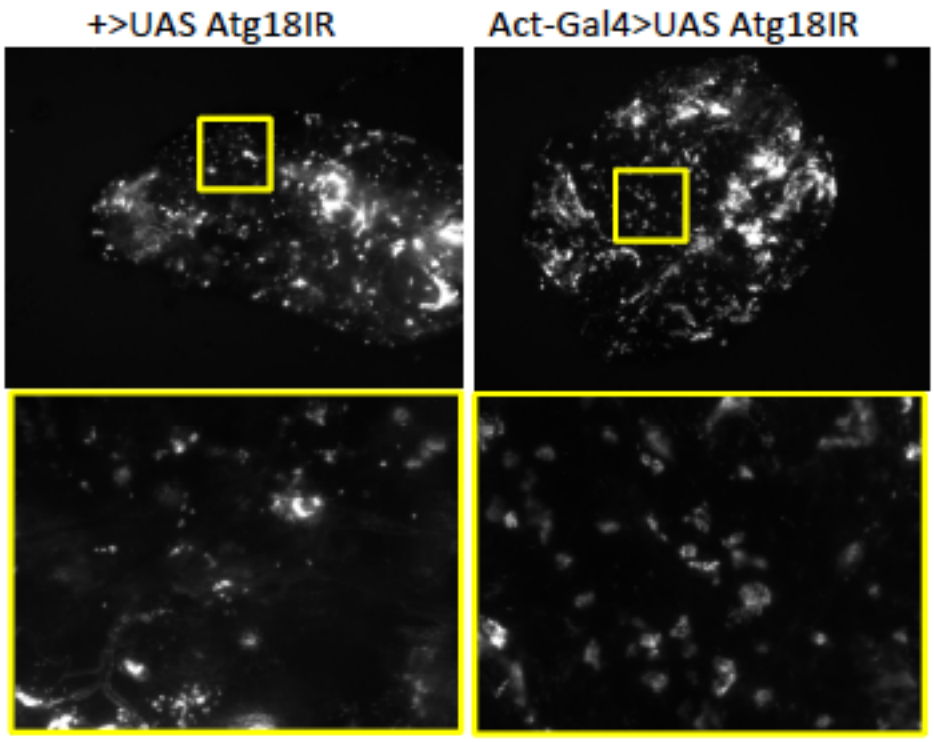

Figure A-S6. Atg18-depleted flies have wild-type numbers of hemocytes that are functional as measured by phagocytic activity. Adult flies were injected with 0.2um red fluorescent beads. Three days later the flies were processed for fluorescence microscopy. Hemocytes are the only phagocytic cells which take up fluorescent beads, which can be readily visualized through the cuticle and are distributed throughout the abdomen. Top panels at low magnification and the indicated inset is shown at higher magnification to show individual cells that have taken up multiple beads. Areas of increased saturation in top panels are likely aggregated hemocytes.

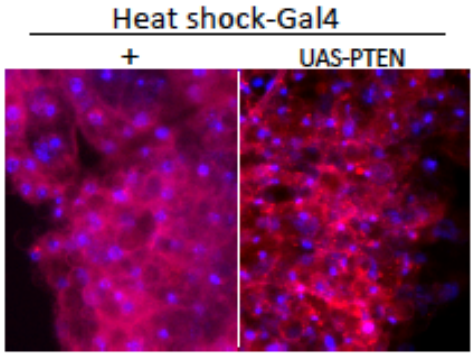

Figure A-S7. Flies carrying a heat shock-inducible Gal4 were crossed to UAS-PTEN or control at room temperature. Progeny were collected and heat shocked at 37C for one hour the day before and the day of staining. Autophagy was monitored using Lysotracker staining to visualize the autophagosomes and counterstained with Hoescht 33342 to observe the nuclei. There are increased acidic compartments in the fat body cells of well-fed flies expressing the negative regulator PTEN compared to the diffuse dim staining in the control fat body cells.

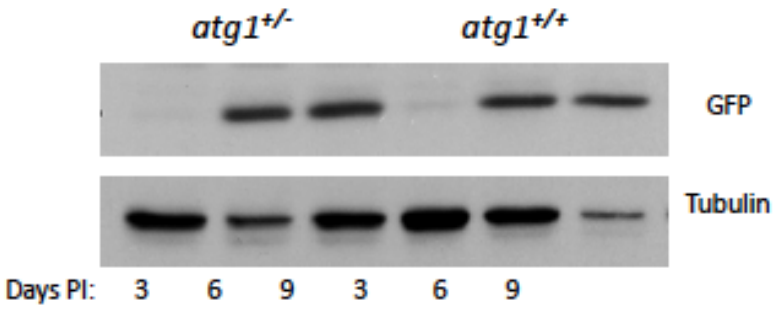

Figure A-S8. Heterozygous ATG1 mutants carry wild-type levels of VSV. Flies of the indicated genotypes were challenged with VSV and monitored by immunoblot at the indicated time post infection.